NASA/TP–2018-219033/Vol. 2

Advances in Above- and In-Water Radiometry, Volume 2:

Autonomous Atmospheric and Oceanic Observing Systems

Stanford B. Hooker, Randall N. Lind, John H. Morrow, James W. Brown, Raphael M. Kudela,
Henry F. Houskeeper, and Koji Suzuki

National Aeronautics and
Space Administration

Goddard Space Flight Center
Greenbelt, Maryland 20771

November 2018

NASA STI Program ... in Profile

Since its founding, NASA has been dedicated to the advancement of aeronautics and space science. The NASA scientific and technical information (STI) program plays a key part in helping NASA maintain this important role.

The NASA STI program operates under the auspices of the Agency Chief Information Officer. It collects, organizes, provides for archiving, and disseminates NASA's STI. The NASA STI program provides access to the NASA Aeronautics and Space Database and its public interface, the NASA Technical Report Server, thus providing one of the largest collections of aeronautical and space science STI in the world. Results are published in both non-NASA channels and by NASA in the NASA STI Report Series, which includes the following report types:

- TECHNICAL PUBLICATION. Reports of completed research or a major significant phase of research that present the results of NASA Programs and include extensive data or theoretical analysis. Includes compilations of significant scientific and technical data and information deemed to be of continuing reference value. NASA counterpart of peer-reviewed formal professional papers but has less stringent limitations on manuscript length and extent of graphic presentations.

- TECHNICAL MEMORANDUM. Scientific and technical findings that are preliminary or of specialized interest, e.g., quick release reports, working papers, and bibliographies that contain minimal annotation. Does not contain extensive analysis.

- CONTRACTOR REPORT. Scientific and technical findings by NASA-sponsored contractors and grantees.

- CONFERENCE PUBLICATION. Collected papers from scientific and technical conferences, symposia, seminars, or other meetings sponsored or co-sponsored by NASA.

- SPECIAL PUBLICATION. Scientific, technical, or historical information from NASA programs, projects, and missions, often concerned with subjects having substantial public interest.

- TECHNICAL TRANSLATION. English-language translations of foreign scientific and technical material pertinent to NASA's mission.

Specialized services also include organizing and publishing research results, distributing specialized research announcements and feeds, providing help desk and personal search support, and enabling data exchange services. For more information about the NASA STI program, see the following:

- Access the NASA STI program home page at http://www.sti.nasa.gov

- E-mail your question via the Internet to help@sti.nasa.gov

- Phone the NASA STI Information Desk at 757-864-9658

- Write to:
  NASA STI Information Desk
  Mail Stop 148
  NASA's Langley Research Center
  Hampton, VA 23681-2199

Advances in Above- and In-Water Radiometry, Volume 2:

Autonomous Atmospheric and Oceanic Observing Systems

Stanford B. Hooker
NASA Goddard Space Flight Center Greenbelt, Maryland

Randall N. Lind
Biospherical Instruments Inc. San Diego, California

John H. Morrow
Biospherical Instruments Inc. San Diego, California

James W. Brown
RSMAS University of Miami Miami, Florida

Raphael M. Kudela
University of California Santa Cruz Santa Cruz, California

Henry F. Houskeeper
University of California Santa Cruz Santa Cruz, California

Koji Suzuki
Hokkaido University Sapporo, Japan

November 2018

S.B. Hooker, R.N. Lind, J.H. Morrow, J.W. Brown, R.M. Kudela, H.F. Houskeeper, and K. Suzuki

Abstract

This publication documents the scientific advances associated with new instrument systems and accessories built to improve above- and in-water observations of the apparent optical properties (AOPs) of optically complex waters. The principal objective is to be prepared for the launch of next-generation ocean color satellites with the most capable commercial off-the-shelf (COTS) instrumentation in the shortest time possible. The Hybridspectral Alternative for Remote Profiling of Optical Observations for NASA Satellites (HARPOONS) is presented as a case example of technologies conceived, developed, and deployed operationally in support of next-generation mission requirements. The field trials, field commissioning, and operational demonstration resulted in a technology readiness level (TRL) value of 9 for a diversity of laboratory and field instrument systems. Separate detailed presentations of the individual instruments provide the hardware designs, accompanying software for data acquisition and processing, and examples of the results achieved. For the laboratory components, calibration and characterization procedures are described along with an estimation of the sources of uncertainty, which culminates in a full uncertainty budget for the radiometers deployed to the field.

Prologue

The HARPOONS sampling paradigm is based on the Hybrid System for Environmental AOP Sampling of the Sea Surface Demonstration (HySEAS3D) concept, wherein an unmanned surface vessel (USV) is used to make above- and in-water optical measurements (Chap. 7) while an appropriately nearby sun photometer characterizes the atmospheric conditions during sampling. The selected USV is a third-generation Wave Glider surface vessel, or SV3, developed by Liquid Robotics, Inc. (LRI) and built as a COTS platform (Sunnyvale, California).

Because the principal HARPOONS objective is obtaining autonomous in-water hyperspectral profiles, the optical instruments are from the Compact-Profiling Hybrid Instrumentation for Radiometry and Ecology (C-PHIRE) suite of next-generation Enhanced Performance Instrument Class (EPIC) radiometers. For C-PHIRE radiometers, an array of microradiometers (15 or 18, depending on the instrument) acquire data in parallel with a hyperspectral spectrograph.

In order to reduce costs, a harmonized architecture is used for all of the above- and in-water optical instruments with differences minimized to the greatest extent practicable. Consequently, all the spectrographs are the same one used for the Compact-Hybridspectral Radiometer (C-HyR) profiler (Chap. 3), which is the Compact Grating Spectrometer (CGS) manufactured by Carl Zeiss Spectroscopy GmbH (Jena, Germany) with tec5USA, Inc. (Plainview, New York) supplying the electronics interface. The CGS has 2,048 pixels spanning a spectral range of 190–1,000 nm.

The anticipated spectral range for validated hyperspectral data products is 305–900 nm, although the future applications discussed in Chap. 8 for supporting next-generation NASA missions anticipates a validated spectral range of 320–900 nm. The CGS spectrograph as implemented here is the result of collaborations between the authors and the manufacturer's representative tec5USA.

The CGS comprises an imaging grating, optical port, and a charge-coupled device (CCD) detector with electric shutter to minimize integration times. The CGS is compact ($74 \times 30 \times 76$ mm^3) and thermally stable with a spectral resolution less than 3 nm (in keeping with PACE mission requirements for vicarious calibration exercises). The spectrometer core is a blazed, flat-field grating for light dispersion and imaging. The CGS has excellent stability coupled with very low stray light and high reliability in rough environments. The CGS was selected based on exhaustive market surveys for the Optical Sensors for Planetary Radiant Energy (OSPREy) activity (2009–2012) with trade study refinements during C-HyR (2013–2014) development (Chap. 3).

The deployment of sophisticated instruments designed to provide the highest quality data products possible requires advances in the technologies used in the laboratory and the field. Consequently, the HARPOONS activity involves five principal instrument systems with the radiometers and support electronics developed by Biospherical Instruments Inc. (BSI) and manufactured as COTS devices (San Diego, California), as follows:

1. A Towable Optical Wave-Following *In Situ* Hybrid (TOW-FISH) profiler, which has downward irradiance (E_d) and upwelling radiance (L_u) C-PHIRE in-water radiometers mounted on a modified Compact-Optical Profiling System (C-OPS) backplane with dual thrusters developed for the Compact-Propulsion Option for Profiling Systems (C-PrOPS) accessory. The TOW-FISH is towed behind an SV3 using a sea cable with internal and external strength members.

2. An above-water instrument suite mounted on the SV3, which principally contains a global solar irradiance (E_s) C-PHIRE radiometer equipped with a

shadow band accessory to measure the indirect or diffuse irradiance (E_i). Additional above-water devices provide the photosynthetically available radiation (PAR), global positioning system (GPS) coordinates, and communications (with antennas). The tallest components are the solar reference and PAR sensor diffusers.

3. An above-water Compact-Optical Sensors for Planetary Radiant Energy (C-OSPREy) sun photometer mounted on a tracker with a quad detector, which is supported by a solar reference (E_s and E_i) similar to what is mounted on the SV3 except the wavelength domain is more expansive. The sun photometer measures the direct solar (or lunar) irradiance (E), the indirect or diffuse sky radiance (L_i), and the total radiance of the sea surface (L_T), location permitting.

4. A laboratory C-PHIRE Transfer Radiometer (CXR) designed to maintain the National Institute of Standards and Technology (NIST) scale of spectral irradiance within a Lamp Library of NIST-traceable standard lamps and seasoned working lamps. Transferring the NIST scale to a working lamp increases the lifetime of the standard lamps by minimizing the amount of time the standard lamps are used.

5. A Compact Quality Monitor (CQM), which is designed to provide a time series of the calibration stability of radiometers. The CQM can be used in the laboratory or the field, and is anticipated to be a routine part of laboratory calibrations.

Control of all the instruments and execution modes is principally through Data Acquisition and Control for Photometric and Radiometric Observations (DACPRO)

software modules hosted on a MacMini computer (SV3). Data collection functions are established by a scheduler set up before the start of the nominal 10 d mission and are executed automatically.

The principal communications for executing commands on the SV3 is through the Iridium link and the Wave Glider Management System (WGMS); the MacMini sends status updates through WGMS. The SV3 is launched, recovered, and can be visited by a small boat. When near the SV3, a Wireless Fidelity (WiFi) connection can be used to interact with the MacMini directly using a remote desktop utility on a or a MacBook Pro laptop. The remote connection allows the user to investigate system performance, change sampling scenarios already established in the scheduler, etc.

The above-water instrumentation operates on the SV3 power system, which includes two large battery units that are recharged with three solar panels. To allow continuous functionality in the presence of onboard faults, the MacMini has a dedicated 12 VDC lithium-ion back-up battery. The in-water instrumentation is powered by a separate set of batteries stored within one of the payload dry boxes with sufficient capacity to complete a 10 d mission without recharging.

DACPRO is strongly linked to the Processing of Radiometric Observations of Seawater using Information Technologies (PROSIT) software package, which is used to derive all of the data products from the field observations. The most recurring data products as a function of wavelength, λ, are as follows: a) the downward irradiance diffuse attenuation coefficient, $K_d(\lambda)$; b) the water-leaving radiance, $L_W(\lambda)$, including normalized and exact forms; and c) the remote sensing reflectance, $R_{rs}(\lambda)$.

Chapter 7

The HySEAS3D Autonomous Profiling Concept

Stanford B. Hooker
NASA Goddard Space Flight Center
Greenbelt, Maryland

John H. Morrow and Randall N. Lind
Biospherical Instruments, Inc.
San Diego, California

Abstract

HySEAS3D is designed to meet the need for a rapidly deployed autonomous observation platform in keeping with calibration and validation data quality requirements. The package is an integration of two COTS technologies each with a TRL of 9, as follows: the LRI Wave Glider and the 19-channel (320–875 nm) BSI C-OPS. Wave Gliders have autonomously transited the Pacific Ocean, e.g., San Francisco (California) to Sydney (Australia), and have been used in the arctic and for hurricane sampling—*they are rugged.* The silicon photodetector (SiP) microradiometer optical sensor technology used in C-OPS has been successfully deployed in more than 40 above- and in-water radiometric systems, including arctic, laboratory, and airborne instrument suites. The integrated Wave Glider and C-OPS hybrid is designed to collect AOPs in previously under-sampled locations and at reduced cost compared to conventional means. The C-OPS is fitted to a modified backplane, which can include additional fairing components as necessary, and is called the TOW-FISH. The TOW-FISH ascends to the surface on command using two small digital thrusters, all the while measuring $E_d(z, \lambda)$ and $L_u(z, \lambda)$, in addition to vertical orientation. The Wave Glider hosts the global solar irradiance, $E_s(\lambda)$, reference instrument. The free-fall descent from the surface yields centimeter-scale (or less) vertical resolution over the upper 5–6 m, which provides characterization of the first optical depth spanning 320–875 nm. Because of the high resolution, determination of the spectral data products are accomplished with equal efficacy as follows: a) $K_d(\lambda)$; b) $L_W(\lambda)$, including normalized and exact forms; and c) $R_{\rm rs}(\lambda)$. The autonomous operation of the Wave Glider is through the existing WGMS architecture using Iridium communications. Automatic control of the payload instrumentation is through the existing DACPRO architecture hosted on a payload MacMini computer. All data processing is accomplished using PROSIT after the end of a nominal 10 d fair-weather mission. To keep integration as simple as possible, the payload does not use the built-in capabilities of the Wave Glider and WGMS. The latter is used for a short command set to start, stop, and reboot the MacMini and to provide power for the above-water instruments; the in-water instruments receive power from a separate battery unit.


7.1 Introduction

HySEAS3D is designed to meet the need for a rapidly and easily deployed autonomous platform in keeping with calibration, validation, and research (CVR) data quality requirements (Hooker et al. 2007). The package is an integration of two commercial-off-the-shelf (COTS) technologies from BSI and LRI, each with a separate TRL of 9. The concept is to use a second-generation Wave Glider (SV2) built by LRI (Sunnyvale, California) to tow a 19-channel (312–875 nm) C-OPS instrument with digital thrusters and solar reference built by BSI (San Diego, California). Wave Gliders have autonomously transited the Pacific Ocean, e.g., San Francisco (California) to Sydney (Australia), and have been used in the arctic and for hurricane sampling—*they are rugged, well proven, autonomous platforms.* The microradiometer optical sensor technology used in C-OPS has been successfully deployed in more than 40 above- and in-water radiometric systems, including arctic, open-ocean, coastal, littoral, riverine, laboratory, and airborne sensor suites.

An SV2 is a wave-powered version of a small surface vessel, with the added advantage that it is almost never becalmed, because *it is able to harness energy from waves of very small amplitude.* In calm and rough seas alike, the SV2 is able to maintain a headway of approximately 0.4–2.0 kt (nominally 1 kt) along an assigned course or keep

station to within a 40 m *watch* circle (SV2 speed versus surface currents permitting). An SV2 consists of a surface *Float* plus underwater *Sub* joined by a 4 m (or longer) Umbilical (Fig. 66) with electrical and strength members. It uses a propulsion technology that utilizes wave energy for thrust and solar panels (80 W peak) for charging onboard batteries (665 W hr). The design of the system is based on deployments in the Arctic, because if the solar panels can satisfy mission requirements in the Arctic, the rest of the world ocean is likely automatically satisfied.
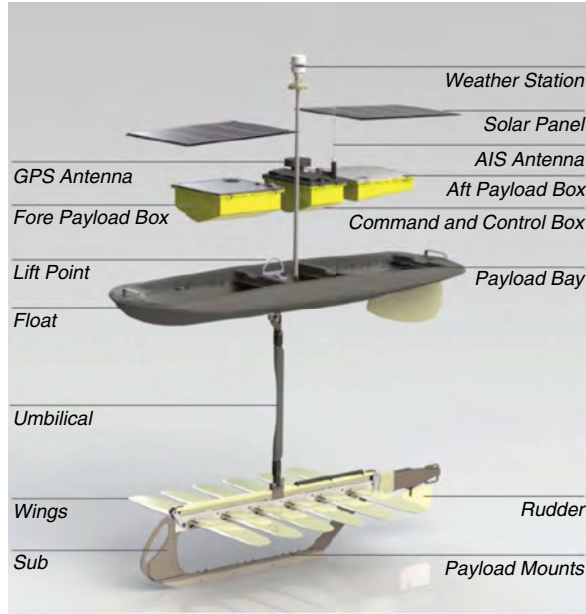

Fig. 66. The base configuration of an SV2 showing the 210 cm × 60 cm Float and 40 cm × 191 cm Sub with 107 cm wide wings. The SV2 has a mass of 90 kg and displaces 150 kg.

The wave-induced thrust mechanism used by an SV2 is purely mechanical and provides effectively limitless propulsion. The batteries provide power for command and control electronics, a rudder module, plus payload sensors in the Float and Sub, or towed behind either (the proposed system is towed behind the Float). The core electronics include a GPS for precision navigation (±3 m), long- (satellite) and short-range (e.g., cellular) communications, a weather station, and an Automatic Identification System (AIS) receiver, which is used for collision avoidance. Both medium- and large-sized vessels that could unequivocally damage the SV2 are required to have AIS.

If payload sensors are mounted on or towed behind the Sub, power and telemetry is provided via the Umbilical; otherwise power and telemetry is via the Float. The latter provides the most expansive option in terms of power transmission and data telemetry, because a separate sea cable satisfying mission requirements can be used (as is done herein). An SV2 is two-person portable, air freight compatible, and can be deployed using a small boat or dock (water depth permitting), so it can be deployed rapidly in remote locations.

Wave motion is greatest at the sea surface, and decreases rapidly as depth increases. The two-part (Float–Sub) architecture of an SV2 exploits this difference to provide forward thrust (Fig. 67). A rising wave lifts the Float, causing the Sub to rise. The articulated wings on the Sub press down and the upward motion of the Sub becomes an up-and-forward motion, in turn pulling the Float forward and off the wave. This causes the Sub to drop, the wings pivot up, and the Sub moves down and forward. This process is continuously repeated as long as there is wave motion on the surface, even if the amplitude is rather small.
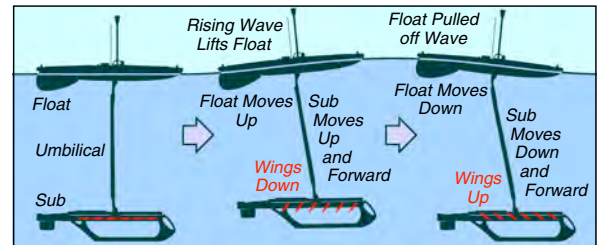

Fig. 67. The SV2 propulsion mechanism *harvests* wave energy with the Sub wings to create forward thrust, thereby allowing the SV2 to move forward and *swim* from one location to another.

7.2 Background

The integrated SV2 and C-OPS with C-PrOPS hybrid can collect AOPs in previously under-sampled locations and at reduced cost compared to conventional means. The C-OPS is already a low-drag device, but if need be, it can be surrounded by a fairing. Hereafter, for the SV2 application, the C-OPS with C-PrOPS is referred to as the TOW-FISH. The TOW-FISH ascends to the surface (from a nominal depth of 5–6 m) on autonomous command using the C-PrOPS thrusters, all the while measuring $E_d(z, \lambda)$ and $L_u(z, \lambda)$, in addition to vertical orientation. The SV2 hosts the $E_s(\lambda)$ solar reference. The free-fall descent from the surface yields centimeter-scale (or less) vertical resolution over the upper 5–6 m, which provides characterization of the first optical depth spanning 320–875 nm. Because of the high vertical sampling resolution, the determination of the spectral data products are accomplished with equal efficacy, e.g., $K_d(\lambda)$, and $L_W(\lambda)$ including normalized and exact forms.

Given typical solar illumination instabilities as a result of cloud coverage, as well as a nominal speed of 1 kt for the USV, the HySEAS3D sampling objective is one optical profile every 30 min during daylight hours for an anticipated deployment time period of 10 d. The 30 min value is a nominal one for power budget planning purposes and is based primarily on the 1 kt speed—more frequent profiling is possible if warranted, but depends on solar insolation (Fig. 68). Without bio-fouling mitigation, the optical sensors require cleaning and refurbishment after this length of deployment to maintain the uncertainty budget (discussed below).
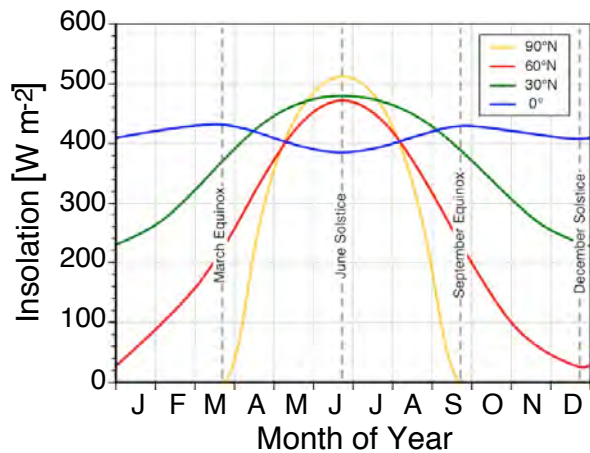
Fig. 68. Solar insolation as a function of the month of the year and latitude in the northern hemisphere (Pidwirny 2006).

A further objective is to conduct nighttime measurements around the period of the full Moon, where applicable, to monitor individual channel performance within the instruments. The nighttime data can also be used for dark measurements under cloud cover. The solar reference shadow band accessory can confirm if there is sufficient lack of light for dark measurements.

7.3 Design

The primary sensor for this project is a TOW-FISH pulled sufficiently far behind (30–35 m) an SV2 (Fig. 66) such that shading from the latter is negligible and an accordion-like isolation section in the sea cable removes tow-induced irregular motions (Fig. 69). The TOW-FISH makes a vertical ascent every 30 min from a 5–6 m depth, and then free-falls back to the stowed depth. The sensor system includes three microradiometer instruments, as well as ancillary sensors for environmental measurements (conductivity, temperature, depth, and attitude) which communicate with a master aggregator coupled with a data-logging sensor management computer (SMC).
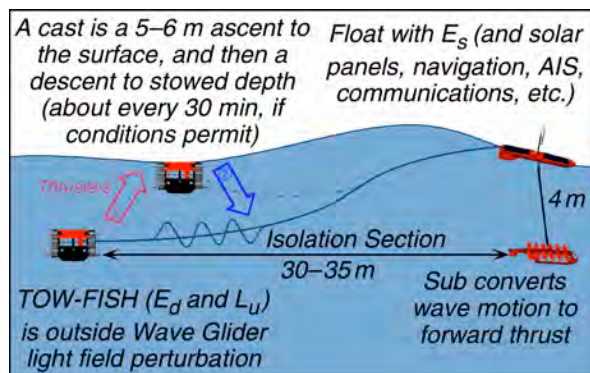
Fig. 69. A diagram of the proposed USV sampling system showing the TOW-FISH tethered 30–35 m behind the approximately 2 m long Float and Sub, with a spectrally matching solar reference (denoted E_s) mounted on the Float.

The four-point *front-on* harness for a standard C-OPS (Fig. 10) is changed to a two-point *side-on* configuration which minimizes drag. This harness arrangement has been tested and implemented as part of the C-PrOPS development (Fig. 17). The profiler can be faired to support passively stable operation in the two-point harness configuration, but this is not anticipated to be necessary. The C-PrOPS digital thrusters provide a low-risk solution for vertical positioning. Control of the vertical position will be achieved with a low-level controller hosted on the master aggregator, which would already have access to data from the ancillary depth sensor, or aboard the SMC.

The USV hosts the SMC with master aggregator and provides all system power from two onboard batteries—a 660 W h battery dedicated to the core command and control functions plus a 1,100 W h expanded battery dedicated to the optical payload. The efficiency of charging the batteries using solar panels is time and latitude dependent (Fig. 68), which influences mission endurance, i.e., the number of fully functional at-sea days. The area of the solar panels and size of the expanded battery factor into endurance as a function of latitude and time. For a 10 d endurance and hourly profiles, the solar panels are expected to provide adequate sustaining power, depending on geographic location and time of year. In the arctic, this corresponds to the time period between the equinoxes (approximately April to early September).

In terms of interface specifications, the power (about 3.2 W) and Recommended Standard (RS) telemetry (RS-232, RS-422, and RS-485) requirements for the optical instrumentation are compatible with the present command and control plus Umbilical architecture, although limiting total thruster power to less than 6 A for depth control provides compatibility with prior Wave Glider designs. The data relay communications default protocol is Iridium short burst data messaging, which will be used to send short performance summaries of completed AOP sampling events, if cellular telephony is unavailable.

The TOW-FISH is pulled behind the Float via a tether (Fig. 69), which includes an isolation segment connected to a neutrally buoyant leader. The isolation segment absorbs the back-and-forth motion induced by the USV onto the TOW-FISH. Catenary drag, which arises on the leader during vertical profiles due to forward motion of the USV, is part of the conceptual design of the profiler depth control and static stability systems. Mitigation of cable drag allows for profiling operations at higher speeds and with reduced thruster power consumption. Such cable drag mitigation is possible by optimizing the cable design to reduce overall diameter, or alternatively by incorporating drag-reduction features, such as fairings on the tether.

The expected instrument power consumption of approximately 30 W is within the range of low power sensors typically employed aboard a USV. At a duty cycle of less than 10% for the optical sensors plus SMC with master aggregator, and in conjunction with a nominal USV
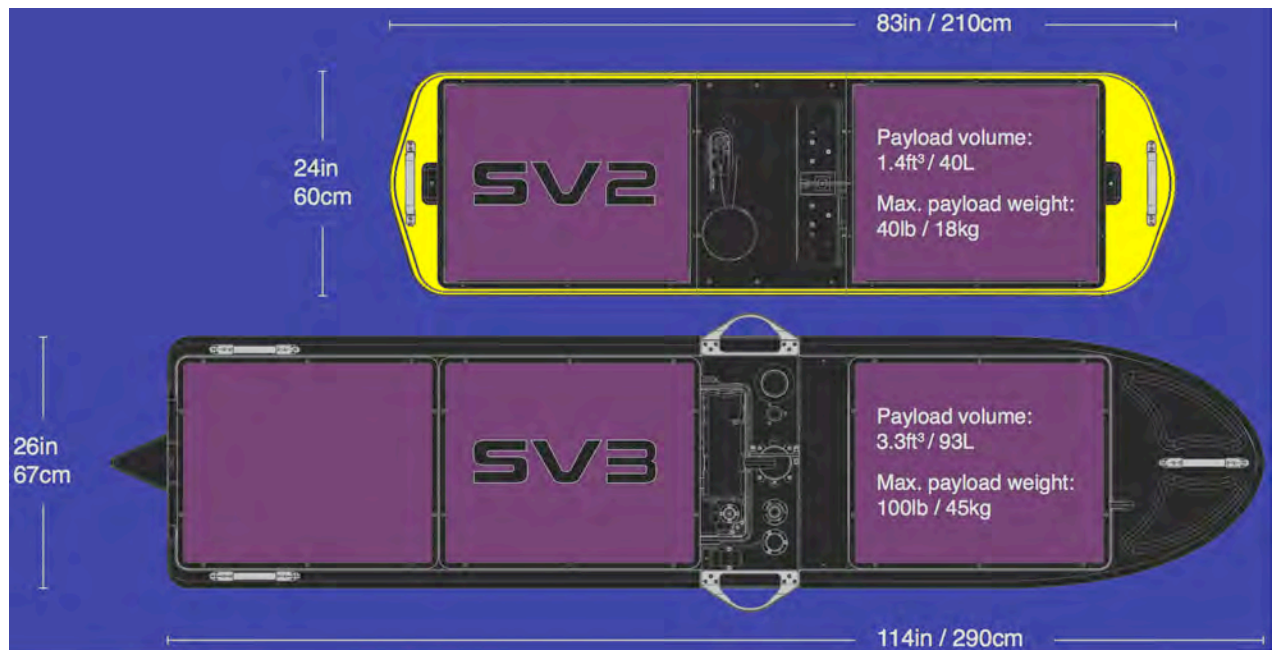
Fig. 70. A scaled line drawing comparison of the SV2 (yellow) and SV3 (black) Wave Gliders, with the former having two solar panels (purple) and the latter three. The principal physical difference in the two models is the greater length of the SV3, and thus enhanced solar panel capability.

core services load of 2.5 W, the net power consumption of the HySEAS3D sensor system is less than 15 W continuous. Assuming a peak power draw of 130 W from the TOW-FISH when the depth of the profiler is controlled using the thrusters, the resultant power use is less than 16 W continuous for the entire system at a sensor duty cycle consistent with hourly observations. Even at the latitude of Barrow (about 70°N) 3.5 W of continuous draw is nominally sustainable through the peak summer months.

Augmenting the onboard batteries with an auxiliary battery (previously demonstrated) substantially extends the operations of the SV2 at high latitudes. This enables the system to persist before or after the time periods when science cruises to the region typically operate. The notional endurance that could be achieved with an expanded battery accessory fitted into the aft payload box, similar to that already used on an arctic Wave Glider prototype, is approximately 11 d in the October–February time period. Further enhancements to the onboard battery storage capacity are anticipated independent of the HySEAS3D concept, and these expand the operational capabilities even further (e.g., in high latitudes).

7.4 Results

The Wave Glider SV model series represents the next generation of Wave Glider technology and includes the Wave Glider SV2 with a compatible growth path to the high-end Wave Glider SV3. The HySEAS3D concept was developed when the SV2 was a COTS item and the SV3 was anticipated, but not yet available.

With over 200 Wave Gliders performing more than four years of customer missions spanning the Arctic to Australia, the original Wave Glider has proven itself both reliable and durable. Since 2009, Wave Gliders have traveled over 480,000 km globally, and set the world distance record for autonomous ocean vehicles. The original Wave Gliders have completed over 100 missions, and navigated through five hurricanes and three cyclones, all the while continuously transmitting data.

SV Series Wave Gliders—individually or operating in fleets—can travel thousands of miles, carry adaptable payloads, power themselves, and gather, process, and deliver data in real time globally. The Wave Glider SV3 and the enhancements to the Wave Glider SV2 will enable around-the-clock, all-weather operations. A physical comparison of the SV2 and SV3 appears in Fig. 70.

The reliability and durability of the Wave Glider was an important aspect of its selection for HySEAS3D. In addition, the robust capabilities of the Float allowed for the potential mounting of the solar reference plus support instruments, e.g., a shadow band and GPS.

7.5 Conclusions

Although, the SV2 is capable of towing (Table 7), towing from the Float is not recommended, and towing the TOW-FISH from the Sub is problematic, because the Umbilical connecting the Sub to the Float cannot support the wattage needed for the TOW-FISH thrusters. Furthermore, the Umbilical is connected to the SV2 power system, which provides power more similar to a power supply than a battery, wherein the instantaneous thruster

loads are sometimes problematic. Consequently, the autonomous HySEAS3D profiling concept required a more advanced Wave Glider than an SV2, e.g., an SV3.

Table 7. A comparison of the SV2 and SV3 series of Wave Gliders with the capabilities critical to HySEAS3D shown in red.

Parameter	SV2	SV3
Environmental Conditions		
Moderate (Sea State 1–4)	•	•
Temporary Severe (Sea State 5–8)	•	•
Fringe (Glassy, Currents, No Sun)		•
Payload Features		
Maximum Weight [kg]	18	45
Multiple Sensors	6	12+
At-Sea Upgrades	•	•
Plug and Play Payloads		•
On-Board Computers		
High-Speed Network (WiFi, Cell)	†	•
High-Performance Navigation		•
High-Performance Payload		•
Operations		
Years at Sea (No Fuel or Crew)§	•	•
Optimized for Towing	‡	•
Optimized for Coordinated Fleets		•
Designed for High Deck Recovery		•

† An SV2 option. ‡ The SV2 is capable of towing.
§ Requires regularly scheduled maintenance.

When the HySEAS3D concept was in preliminary design and development, the SV3 was still in the design stage and was not a COTS item. The COTS capabilities of the SV3 are now known, and it is optimized for towing (Table 7). The SV3 can also support towing from the float, however, the onboard power system functions more like a power supply than a true battery, i.e., like the SV2. This means the TOW-FISH conceived for HySEAS3D would have to be operated from a second set of batteries, which means the extra payload capacity of the SV3 is a requirement.

Future opportunities to deploy an optical instrument suite from an SV3 anticipate the missions would be conducted in exclusively fair-weather conditions, wherein calm sea states are more likely. The increased likelihood of becalming the SV3 means the propulsion capabilities enabled by the SV3 thrudder provides additional confidence in successful mission outcomes, albeit at the expense of higher power consumption. Additional payload battery capacity, however, could ensure the SV3 power system had sufficient reserves to accommodate limited use of the thrudder. The expectation is that the instrumentation comprising the TOW-FISH would become more sophisticated over time, and the onboard high-speed network with WiFi and cellular connections would be required to ensure all of the instruments were functioning properly before a sampling mission was begun. The exploitation of all these SV3 features is presented in Chap. 8 as part of documenting the HARPOONS activity.

Chapter 8

The HARPOONS Vicarious Calibration Project

Stanford B. Hooker and Carlos del Castillo
NASA Goddard Space Flight Center
Greenbelt, Maryland

Randall N. Lind, John H. Morrow, and Charles R. Booth
Biospherical Instruments, Inc.
San Diego, California

James W. Brown
RSMAS University of Miami
Miami, Florida

Raphael M. Kudela and Henry F. Houskeeper
University of California Santa Cruz
Santa Cruz, California

Koji Suzuki
Hokkaido University
Sapporo, Japan

Roy A. Armstrong
University of Puerto Rico
Mayaguez, Puerto Rico

Abstract

The HARPOONS paradigm for autonomous CVR activities involves five principal C-PHIRE instrument suites, as follows: a) an in-water thruster-assisted profiler towed behind an SV3 that is launched and recovered with a small boat; b) above-water instruments mounted on the SV3 to provide solar reference measurements with a shadow band accessory plus PAR, GPS, and communications antennas that are lower than the reference and PAR diffusers; c) a nearby (coastal) sun photometer mounted on a tracker with a quad detector and solar reference similar to what is on the SV3 (the wavelength domain is more expansive); d) a laboratory transfer radiometer; and e) a field stability monitor. Control of the instruments and execution modes is through DACPRO modules hosted on a MacMini computer with a back-up battery. Data acquisition uses a scheduler set up before a 10 d clear-sky mission and executes automatically. The principal communications for executing commands and receiving status messages is through an Iridium link. The SV3 can be visited by small boat and a MacBook laptop using WiFi provides detailed monitoring of system performance, uploading scheduler changes, etc. The above-water instrumentation operates on SV3 power, which includes two large battery units recharged with three solar panels. The in-water instrumentation is powered by a separate set of payload batteries.

8.1 Introduction

The HARPOONS project applies the HySEAS3D autonomous profiling concept (Chap. 7) to the challenge of obtaining high quality optical data for the vicarious calibration of ocean color satellites, in this case the next-generation Plankton, Aerosol, Cloud, ocean Ecosystem (PACE) mission. The overall objective is to develop and mature a compact, flexible autonomous optical system that meets or exceeds the *in situ* performance requirements established by the research solicitation that funded the HARPOONS project. The solicitation was based on the recommendations the PACE Science Definition Team (SDT) made for vicarious calibration activities.

The autonomous approach documented herein uses a USV to tow a state-of-the-art optical package capable of making autonomous profiles in the near-surface portion of

the water column in suitably clear and spatially homogenous oceanic waters. The profiling capability is made possible by small digital thrusters mounted on the profiler backplane (Sect. 2.3.1). At a certain level, HARPOONS has been under development for the last 10 yr through NASA investments in Small Business Innovative Research (SBIR) proposals, Science Innovation Fund (SIF) awards, mission office research activities, Internal Research and Development (IR&D) projects, and NASA Research Announcements (NRAs). Because of this legacy, there are multiple secondary objectives of the HARPOONS project which enhance the reliability of many subsystems, e.g., the sea cable has terminated internal and external strength members to mitigate risk.

HARPOONS is based on the perspective that an instrument capable of high quality observations should be available as a COTS product, and that the engineering applied to develop the instrument should allow the deployment of the instrument in as many CVR activities as possible. Consequently, the technology documented here is anticipated to be applied to not only the vicarious calibration problem set, but also to algorithm validation and baseline research, i.e., all CVR activities. Indeed, the new technology that was developed was applied to all three as part of field commissioning activities (Sect. 8.3.8).

Because the PACE mission is anticipated to require coupled ocean-atmosphere science teams, e.g., to improve the atmospheric correction of the satellite data, the field instrumentation for HARPOONS includes a C-OSPREy sun photometer with sky photometer capabilities to support the derivation of atmospheric data products. The C-OSPREy instrument has sufficient dynamic range that it can also be used to view the Moon, as well as the sea surface, and thereby provide an unprecedented number of data products for ocean-atmosphere investigations.

The HARPOONS CVR paradigm ultimately anticipates replacing the in-water approach with a more nimble and extensive mapping capability of an unmanned airborne vehicle (UAV). The airborne trajectory is inevitable, because the spectral domain of interest for remote sensing—which will continue to expand over time—includes wavelengths that are difficult to obtain with an in-water instrument because the attenuation at many wavelengths can be so large the vertical scale for deriving data products is very small. For example, the near-infrared (NIR) wavelengths in clear waters for calibration, or the ultraviolet (UV) wavelengths in turbid water for validation and research, must be measured in the top 1 m of the water column or less. In comparison, data products at these wavelengths can be obtained directly using an above-water (i.e., airborne) method.

The expansion of observational capabilities to an airborne platform would allow inland water masses or more heterogeneous phenomena, like red tides, to be sampled with the same efficacy and technology developed for the world ocean. The first step of the trajectory from USV to UAV would be aboard the Center for Interdisciplinary Remotely-Piloted Aircraft Studies (CIRPAS) Twin Otter, which has been used to deploy autonomous radiometric systems built with SiP microradiometers (Chap. 1); the optical instruments described herein include a 15–18 microradiometer cluster, depending on the radiometer.

A pictorial representation of the HARPOONS CVR perspective is shown in Fig. 71, wherein autonomous sampling is provided by an SV3 towing an in-water optical package with contemporaneous above-water instruments providing incident solar reference and shore-based atmospheric correction data. An in-water profile of optically significant constituents is achieved by using small digital thrusters to ascend the in-water package to the surface, whereupon it slowly returns to the resting depth. An isolation unit on the sea cable dampens the cyclical tugging imparted by the SV3. A nearby shore facility (not shown) provides SV3 deployment, recovery, emergency response, plus radiometric calibration and stability monitoring.
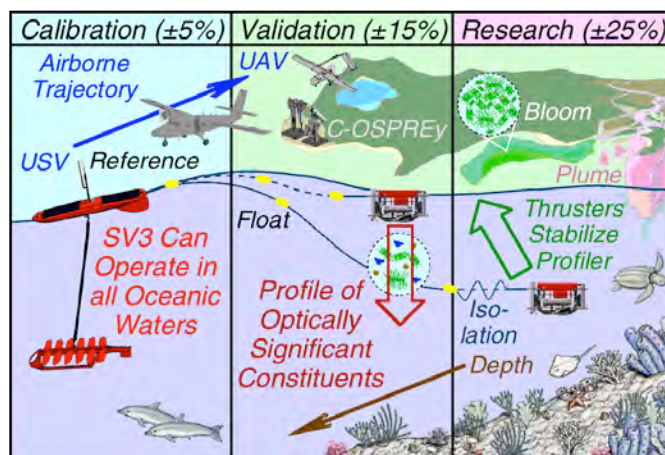
Fig. 71. The HARPOONS CVR paradigm wherein autonomous data are collected in all oceanic waters from shallow to deep, heterogenous to homogenous, and optically complex (case-2) to optically simple (case-1). Supporting atmospheric observations are acquired at a nearby shore station using C-OSPREy and aerial observations provide optional spatial mapping.

Data collection in Fig. 71 is expected to occur during fair-weather time periods forecast to last approximately 10 d. Shorter or longer deployments are feasible, but this duration is selected for sampling and power consumption purposes. If the weather forecast is favorable for both sun and sea conditions, the SV3 is launched; otherwise, deployment is delayed until conditions improve. Validation stations comprised of independent measurements of inherent optical properties (IOPs) and AOPs, plus water collection for laboratory analyses (e.g., pigments, absorption, etc.) is conducted in close proximity to the SV3.

While at sea, and depending on local heterogeneity, additional validation stations are conducted. For example, if the SV3 is launched into a phytoplankton bloom, one or more daily validation stations are anticipated; but if the

SV3 is launched into clear open-ocean waters, validation stations once every few days are appropriate. If conditions deteriorate before the 10 d period expires, the SV3 is commanded to turn towards shore for recovery. When the SV3 is recovered, a final validation station is conducted.

Before and after SV3 missions, the sampling systems are inspected with appropriate cleaning and maintenance performed as required. The instruments are checked for nominal performance and recency of calibration, wherein repairs or recalibration are performed as required. In addition, the optical instruments are monitored with a portable source to ensure a time series of observations are available for data quality assessment. These data are used in conjunction with the validation data to detect anomalies in performance. The DACPRO and PROSIT acquisition and processing software, respectively, along with the state-of-the-art instrumentation described herein ensures the CVR uncertainty objectives (to within $\pm 5\%$, $\pm 15\%$, $\pm 25\%$, respectively), which are compatible with the PACE SDT recommendations, are achievable.

The spectral requirements for the PACE mission span 350–900 nm and require hyperspectral resolution (less than 3 nm). Spectrographs present challenges in terms of stability and compactness, so the approach presented here is based on the hybridspectral C-PHIRE and C-OSPREy designs, wherein 15–18 highly accurate SiP microradiometers (depending on the instrument) obtain data simultaneously with a 2,048 pixel spectrograph. The two detector systems have NIST traceable calibrations and are intracompared during data processing to detect drift or anomalies in nominal performance.

The expectation is that the faster sampling (15 Hz) of the highly accurate microradiometers will help maintain the calibration of the slower sampling and inherently noisier spectrograph (approximately 2 Hz depending on flux levels, i.e., depth). Intercomparisons with a C-OPS instrument equipped with the C-PrOPS accessory, plus a time series of measurements from a CQM portable source, provide additional evaluations of instrument stability in the field.

To facilitate the replication of the instrumentation presented, another adopted perspective is that as many of the components as possible are COTS items; this lowers the cost of subsystems, and further reduces costs by minimizing non-recurring engineering (NRE) expenses. Consequently, all of the instruments and systems described herein are built primarily with COTS components and the completed instruments, ancillary devices, and accessories needed to deploy the instrument systems are anticipated to be available as COTS procurements.

8.2 Background

As noted in Chap. 7, the SV2 was not considered adequate for towing a smaller instrument package than what is anticipated for HARPOONS (the hybridspectral instruments will require a larger backplane). Consequently, the HARPOONS autonomous sampling platform is the SV3, which is now a COTS procurement.

The three principal subsystems of an SV3 are shown in Fig. 72, wherein the mounting locations for above-water instruments are the cover and mast plates. The Float rides on the surface of the water and contains the batteries, command and control unit (CCU) electronics, and optional payloads. The CCU radome provides the Iridium communications, the GPS antenna, and the bulkhead connections for the cellular and AIS antennas. The Resilient tracker provides the GPS location of the SV3 at a coarser (user selected) temporal resolution and continues to function if the Float is flipped upside down. Three solar panels on the Float deck maintain the battery charge.
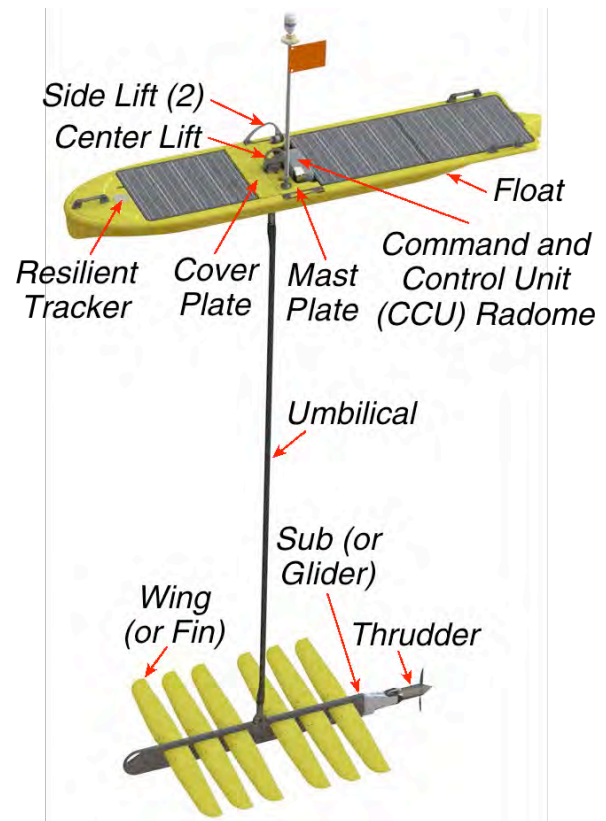
Fig. 72. The three principal subsystems of a Wave Glider are shown as follows: the Float, Umbilical, and Sub.

The Float deck typically has additional instrumentation and communications devices installed on the mast plate. For HARPOONS, a solar reference system with multiple devices was added to a custom (reinforced) cover plate. Normally, the cover plate is not used, because its original purpose is to cover the top of an optional auxiliary power unit (APU), which is housed directly below. Also for HARPOONS, a harness for towing the TOW-FISH profiling optical sensor suite was added to the aft handle assemblies. A buoy with a retrieval line can be released from the back of the float to simplify recovery (discussed

below). Dimensions for the SV3 Float are provided in Fig. 70.

The Umbilical (4 m long for HARPOONS) is a streamlined connector containing high-strength reinforcement cables designed to support the weight of the Sub and the tension the Sub exerts on the Float as it responds to wave motion. The Umbilical also contains electrical wiring for power, thrudder control, auxiliary propulsion, and payload communications.

The Sub (or Glider) is submerged (about 4 m) below the Float during operation. It provides the propulsion for the Wave Glider system by converting wave motion into forward thrust. The attached thrudder steers the Wave Glider system and provides supplemental thrust on demand with a motorized propeller. The Sub is 56.22 in (142.80 cm) wide, 86.55 in (219.84 cm) long, and 8.16 in (20.72 cm) high, ignoring the skeg and thrudder propellers (compare to Fig. 70). The Sub can be used as a platform to mount underwater sensors or to attach an instrument package that is towed. Power and communications wiring connections on the thrudder module can accommodate these sub-surface payloads. This approach is not used in the HARPOONS project, because the Umbilical cable conductors cannot support the power requirements for the digital thrusters on the TOW-FISH.

A motion isolator provides a shock absorber between the Umbilical and Sub. The motion isolator assembly is located directly under the center lift (or *pick*) point on the mast plate of the Float. The motion isolator shaft on the Umbilical assembly inserts into the motion isolator assembly and is locked in place with a shoulder bolt that passes through the motion isolator shaft. A spring in the motion isolator assembly absorbs shock in rough water and high seas. The Umbilical cable passes through a protective shroud and continues on to the CCU.

The lift points for launching and recovering the SV3 are on, or in line with, the mast plate in Fig. 72. Recovery is also facilitated by commanding the SV3 to release a buoy with 30 ft of floating, non-fouling line. The line is stored below the aft solar panel. Two spring loaded latches retain the buoy by clasping a latch plate that extends from the buoy.

The Recovery Buoy cannot be used to lift the Wave Glider system; even without a payload, the Recovery Buoy, and the hardware where the line attaches to the Recovery Buoy, will not support the weight of the Wave Glider system (Float plus Umbilical and Sub).

When the release command is issued, a linear actuator forces a piston to open the latches and continue extending to push on the latch plate until the buoy is released from the Float. The release command and other aspects of communicating with the SV3 (e.g., to receive alerts, check the status of batteries and solar panel charging, etc.) are accomplished using the WGMS architecture. The piloting and navigation of the SV3 is also established, monitored, and revised using WGMS (e.g., way points can be

set, thrust from the thrudder can be activated and deactivated, etc.). The recovery buoy and other components of a typical SV3 configuration are presented in Fig. 73, wherein the low freeboard of a Wave Glider requires the use of *dry* (waterproof) boxes for all sensitive payload items (e.g., electronics and batteries) located within the SV3. The likelihood of rough surface conditions during any deployment also requires waterproofing for all above-water payloads.
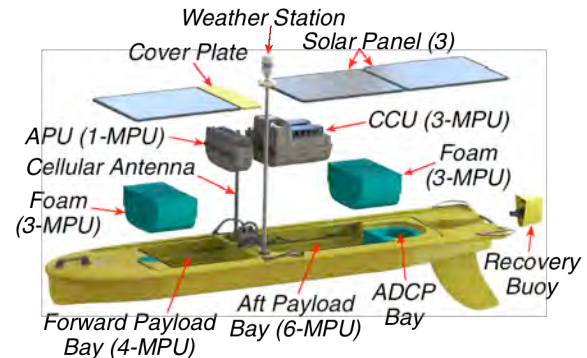
Fig. 73. The components of a typical SV3 configuration, wherein an optional APU with the battery capacity of the CCU, which was used for the HARPOONS activity, is added. The weather station includes a marker light that can be turned on and off remotely.

The available above- and in-water SV3 payload space in Fig. 73, respectively, is principally restricted to the cover and mast plates plus the modular payload units (MPUs) in the forward and aft payload bays and a cylindrical area for an optional acoustic doppler current profiler (ADCP). The deck of the Float is almost completely covered with three solar panels constructed with fiberglass and foam laminate with hard points and a top sheet made of glass. Each panel is identical and is rated for 52 W, for a maximum power generation of 156 W. The design of the solar panels provides connections for bypass diodes that allow the use of half of a panel to provide power when a single cell is shaded.

If one or more cells in each half of a solar panel are shaded, the panel provides zero output.

The dividing line between the two halves of each panel is located half way between the forward and aft panel ends.

Shading in general comes from environmental conditions such as cloud cover, and from system components mounted on the vehicle. Shading from environmental conditions is typically temporary and beyond mitigation. To optimize total power input, all sensors would have to be mounted below the solar panels to prevent shading. Because this is not practical for HARPOONS, wherein a solar reference must be mounted on the mast plate and antennas are required for communications, the masts are kept as short as possible, while not exceeding the height of the solar reference and PAR diffusers, which also cannot

be shaded. The shortening of the masts required minor modifications to the standard configuration of the SV3 (Sect. 8.3.5).

To maximize solar charging, a course perpendicular to the principal solar plane is preferred (i.e., the Sun is on the beam). During early morning and late evening, a north-south course minimizes solar shadowing. In late morning and late afternoon, a northeast-southwest and southeast-northwest course can be advantageous. During the mid-afternoon, an east-west course maximizes solar charging.

The CCU is a special version of a three-bay MPU (3-MPU), and the APU is a version of a one-bay MPU (1-MPU). The configuration shown in Fig. 73, allows two 3-MPU dry boxes to be added to the SV3 plus the ADCP bay can be used for a cylindrical housing, which is what was done for the HARPOONS project. The aft 3-MPU contained a payload development kit, and once the HARPOONS instrumentation matured to the point of operational demonstration for the fourth deployment of the SV3, the development kit was permanently removed.

8.3 Design

The design objective presented herein is to create autonomous sampling systems based on as many COTS components as possible, and to make as few changes to the COTS instrumentation, including the SV3, as practicable. If changes are needed, COTS solutions are used so a future user can implement the change (assuming availability or a compatible replacement). Consequently, only a minimal attempt is made to integrate the scientific equipment into the SV3 payload support capability. All the added electronics to support the above- and in-water instrumentation are contained within two 3-MPU dry boxes plus a cylindrical housing that fits within the ADCP bay (Fig. 74).
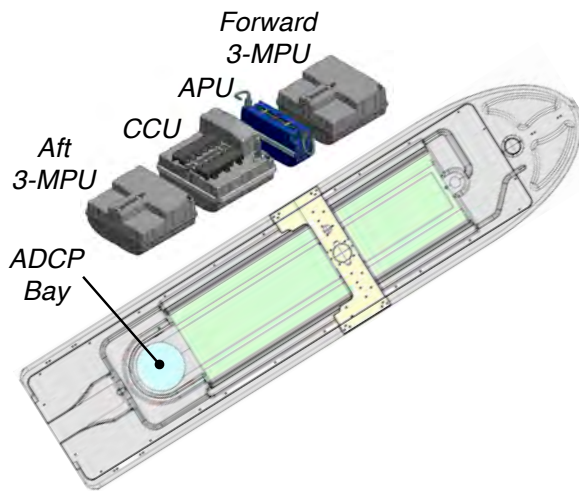
Fig. 74. The four dry boxes in the HARPOONS SV3, which fit into the green shaded area. An additional battery cylinder fits into the ADCP bay shown in blue. The mast plate is shown in yellow.

The SV3 CCU plus the mast and cover plates (Figs. 73 and 74) are the mounting locations for the above-water instruments, masts, and antennas, as follows:

- The CCU has a built-in mount for the AIS antenna;
- The mast plate has weather station (with light) and cellular antenna mounting locations; and
- The purpose-built cover plate has a mount for the solar reference system and fixtures for the cabling associated with the above-water instruments.

The solar reference system (Fig. 75) is comprised of a global solar irradiance C-PHIRE radiometer, the Biospherical Shadow band Accessory for Diffuse Irradiance (BioSHADE) and Biospherical Global Positioning System (BioGPS) accessories, a PAR sensor, and two WiFi antennas. The BioSHADE consists of a controller and a fixture to hold the shadow band. Because the reference system is the largest and heaviest above-water instrument, the cover plate it is mounted to is reinforced and attaches to the mast plate with wishbone gussets. The cover plate is positioned over the APU (Fig. 73) and does not need to be removed to access the forward and aft 3-MPU payload dry boxes (Fig. 74).
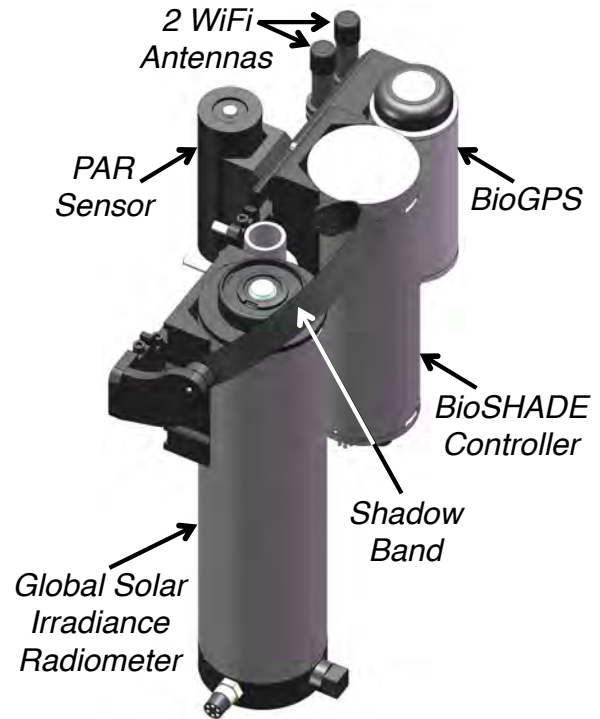
Fig. 75. The SV3 solar reference system, which is mounted to the custom (reinforced) cover plate.

Aspects of the design perspective adopted for the HARPOONS project depend on the command, telemetry, and communications management for the SV3, which is managed by a computer contained within the CCU. The CCU handles communications between the Wave Glider and remote applications. The CCU automatically sends telemetry data over specified communications channels at regular, user-configurable, intervals. Telemetry data includes

the position and general status of the vehicle, as well as any alarms. There are different telemetry data types, and each type can be sent out on a different schedule.

The standard CCU communications channels are Iridium relay link, cellular communications, and WiFi. Specific deployments use a subset of the communications links presented in Fig. 76, as follows:

- Iridium relay communications depend on an internet connection between the Iridium relay and an Iridium network server. The connection between the Iridium network server and the CCU is over the Iridium satellite network.

- Cellular communications depend on an internet connection between the virtual relay and a cellular network server. The connection between the cellular network server and the CCU is over a cellular network.

- WiFi communications do not require an internet connection; data is transmitted directly between the CCU (plus any other connected device in the SV3) and a WiFi enabled device.

A 12-pin general purpose expansion port connector is used to link the payload 3-MPU dry boxes through the CCU and APU in a daisy-chain fashion. This connector provides power, switched $10/100\,\mathrm{Mbit\,s^{-1}}$ Ethernet and communications channels to payloads and other Adaptable Modular Power System (AMPS) domains. The latter enables extremely efficient power management for a wide range of possible Wave Glider configurations.
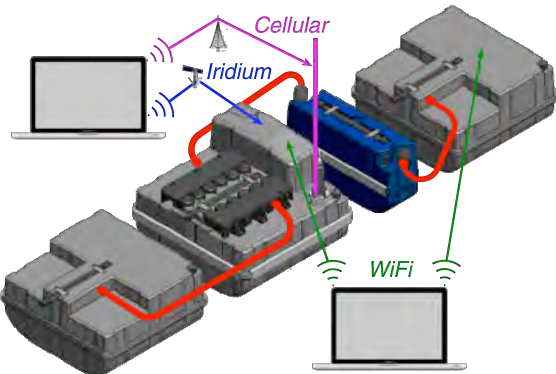
Fig. 76. The standard network communications for an SV3, wherein the red cabling shows how the payload 3-MPU dry boxes are expected to be connected in daisy-chain fashion through the CCU plus (optional) APU. A WiFi link is shown to the forward 3-MPU dry box, because that is where the MacMini payload computer, which has a separate WiFi router and antennas, is located.

The Iridium satellite network is an *always-on* system with global coverage. It is the primary communications link for the Wave Glider, because it does not have distance limitations. The Wave Glider is typically linked to remote applications through an internet connection to the Iridium satellite system.

The Iridium satellite network is the standard means of controlling and monitoring the SV3, which means that *a loss of connection to the Iridium system is a critical failure requiring a rapid response.*

The Iridium modem inside the Wave Glider sends and receives data over the Iridium satellite network using Iridium Short Burst Data (SBD) packet sessions. The Iridium satellite network exchanges data with Iridium network servers in the Iridium data center. Iridium network servers use Transmission Control Protocol/Internet Protocol (TCP/IP) to exchange data with remote applications using the Iridium relay.

The Iridium SBD protocol allows for *economical* transmission of relatively small data packets. Iridium refers to messages from the modem as mobile-originated (MO) and messages to the modem as mobile-terminated (MT). The SBD format supports packets of limited size, depending on the modem used and the direction of the packet. Iridium 9601/2/3 modems can send messages (MO) of up to 340 bytes and receive messages (MT) of up to 270 bytes, whereas Iridium 9522B and 9523 modems can send messages (MO) of up to 1960 bytes and receive message (MT) of up to 1,890 bytes.

A cellular connection to a Wave Glider allows much greater bandwidth than an Iridium connection, but it requires a shore installation, which necessarily has a limited range for a connection, i.e., typically less than 22–45 mi (35–72 km). The greater bandwidth supports more responsive interactions with WGMS and the MacMini payload computer. Under most cellular connections, the operation of the above- and in-water instruments under the autonomous control of the MacMini can be viewed in real time, and the configuration of the autonomous environment can be controlled directly.

A WiFi connection to a Wave Glider provides a second high bandwidth communication link. It has the shortest range, but does not require a shore installation connection. This means the vessel used to deploy the SV3 can communicate directly with the SV3 and the payload computer using a WiFi connection. For the payload design considered here, WiFi allows complete confirmation of SV3, surface reference system, and TOW-FISH functionality before the deployment vessel leaves the deployment site, which is a significant advantage, particularly if the deployment site is beyond cellular range.

The inherently short distance of WiFi communications is even shorter on a Wave Glider, because the CCU, APU, and payload 3-MPU dry boxes are underwater. To prevent the extra attenuation of signal strength and, thus distance, two above-water WiFi antennas were installed on the reference system opposite the BioGPS prior to the fourth deployment of the SV3 to demonstrate operational readiness.

The complexity of integrating a payload design on a Wave Glider increases as a function of how many inherent

SV3 capabilities are relied upon, i.e., the simplest integration uses a minimum number of SV3 capabilities. A partial description of the potential complexity can be constructed by considering the capabilities provided by the CCU, which contains the following:
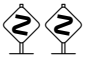
- Vehicle Management Computer (VMC);
- CCU AMPS power domain;
- Iridium 9603 SBD modem;
- Primary GPS module (UBLOX NEO-6Q) and secondary GPS module, which is integral to the CPU module;
- Radome with Iridium antenna, primary and backup GPS antennas, plus 2.4 and 5.0 GHz WiFi antennas;
- Global System for Mobile (GSM) communication cellular modem;
- Water speed sensor interface electronics;
- Expansion switch matrix;
- 8-port managed Ethernet switch;
- AIS receiver;
- Ten 89 W h lithium-ion batteries;
- 9-axis accelerometer; and
- Compass.

The CCU manages power for sensors and other payload components (if so designed), and it provides communications paths for data retrieval, as well as Wave Glider command and control (e.g., navigation).

⬦⬦⬦ *The CCU, as well as the APU, contain no customer-serviceable components*, and should not be opened.

A more complete description of the potential complexity of SV3 integration can be created by considering the three types of CCU connectors (Fig. 77) available to SV3 system integrators, as follows: a) general purpose expansion (G1, G2, and G3) ports; b) sensor (S1, S2, S3, and S4) ports; and the high voltage (HV) port. The Umbilical (U1) connector and the debug (D1) port are dedicated expansion ports. The other CCU connections depicted in Fig. 77 are as follows:

PK The power key access cover, which is used to turn the SV3 on and off.

PP The pressurization port cover, which is used to access the pressurization valve to purge the volume of air in the CCU case and positively pressurize it with a non-condensing gas (e.g., N_2 gas at approximately 2 psi) after the case is sealed.

⬦⬦ *The dry boxes do not have a vacuum rating and can crack if subjected to a vacuum*, e.g., while trying to fill them with a non-condensing gas.

AA The AIS antenna base, which was replaced by an LRI engineer to accommodate a shorter AIS antenna for the design presented here.

CA The cellular antenna connector mount.

O1 The O1 system port.

O2 The O2 system port.
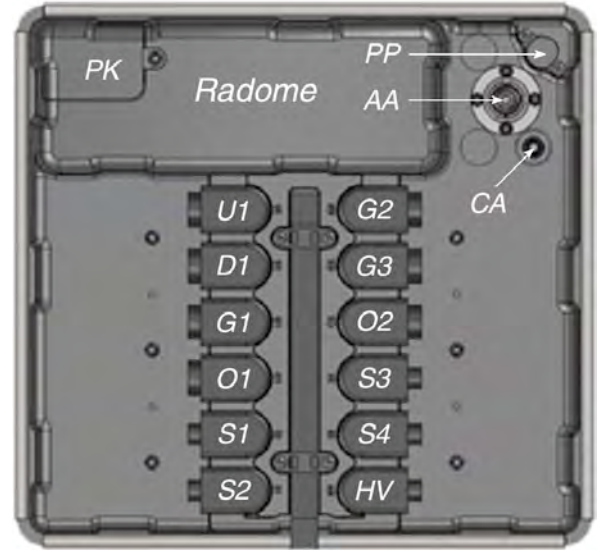
Fig. 77. The connections and port assignments on the CCU. The cable bridges, which hold the connectors in place, are omitted for clarity.

The 12-pin G1–G3 connections provide SV3 DC power, switched $10/100\,\mathrm{Mbit\,s^{-1}}$ Ethernet, and communications channels to payloads and AMPS domains. The 8-pin S1–S4 connections provide compatibility for SV2 payloads to be used on SV3 vehicles. The 6-pin HV connection provides up to 48 VDC power for high voltage sensors (e.g., the ADCP), and RS-232 communications with the CCU.

The 12-pin U1 connector is the power and communications connection between the Float and the Sub (or Glider). The Umbilical transfers power from the Float to the thrudder module, and from there to Sub and towed payloads. The Umbilical also transfers data between the CCU and Sub payloads, the thrudder module, and a towed payload if connected to the Sub.

The 12-pin D1 connection is reserved for Wave Glider system troubleshooting and battery charging using an AC adapter. The 16-pin O1 connection uses an *octopus* cable to connect two solar panels and the water speed sensor to the CCU. The 16-pin O2 connection uses an octopus cable to connect a solar panel, a radar target enhancer, the recovery buoy release mechanism, and the marker light mounted on the weather station mast to the CCU.

The power key turns the SV3 system on and off. It plugs into a 3-pin male electrical connector held in place with a retaining nut. The system is powered on when the key is inserted. When the power key is removed, the system shuts down. When the system is shut down, the batteries are individually disconnected and the solar panels

plus APU(s) are disconnected from the system. A light-emitting diode (LED) indicator light in the handle of the power key provides error or warning information using a pattern of light flashes.

⬦⬦⬦ *If the power key is inserted, but the light remains off, no power is available.* If the SV3 CCU (and APU) batteries are charged and this condition persists, LRI should be contacted for assistance.

If the power key is inserted, and the light flashes, power is available, and SV3 status is established as follows:

- If no software updates are required, the light blinks at a rate of 1 s on and 1 s off for 10 s, and then blinks at a rate of 0.2 s on and 2.8 s off. The light continues to blink at this rate as long as the power domain controller (PDC) for the CCU is running.

- If a software update is required, the light blinks at a rate of 1 s on and 1 s off for 10 s, and then blinks at a higher variable rate during the software update.

  ⬦ *When the software update completes, the light continuously blinks at a rate of 0.2 s on and 2.8 s off*, as long as the PDC for the CCU is running.

- If after 10 s the light blinks at a rate of 1 s on and 1 s off, the SV3 is not performing nominally.

  ⬦⬦ *If the light blinks continuously at a rate of 1 s on and 1 s off, there is a fault condition*, and LRI should be contacted for assistance.

The design of an SV3 payload is influenced by multiple parameters associated with the Float and Sub (or glider), e.g., buoyancy, power, and communications requirements. In regards to communications options that are available, especially for payloads only associated with the Float (like the HARPOONS activity), these depend on which CCU connector ports (Fig. 77) are used.

Payloads that include a modem can communicate directly with remote applications. Payloads connected to the S1–S4 ports can communicate directly with the CCU using RS-232, RS-422, or RS-485 serial communications. Payloads connected to the HV port can communicate directly with the CCU using RS-232 serial communications. Through the CCU, S1–S4 and HV ports can also communicate with other payloads, or with remote applications over the Iridium network.

Payloads connected to the G1–G3 ports use switched $10/100\,\mathrm{Mbit\,s^{-1}}$ Ethernet communications. All communications sent or received by payloads connected to G ports pass through an Ethernet switch that can be configured to allow payload-to-payload communications or direct communications between payloads and the CCU. Because of the aforementioned CCU communications capabilities as a function of the available CCU ports, the payload design described herein relies on the S ports. The G ports are only used to connect power and $10/100\,\mathrm{Mbit\,s^{-1}}$ Ethernet to the dry boxes (Fig. 76).

The time evolution of the hardware and software designs to fulfill the vision presented in Fig. 71 are based on starting points wherein prior accomplishments are leveraged to ensure success is likely and the risks are significantly mitigated, to the extent practicable. For this discussion, the hardware designs include optical, electrical, and mechanical components, or combinations thereof. In some cases, the hardware and software (with firmware) requirements are coupled and evolve in unison, which facilitates the scheduling of the two broadly defined development activities.

The prior hardware accomplishments that reduce risk are as follows:

- The hybridspectral instrument design for both the C-PHIRE and C-OSPREy radiometers are based on the OSPREy instrument architecture, wherein the irradiance OSPREy radiometers are the most similar to the C-PHIRE design, which were successfully built and deployed (Hooker et al. 2012a) with updated protocols (Hooker 2014), including solar and lunar observations obtained at the Mauna Loa Observatory (MLO);

- The TOW-FISH backplane with digital thrusters is based on the significantly proven C-OPS backplane with the C-PrOPS accessory (Chap. 2);

- The hybrid control (HyControl) box is designed to support two hybridspectral (C-PHIRE) radiometers, although one may be connected with a standard Universal Serial Bus (USB) cable, and is based on the successfully deployed components of the Hybridspectral Power (HyPower) box (Sect. 3.3.3) developed for the C-HyR profiler;

- The sea cable (Sect. 3.3.1), plus all other cabling, are COTS items;

- The direct current (DC) to alternating current (AC) inverter is a COTS item;

- The lithium-ion batteries to operate the TOW-FISH and protect the MacMini are COTS items;

- The shadow band, GPS, and PAR sensor are BSI COTS items;

- The extension of the WiFi communications range is accomplished using two COTS antennas and a COTS router;

- The MacMini and support electronics (i.e., the USB hub) are COTS items, which use COTS software for all programming tasks; and

- The validation instruments are COTS items with well established histories of use, i.e., C-OPS with C-PrOPS for the TOW-FISH and a MicroTops II built by Solar Light Company, (Glenside, Pennsylvania) for C-OSPREy.

15

The prior software accomplishments that reduce risk are as follows:

- The DACPRO software has been in continuous use since 1992;

- The PROSIT software has been in continuous use since 1995, wherein the kernel for controlling processing has been in continuous use since 1985 (Hooker and Brown 1985); and

- An international user group evaluates DACPRO and PROSIT functionality during recurring field campaigns, workshops, and training sessions, which result in recommendations to improve the software by identifying problems and desirable new features.

The only instruments that are powered continuously in are the MacMini, the HyControl printed circuit assembly (PCA), and the PAR sensor. All other instruments are only turned on when data acquisition requires; otherwise, the instruments are off to preserve battery charge. The HyControl PCA and PAR sensor receive power from a MacMini USB port. The MacMini is powered by the SV3 power system, but to allow continuous functionality in the presence of onboard faults, the MacMini has a dedicated 12 VDC lithium-ion back-up battery.

Because the MacMini operates on 120 VAC power, a COTS DC-AC inverter is required and is also powered continuously. To ensure continuous access to the MacMini and the CCU at an extended range, a COTS WiFi router with two external antennas mounted on the SV3 cover plate is also powered by the inverter.

8.3.1 Overall Hardware Design

One mechanism to limit payload integration complexity is to minimize how many SV3 (i.e., CCU) functions are used. The design philosophy presented herein makes the payload as standalone as possible by using the fewest SV3 functions possible. In such a framework, the payload is essentially an accessory to the SV3. A separate computer, in this case a MacMini, manages the payload and the (minimal) interactions with the SV3. The principal purposes of the SV3 are to provide power and transport for the payload, wherein the power requirement is also minimized to the extent practicable. Consequently, the payload contains two separate power sources to mitigate risks and ensure the anticipated mission scenario can be completed if an SV3 solar panel fails during the mission.

The overall hardware design of the instrumentation deployed with the SV3 is based on the requirements for collecting high quality data with the radiometers and the need to communicate with them, as depicted in Fig. 78, wherein the sea cable is the C-HyR cable (Sect. 3.3.1) with terminated strength members. The basic approach (Fig. 71) is to tow a profiling package from the SV3 Float with a solar reference mounted on the Float (on a reinforced cover plate) while a C-OSPREy system (Chap. 10)
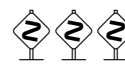
provides contemporaneous measurements from a nearby shore facility to provide atmospheric data products in support of improved atmospheric correction. The solar reference instrument suite is mounted close enough to the HyControl box that the new interface cable uses standard USB, but the much longer sea cable requires a new USB extender capability (Sects. 3.3.2 and 3.3.3).
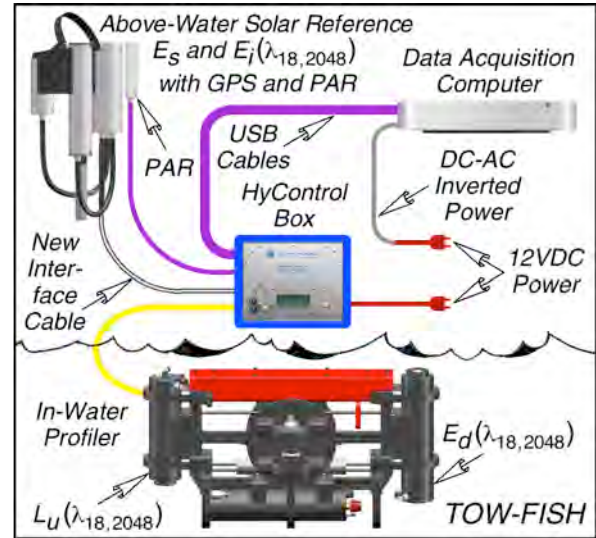
Fig. 78. The overall hardware design from the perspective of the radiometers to be deployed with the SV3 (not shown), wherein all the equipment above the surface are deployed on the Float and the TOW-FISH is towed from the Float.

The basic SV3 towing configuration is presented in Fig. 71, but without the details of the sea cable routing and the harness attached aft of the SV3. For the former, custom solar panel rails were designed to safely route the sea cable aft from the forward payload compartment along the port rail of the Float and into the water. The rails were designed to securely hold the sea cable in place with rubber lined stainless steel P-clamps and to route the cable clear of the solar panel active area while presenting minimal opportunity for snagging or fouling. The P-clamps are fastened to dedicated holes in the custom rails so they do not share the existing solar panel mounting holes. This ensures that in the event of an unanticipated load being applied to the sea cable it will be distributed evenly along the rail and, thus, provide protection to the solar panel.

At the stern of the Float, there are handles used for stabilizing the SV3 during launch and recovery, and as a swimmer aid during in-water servicing operations.

*The aft Float handles are not to be used for lifting the SV3* and are marked "NO HOIST."

Custom harness brackets mount beneath the aft stabilizing handles to secure line guides used as the attachment point for the harness connected to the sea cable. This harness attaches to a shackle, which is in turn attached to a synthetic Kellems grip secured to the sea cable. The

harness centers and distributes the load of the TOW-FISH behind the Float, and the Kellems grip transfers the tow forces from the sea cable to the harness. The harness provides the strain relief for the sea cable and ensures the sea cable bulkhead connector on the forward 3-MPU dry box is not under tension. A cable tie is used to secure the shackle pin, so it cannot rotate and come loose.

The bracket on the port side of the Float where the sea cable exits the Float was modified to permit the mounting of a purpose-built cable guide that safely holds the sea cable as it enters the water, preventing sharp bends, and holding it clear of the trailing edge of the Float.

⚡⚡ As an added precaution, *500 lb (226.8 kg) breaking strength Spectra fishing line is routed from the Float harness shackle to the TOW-FISH harness shackle.*

A picture of the Float harness that provides the strain relief for the sea cable during towing is shown in Fig. 79.
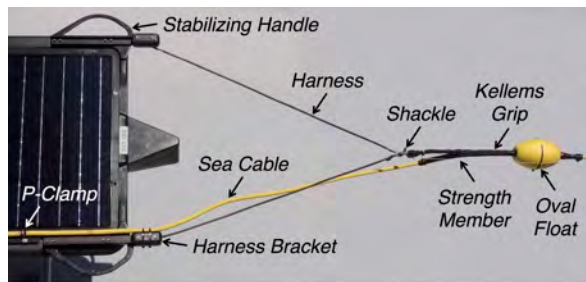
Fig. 79. The harness components for towing the TOW-FISH from the SV3 Float unit.

The towing harness attached to the SV3 is constructed of stainless steel wire rope coated with a plastic sheath and an outer diameter (OD) of 3/32 in (2.4 mm). The rope has 7×7 stranded construction and a rated capacity of 150 lb (68.0 kg) with a nominal breaking strength of 750 lb (340.2 kg). Each length is approximately 32 in (81.3 cm) long and the plastic sheath improves abrasion resistance, handling, and the tensile properties of the harness for in-water operations.

Just beyond the strain relief of the sea cable (in the direction towards the TOW-FISH), a 6 in (15.2 cm) oval-shaped float keeps the harness at the surface. The float is the first in a series of floats to control sea cable buoyancy in order to optimize the performance of the TOW-FISH and to indicate the trailing profiling package. An isolation segment close to the TOW-FISH absorbs the irregular cable tension created by the Float towing the profiling package (Sect. 9.3.7).

The floats can be added or removed at sea by a swimmer as part of fine tuning profiling operations. The floats and sea cable are yellow to improve their visibility, although the closest one to the TOW-FISH is black to minimize any perturbation to the underwater light field. The harness assembly designed for attaching the sea cable to the TOW-FISH is similar to the harness design for attaching the sea cable to the SV3, in terms of the basic functionality and components.

8.3.2 Overall Electrical Design

A generalized wiring schematic for the HARPOONS scientific payload (i.e., the instrumentation and components shown in Fig. 78) is presented in Fig. 80 as revealed with respect to the overlying solar panels. The schematic represents the connection source and destination, and not necessarily the exact cabling that ultimately connects the source to the destination. The figure shows where the single MacMini back-up battery and four payload batteries are located.
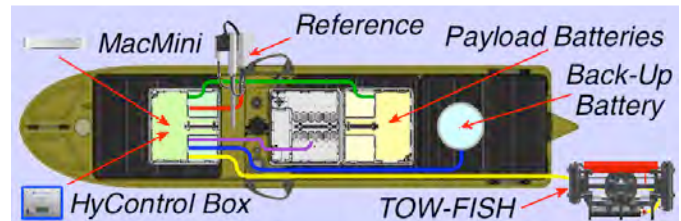
Fig. 80. A generalized wiring diagram for the payload boxes used to implement the hardware design in Fig. 78, wherein only the principal scientific payload connections are shown for the forward (light green) and aft (light yellow) 3-MPU dry boxes, with the CCU (light gray) in between, and the ADCP bay (light blue) cylinder. The APU is located under the custom cover plate, which the reference system is mounted to, and is not shown.

There are five principal connections associated with the forward 3-MPU dry box, which is where the MacMini and HyControl box are located, along with the inverter required for the MacMini and the WiFi router. The five connections are to the surface reference system, the CCU and APU, the aft 3-MPU dry box, the ADCP bay, and the TOW-FISH (towing apparatus details are shown in Fig. 79). The five connections are shown in arbitrary colors in Fig. 80, as follows:

1. The power and telemetry (red) for the surface reference system mounted on the SV3 custom cover plate;

2. The power, telemetry, and Ethernet connection (purple) to the CCU and APU, wherein the latter two are joined together;

3. The power connection (green) to the aft 3-MPU dry box containing four 24 VDC payload batteries, which are serially wired in two pairs to provide 48 VDC;

4. The power connection (blue) to the back-up battery in the ADCP bay; and

5. The power and telemetry sea cable connection (yellow) to the TOW-FISH in-water instrumentation.

The cable length for the surface reference system is short enough that USB extension hardware is not required (e.g., as provided by a HyPower or HyControl box).

The Ethernet connection between the forward and aft 3-MPU dry boxes is normally part of the daisy-chain connection of all dry boxes using a 12-pin general expansion cable, as shown in Fig. 76. During the fourth operational

demonstration in Puerto Rico, the Ethernet connection between the APU and the forward dry box was problematic. Consequently, the connection between the APU and forward dry box was removed, and an alternative Ethernet connection was established from the CCU (G2 port) to the forward 3-MPU dry box using a 12-pin general expansion cable. This configuration improved cable-routing clearances, which are restricted within the confines of the Float below the solar panels, and was retained. In this new configuration, the APU only functions as a second 890 W h battery, in addition to the CCU 890 W h battery.

8.3.3 Overall Software Design

The control of the instrumentation and the recording of the data obtained during HARPOONS field campaigns are accomplished using the DACPRO software environment, and data products are derived using the PROSIT software application. Both DACPRO and PROSIT are strongly linked and strictly adhere to the NASA Ocean Optics Protocols (Mueller and Austin 1992 and 1995 plus Mueller 2000, 2002, and 2003), hereafter Protocols, in order to facilitate the collection of the highest quality data and subsequent data products across all measured wavelengths. The DACPRO and PROSIT software systems are accessible using more than one operating system (OS), but they are both optimized for Macintosh OS X.

The complete implementation of the DACPRO and PROSIT software requires multiple languages and compiler environments. From a graphical user interface (GUI) perspective, DACPRO is written primarily in the LabVIEW programming language developed by National Instruments (NI) Corporation (Austin, Texas), whereas the PROSIT GUI is written in the ActionScript language and uses the Flex framework developed by Adobe Systems Inc. (San Jose, California).

Both the DACPRO and PROSIT software environments are written and compiled to be run as Macintosh OS X applications, although DACPRO can be ported (or built) to run on a Windows OS computer. The DACPRO and PROSIT programming environments are significantly different, but the core routines are the same in each environment and are written in the C programming language. The computationally intensive components that are used by DACPRO and PROSIT are algorithmically identical.

One of the challenges with extending DACPRO to support HARPOONS data acquisition is that the Zeiss CGS is a USB device, which means a driver and dynamic link library (DLL) is required to access the instrument, control it, and acquire data.

Zeiss and the tec5USA support company do not provide a CGS driver or DLL for the Macintosh OS.

Consequently, a driver and DLL compatible with the Macintosh OS was created using a combination of tec5USA technical support (when available), reverse engineering, and limited documentation for the PC driver and DLL.

8.3.4 Risk Mitigation

Identifying and mitigating the risks threatening the completion of a 10 d mission is an important exercise. Although some risks can be investigated shortly after defining what constitutes a successful mission, many are not well known until the overall system has been assembled and tested in an operational environment. For the HARPOONS activity, a successful mission is to launch the SV3 with the scientific instruments at the start of an approximately 10 d forecast for clear skies and fair seas, to remain at sea collecting data from all instruments until a point in time wherein poor conditions are anticipated or the 10 d time period elapses, and to recover the SV3 and instrumentation without incident.

The most significant risk for the HARPOONS activity is an unanticipated problem with the autonomous vehicle. This risk is mitigated by choosing a Wave Glider as the autonomous platform, because the Wave Glider is a reliable and durable autonomous platform that has crossed the Pacific Ocean (San Francisco to Tokyo and San Francisco to Sydney), navigated through hurricanes and cyclones, and moves by mechanically harvesting the (almost) ceaseless energy of surface gravity waves.

Because the Wave Glider is propelled by harvesting wave energy, it cannot stop moving due to a loss of fuel or battery charge, *although it can be becalmed in glassy conditions, has a very slow speed in calm conditions, and has difficulty maneuvering in a desired direction in the presence of strong and unfavorable currents.*

Consequently, almost all of the energy collected by the three solar panels (52 W each), which provide approximately 936 W h per day (assuming a conservative 60% solar charging efficiency over a 10 h illumination time period) are available for the scientific payload and mission.

The second most significant risk is inadequate power for the scientific equipment. The scientific equipment is only marginally integrated into the SV3 payload architecture, which makes the system less complicated and allows simpler replication for another user. A principal reason for this architecture is the SV3 battery system is more like a power supply, which means instantaneous loads (e.g., from thrusters) are sometimes problematic.

To minimize risk associated with the power budget, the most power intensive or important scientific equipment, the TOW-FISH thrusters and the MacMini, respectively, each have their own battery reserves. The TOW-FISH batteries are completely independent of the SV3 power system and are sized to last the entire 10 d mission without a need for recharging. The MacMini back-up battery ensures a continuous supply of power without transient faults. The battery reserves also allow the anticipated 10 d missions to complete successfully if a solar panel fails.

The MacMini plus the solar reference with shadow band, GPS, and PAR sensor are the only scientific devices connected to the SV3 power system. These devices

with their support electronics (DC-AC inverter, HyControl box, USB hub, etc.) place the largest demand on the SV3 power supply, which is comprised of the CCU battery (890 W h), APU battery (890 W h), and three solar panels (3×52 W). The total battery charge when the SV3 is launched is 1,780 W h. *When the SV3 is deployed for a 10 d vicarious calibration mission, a significant portion of the mission can be supported with the internal charged batteries alone* and if one of the three solar panels fails, the mission can still be successfully completed (Sect. 8.9).

With risks to propulsion and power significantly mitigated, the subsequent concerns are associated with possible, but unlikely, threats to the entire system or important subsystems. The threats to subsystems are not considered rather likely, because the components are principally COTS and have already been extensively tested. The SV3 has inherent mitigators for risk, as do the mission parameters required for vicarious calibration data.

Short-duration (10 d) missions are anticipated, wherein the SV3 is only deployed during fair-weather conditions (i.e., good satellite viewing) and forecasts, thus, unanticipated risk due to severe weather is small. During these missions, the SV3 is (almost) always in motion, so it is not an established fish aggregation device (FAD) like a permanent mooring.
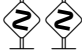
⬨⬨ Like any device or structure placed in water, however, *some wildlife will be attracted to the SV3 and the instrumentation deployed above or in the water.*

The location of the SV3 is not known to fisherman or recreational boaters, so vandalism, whether intended or accidental, is significantly minimized. The anticipated *launch* location is beyond the usual distance from shore for recreational boaters, i.e., approximately 20 nmi.

To be spotted by another vessel, the SV3 has to be discovered accidentally, i.e., randomly. The low vertical profile of the SV3 and the black paint scheme reduce the likelihood of discovery.

⬨⬨⬨ If the SV3 is accidentally discovered, *the most significant risk is an inquisitive boater colliding with the Float or crossing behind the Float and cutting the sea cable plus external strength member.*

Consequently, the cable is a high visibility yellow and yellow floats are attached to the cable to indicate a trailing apparatus. Similarly, when the profiler ascends, yellow floats become visible to mark the extent of the towed package behind the SV3.

⬨⬨ The SV3 has an AIS antenna, which receives reports from class A and class B vessels in the vicinity (i.e., vessel identification, position, heading and other standard AIS data), and *the SV3 automatically executes an avoidance maneuver when detecting an AIS target.*

The SV3 also has a Resilient tracker or beacon (Fig. 72), which provides another source of GPS location information transmitted over the Iridium network, in addition to the tracker included in the CCU radome.

⬨⬨⬨ If the SV3 is flipped over, *a capsized Resilient tracker nonetheless broadcasts the GPS location of the SV3.*

Another recurring risk to the SV3 is damage caused during launch or recovery. If the former occurs, the SV3 is immediately recovered. A recovered and damaged SV3 is returned to the shore facility for maintenance and team debriefing with retraining depending on the circumstances causing the damage.

With these inherent risk mitigators in mind, there are three categories of threats that are considered next, as follows (Table 8):

- The 10 d mission is threatened, such that no further useful data is likely to be obtained (e.g., the weather forecast suddenly changes for the worse with a high likelihood of severe weather).l

- Daily operations are threatened and might have to cease (e.g., forward progress of the SV3 is too slow, due to glassy conditions, and the profiler sinks to 20 m or more); and

- Data quality is threatened during individual profiles (e.g., the altimeter and rate gyros fail).

Regardless of mitigation strategies, some risks can suddenly and uniquely materialize to threaten mission success and require an intervention (e.g., another vessel is on a collision course with the SV3). Three advantages of using the SV3 as the deployment platform are as follows: a) it is autonomous, so it can be commanded to return to shore to facilitate recovery; b) the AIS system provides built-in avoidance capabilities; and c) it can be intercepted by smaller, high-speed, and more nimble vessels to rapidly recover it.

The categories of risk and their likelihood (possible, unlikely, and rare) led to design efforts to remove or substantially mitigate risks that required an abundance of caution to prevent. Notable exceptions that could not be completely designed out of the SV3 and scientific instrument system are those risks associated with random misfortune, e.g., a critical shipping container goes missing while being shipped. Rare events that require extreme caution typically must be accepted, because the cost of completely removing them is frequently prohibitive, e.g., a passing large vessel flips the SV3 upside down. The same is true for unlikely risks, e.g., a small boat passes to the aft of the SV3 and severs the sea cable plus the external strength member.

An example of a risk that was mitigated with additional engineering was the low height of the standard center lift (pick) point on the SV3 (Fig. 72). The original pick-point assembly consisted of a 6 in (15.2 cm) tall stainless steel pad eye attached to the SV3 float body via two forked mounts bolted through the SV3 top plate. The Wave Glider is launched from research vessels by attaching a cable hoist, lifting the SV3 vertically, and then transferring the SV3 to the water. Normally Wave Gliders are

Table 8. The categories of risk for an SV3 and TOW-FISH deployment, with the mitigation strategies and response (if necessary, and in parentheses), wherein purple is considered possible, red is unlikely, and green is rare.

Category	Risk	SV3 Mitigation and Response
(purple ×3)	One or more shipping containers go missing during transport	High-priority boxes, e.g., SV3 wooden crates and lithium-ion MPUs, each have a global GPS package tracker inside
(purple ×2)	SV3 release mechanism fails during launch of SV3	Double-check prior to launch (immediately recover SV3 while attached to cradle, recheck, and attempt re-deployment)
(green ×3)	A passing large vessel flips the SV3 upside down	All mast instruments are waterproof, tracker works inverted (rapid recovery from nearby shore facility)
(red ×2)	A boater or fisherman vandalizes the SV3	SV3 hard to detect and is beyond recreational distance to shore (rapid recovery from nearby shore facility)
(purple ×1)	A calm sea state or unfavorable current becalms the SV3	Oceanic operational area usually has a sea state above 1 (the the thrudder to be used to increase speed)
(green ×2)	Potential collision with a large- or medium-sized vessel	SV3 difficult to detect, AIS automatic avoidance maneuvers (the thrudder is used to increase speed)
(purple ×1)	Fish or marine wildlife are attracted to the SV3	Short 10 d mission with no instruments under the SV3 to be affected (thrusters are a deterrent for TOW-FISH)
(red ×1)	One of the three solar panels fails or is shaded	Short (10 d) mission requires two functional panels (rapid recovery from nearby shore facility if more than 1 fails)
(green ×2)	An SV3 or payload battery fails or discharges early	Short mission needs 1 (or 2) SV3 battery and 2 (of 4) payload batteries (recovery from shore facility if more failures)
(green ×3)	The CCU fails or becomes unresponsive	Tracker (beacon) provides location (rapid recovery from nearby shore facility)
(red ×1)	DACPRO or OS X freezes, or is unresponsive	In 25+ yr, freezes are rare, interfaces idled if not used, system reboots daily (rapid intervention from nearby shore facility)

Category	Risk	In-Water Instrumentation Mitigation and Response
(red ×1)	New technology sensor fails prematurely	New technologies are well tested (COTS) and redundant (old technologies are usually retained in instruments)
(red ×3)	Sea cable run over and severed by a small boat with no AIS	Sea cable marked with floats, SV3 beyond recreational distance to shore (recovery from nearby shore facility)
(purple ×2)	Digital thruster fouls and the thrust levels degrade	TOW-FISH ascends with one thruster, but is slower (recovery from nearby shore facility if start of mission)
(red ×3)	TOW-FISH run over by a small boat with no AIS	TOW-FISH rarely at surface, sea cable marked with floats (rapid recovery from nearby shore facility)
(purple ×1)	SV3 becalmed, so TOW-FISH resting depth is too deep	Reduced profiling frequency if TOW-FISH deeper than 10 m (thrudder to be used to increase speed prior to profile)
(purple ×1)	TOW-FISH attracts fish and marine wildlife	Vertically moving TOW-FISH with thrusters on is a deterrent to loitering fish and marine wildlife
(green ×1)	One or more optical apertures are bio-fouled	Short mission, apertures in motion cleansed by water passing over them (rapid field maintenance from shore facility)
(purple ×2)	Unforeseen bad or severe sea state or weather	Short, fair-weather mission (SV3 turns to shore, and rapid recovery from nearby shore facility)

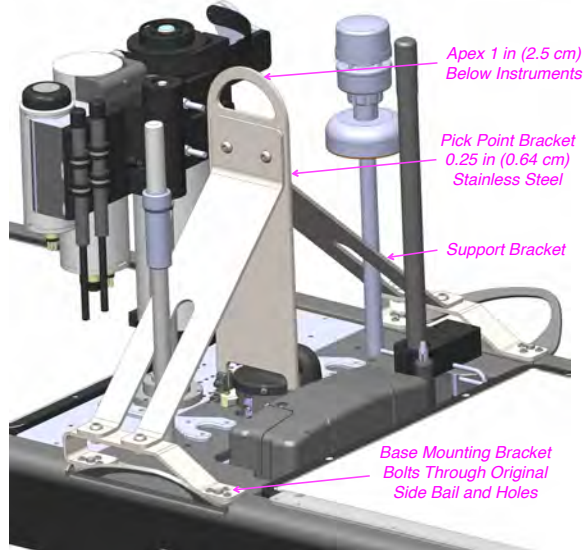| Category	Risk	Above-Water Instrumentation Mitigation and Response
(green ×3)	New AIS or WiFi antenna fails prematurely	WiFi is not mission critical; AIS made by cellular antenna manufacturer (rapid recovery from nearby shore facility)
(green ×2)	Shadow band fails to rotate correctly or freezes	Could shade E_s, not critical data, redundant C-OSPREy data (rapid recovery from nearby shore facility if frozen)
(green ×1)	Airborne particle deposition fouls optical apertures	Short mission reduces fouling opportunity and air flowing over the apertures deters the deposition of particles
(purple ×2)	Reference and masts attract birds and pick point is too short	Shadow band sweep deters birds landing (field maintenance from shore facility) and modified pick point is taller

(icon) Caution warranted to protect performance. (icon ×2) Extra caution needed to avoid compromising performance. (icon ×3) Extreme caution required to ensure integrity of equipment or data.

recovered in the same fashion they are launched, but the SV3 outfitted for HARPOONS necessarily includes an instrument cluster and antenna mounts adjacent to the pick-point location.

The 18 in (45.7 cm) tall instrument cluster complicates recovery in regards to the original height of the pick point, because the SV3 is usually many feet from the vessel during recovery and cannot be lifted vertically at a distance. Consequently, the cable hoist is connected to the SV3 side bail, which causes the craft to rotate 90° on its side, so the hoisting cable is at an angle during recovery and may damage the above-water instrument cluster. Recovery with the side bail also poses a potential risk of damaging the instrument cluster as it passes through an A-frame.

The vulnerability of the original pick-point assembly was well demonstrated during the first deployments in Hawaii, Monterey Bay, and Puerto Rico. After the latter campaign, an elongated pick point was designed to allow the recovery of the SV3 from the existing pick point location. The extended pick point allows recovery of the SV3 from the water in a vertical orientation while minimizing the risk of damaging the instrument cluster or other sensors. The new pick point attaches to the SV3 with the same forked mounts of the original pick-point assembly and is reinforced with angle brackets on both sides (Fig. 81). The height of the extended pick-point assembly above the mast plate is less than the height of the solar reference above the cover plate.

Apex 1 in (2.5 cm) Below Instruments

Pick Point Bracket 0.25 in (0.64 cm) Stainless Steel

Support Bracket

Base Mounting Bracket Bolts Through Original Side Bail and Holes

Fig. 81. A three-dimensional drawing of the extended pick-point assembly for the SV3 mounted on the mast plate.

8.3.5 SV3 Communications

Because the optical measurements require a solar reference radiometer mounted on the mast plate, the height of the other structures on the mast plate (e.g., antennas) cannot exceed the height of the solar reference and PAR diffusers, which are 18.25 in (46.4 cm). The latter is the minimum height to ensure the moment arm created by the mass of the reference radiometer with accessories (shadow band, GPS, and PAR sensor) is as short as possible and within tolerances established by the LRI engineers. A secondary advantage of minimizing the height of the above-water instrumentation is that it makes the SV3 harder to detect by fisherman or recreational boaters.

The Resilient tracker was not modified and is a Rover beacon made by Xeos Technologies Inc. (Dartmouth, Nova Scotia). The height above the mast plate is 2.5 in (6.4 cm). The Rover is an independently powered, self-contained satellite transceiver designed to work in rugged ocean environments. The Rover features independent dual GPS and Iridium patch antennas, so in the event the SV3 is flipped over (i.e., capsized), the Rover will continue to record and transmit its position. The frequency of transmission is user programmable. For autonomous HARPOONS deployments, the transmission frequency was hourly. The Rover beacon contains 18 AA (1.5 VDC each) batteries, which allow for a 2 y deployment using a 3 h reporting interval.

The cellular antenna was not modified, and is a model 3D0819V-XS-4-3 made by Antcom (Torrance, California). The mast for the antenna was shortened to achieve a final height above the mast plate of 17.125 in (43.5 cm).

The AIS antenna was modified twice. The original model was a 5250-AIS stainless steel half-wave antenna made by Shakespeare Marine Antennas (Columbia, South Carolina), wherein the height above the mast plate was about 3.6 ft (1.1 m). For the first deployment of the SV3, wherein the SV3 was always in near proximity to the vessel used to deploy the SV3 and TOW-FISH, the antenna was reduced in height to make it compliant with the height restriction required for the solar irradiance reference. Although this remedy worked for the attended deployments associated with field testing, it was not considered a long-term solution for unattended operations. Consequently, the AIS antenna was replaced with a model 18R-161-162P-18CPA2155-U made by Antcom (Torrance, California), i.e., the supplier of the cellular antenna. The height of the new antenna above the mast plate is 18.125 in (46.0 cm).

The weather station is an Airmar 200WX made by Fondriest Environmental (Fairborn, Ohio). The mounting mast supplied by LRI was shortened from 46.0 in (1.2 m) to 16.875 in (42.86 cm) above the mast plate. The Airmar 200WX is a compact weather instrument designed for moving platforms and includes the following sensors: a 3-axis compass, rate gyro, GPS, tilt, temperature, pressure, plus apparent and true wind speed. The equipment mounted on the weather station mast was not modified. Also, the Iridium antenna, which is contained within the CCU radome, was not modified. The configuration of the above-water equipment mounted on the Float during the second deployment of the SV3 is shown in Fig. 82.
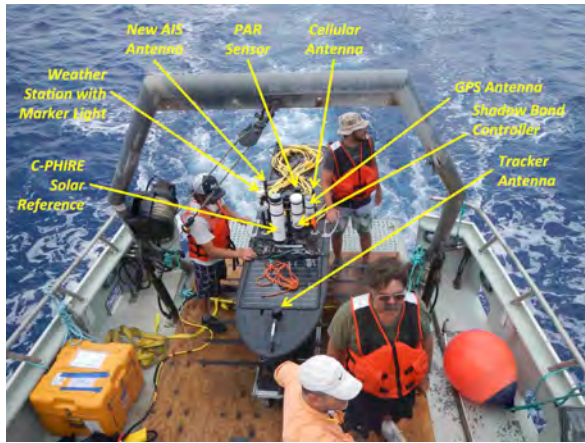
Fig. 82. The SV3 above-water instruments and antennas as configured during the R/V *Huki Pono* deployments (the CCU radome is obscured by the equipment mounted on the mast plate).

To improve communications with the SV3 local area network (LAN) using WiFi, thereby allowing communications with the MacMini from a small boat (e.g., the vessel used to launch or recover the SV3) in near vicinity of the SV3, two height-compliant WiFi antennas were added to the reference system before the operational demonstration in Puerto Rico. The selected WiFi antenna is a model RAF whip antenna made by Linx Technologies (Merlin, Oregon). The RAF is a dual-band, half-wave antenna covering the 2.45 GHz and emerging 5 GHz bands. The WiFi antennas are connected to a O2Wind router made by RadioLabs (Fortuna, California) as is the MacMini and the SV3 LAN.

8.3.6 SV3 and Payload Batteries

The CCU contains a battery pack that supplies power to the core system and payloads as needed to supplement input from the solar panels. The CCU battery pack consists of 10 lithium-ion 89 W h batteries. An APU is a self-contained AMPS power domain and has identical battery specifications as the CCU. AMPS allows energy sharing between the core electronics and all payloads connected to the system. The CCU and APU are charged by the three 52 W solar panels mounted to the Float deck (Fig. 73).

The maximum continuous current available to any payload depends on its connection to the CCU and APU system. The maximum battery voltage for the CCU and APU batteries is 16.6 VDC, the maximum continuous current is 20 A, and the fully charged (theoretical) energy capacity is 890 W h. The allowed voltage range for a payload connected to the Umbilical is 14–23 VDC with a maximum current of 6 A, which does not satisfy the requirements for the pair of digital thrusters on the TOW-FISH backplane.

Although the CCU and APU batteries nominally satisfy the power requirements for the digital thrusters, *the SV3 power system architecture functions more like a*

power supply than a battery, so the instantaneous loads of the thruster DC motors are sometimes problematic and require a true battery power source, which is housed in the aft 3-MPU dry box.

The use of a separate battery source for profiling is a positive impact on the SV3 power budget, as discussed below (Sect. 8.9).

The principal reasons the TOW-FISH is towed from the Float is the Umbilical cannot provide the needed amperage for the TOW-FISH digital thrusters, and towing from the Float allows the TOW-FISH sea cable to be connected to the four payload batteries in the aft 3-MPU dry box (using the HyControl circuitry).

The MacMini power is supplied by a COTS DC-AC 120 W model XP 125 true-sine-wave inverter manufactured by EXELTECH (Fort Worth, Texas). The inverter is connected to CCU port S1, and is also supported by a 12 VDC lithium-ion battery rated at 120 W h (10 A h) made by K2 Energy (Henderson, Nevada). The 12 VDC battery enclosure occupies the ADCP bay (Fig. 80) and has a pressure relief valve for safety purposes.

The MacMini back-up battery system includes a PCA to allow the following functions: *a) power the MacMini on and off remotely using WGMS (Sect. 8.3.7); b) ensure instantaneous amps are available during operation; and c) prevent power transients that might otherwise impair MacMini operations while data is collected and recorded.*

The TOW-FISH batteries are made by BiX International (Santa Ana, California) and are 24 VDC lithium-ion batteries rated at 300 W h (12.5 A h). For the first three deployments of the SV3 (twice in Hawaii and once in California), two of these batteries were installed in the aft 3-MPU dry box. They were connected in series to produce 48 VDC. For the fourth deployment (Puerto Rico), four of these batteries were connected in two serial pairs for a total of 1,200 W h (50 A h).

8.3.7 Payload Electronics

The cabling depicted in Figs. 78 and 80 represent simplified (but functionally correct) schematics, with Fig. 80 emphasizing that the forward 3-MPU dry box is connected to all components mounted on, or towed by, the SV3. The forward 3-MPU dry box was selected for this purpose as part of weight balancing the Float with respect to the equipment loaded into or mounted onto the Float.

For the C-PHIRE radiometers, EPIC Remote Interface (ERI) electronics modules provide power conditioning and the communications channel conversion for USB to support EPIC radiometers when they are located more than 2–3 m from the data acquisition computer. There are two versions of the ERI, as follows: a) above-water atmospheric, which is designated ERA; and b) in-water

profiling, which is designated, ERP. The C-OSPREy solar irradiance reference and the C-OSPREy radiance instrument both use identical ERA modules; the solar irradiance reference on the Float does not require an ERA, because the HyControl box is positioned close enough to allow a direct USB connection. Only the TOW-FISH uses the ERP module.

The ERP and ERA electronics modules are similar. Both share the 4 in (10.2 cm) OD form factor of the EPIC architecture, and contain all of the required electronics to support EPIC instrument deployments at distances up to 100 m from the data acquisition computer. There are two primary distinguishing capabilities of the ERP relative to the ERA: a) the ERP supports both the power and telemetry requirements of a dual thruster architecture; and b) the ERP supports the simultaneous operation of two EPIC instruments, which is required for the TOW-FISH configuration, whereas the ERA supports only one.

The cabling and connections that permit the detailed command and control of the electronics needed for autonomous sampling with the SV3 are shown in Fig. 83, wherein serial communications are shown as blue lines, including transistor-transistor logic (TTL) communications; USB communications are shown as pink lines; power routing is shown as green, brown, and red lines; Ethernet communications are shown as black lines; and antenna connections are shown as dark gray lines.
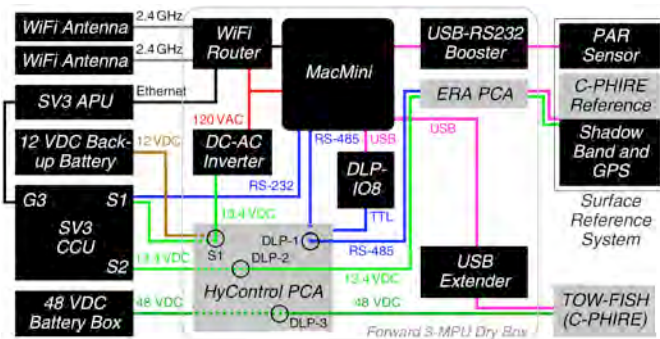
Fig. 83. An overall wiring diagram for the scientific equipment installed on the SV3 with respect to the components mounted in the forward 3-MPU HyControl dry box (large center rectangle with rounded corners). All COTS items are shown as black boxes and the devices built for HARPOONS are shown as gray boxes, with the surface reference system a combination of both.

The COTS payload electronics in Fig. 83 are shown as black rectangles, and custom electronics are show as gray. The aforementioned HyControl box (Figs. 78 and 80) is a combination of the HyControl PCA plus all the equipment contained within the light gray rectangular outline denoted as the *Forward 3-MPU Dry Box*, including the MacMini, WiFi router, DC–AC inverter, the ERA PCA for the C-PHIRE solar reference radiometer, etc. A companion ERP PCA is mounted on the TOW-FISH backplane (not shown in Fig. 83).

The scientific electronics presented in Fig. 83 are contained primarily in the forward 3-MPU dry box. A payload development kit was originally part of the aft 3-MPU dry box, but it was permanently removed for the fourth SV3 deployment to demonstrate operational readiness off the southwest coast of Puerto Rico, because the number of lithium-ion payload batteries therein was increased from two to four. The batteries are serially wired in pairs to power the TOW-FISH electronics at 48 VDC.

The embodiment of the HyControl box in Fig. 83 is as a PCA, because a separate enclosure is not needed, given the electronics are stored in a dry box. The HyControl PCA is a more sophisticated version of the HyPower box developed and deployed for the C-HyR activity (Sect. 3.3.3) The HyControl PCA uses a COTS USB-serial module to turn C-PHIRE subsystem voltages on and off, as well as to provide measurements of relevant supply voltages and high-voltage current draw. The PCA provides reverse voltage input protections, power routing, logical control of field-effect transistor (FET) switches, voltage dividers for voltage measurements, a shunt resistor for current measurement, and a precision 2.5 VDC voltage reference accurate to better than 0.5%.

The COTS USB-serial module in Fig. 83 is made by DLP Design (Allen, Texas). The module provides input/output (I/O) control of eight data channels and is designated the DLP-IO8. The DLP-IO8 is a low-cost, easy-to-use data acquisition system for measuring voltages, controlling and monitoring processes, and acquiring temperature data. Each of the eight available channels can be configured for any of the digital, analog, or temperature modes via single-byte commands. All operational power is taken from the host computer via the USB port.

The DLP-IO8 utilizes Future Technology Devices International (FTDI) drivers (Glasgow, United Kingdom) to convert RS-232 or TTL serial transmissions to USB signals. This provides support for legacy devices with a modern computer architecture (e.g., the MacMini). The DLP-IO8 FTDI drivers are the same as the other FTDI USB-serial components used in the C-PHIRE architecture, including user-programmable *branding* (text fields) that is useful for port identification.

The HyControl PCA supports all three C-PHIRE radiometers (two on the TOW-FISH and one solar reference) by implementing command and control procedures using the CCU (WGMS commands) and the DLP-IO8. These procedures implement basic functionality of the system design (e.g., turning components on and off), as follows:

- After the WGMS command to turn on CCU port S1 is acknowledged, the resulting 13.4 VDC power turns on the inverter, which turns on the MacMini. The 12 VDC back-up battery supports the dynamic load the inverter presents to the SV3 power supply (through S1), and is forced off when S1 is switched off. Toggling S1 allows a reboot of the MacMini in the event of a hardware or software fault. S1 cannot

power the inverter alone, however. Switch S1 must be on for the MacMini, and thus the entire C-PHIRE system, to operate.

⚖ *The power settings on the MacMini are configured to automatically log on and start executing the data acquisition schedule as long as the MacMini is receiving power after what it perceived to be a power fault*, which is how it interprets every instance of power cycling when operating in automated mode to support a mission.

- After the WGMS command to turn on CCU switch S2 is acknowledged, the resulting 13.4 VDC power is used for the surface reference system, wherein DLP-1 and DLP-2 are used to turn on the basic master aggregator and pass this power to the reference, respectively. S2 must be on for the surface reference system to operate.
- 48 VDC power from the aft 3-MPU dry box is used to power the TOW-FISH, wherein DLP-3 is used to pass the power to the backplane.

Consequently, each of the major components shown in Figs. 71 and 78 can be turned on and off, as follows: port S1 controls the operation of the inverter and, thus, the MacMini; port S2 plus DLP-1 and DLP-2 control the operation of the solar reference instrument suite; and DLP-3 controls the operation of the TOW-FISH instrumentation.

The PAR sensor in Fig. 83 (a BSI QCP2150) is not controlled by the DLP-IO8. It is powered by a USB-serial converter. The other five communications channels on the DLP-IO8 provide additional status data, while mitigating risk (Table 8), as follows:

- The DLP-4 channel provides an analog voltage measurement of the 48 VDC battery supply in the aft 3-MPU dry box (that provides all the power for the TOW-FISH).

  ⚖⚖ *If the voltage of the 48 VDC battery box drops to 42 VDC or less while the battery is supplying greater than 5 A, the profiling portion of the mission should be terminated* (thruster use should be stopped); this corresponds to about 3 A per thruster, which approximates a thrust level of 66%.

  Lower currents (i.e., thrust levels) allow the voltage to drop further before the mission is terminated.

  ⚖⚖⚖ *The 48 VDC battery automatically shuts off if the voltage drops to 40 VDC.*

- The DLP-5 channel provides an analog amperage measurement of the 48 VDC battery supply in the aft 3-MPU dry box. This is a coarse measurement and is intended to verify that the TOW-FISH instrumentation is approximately performing (or is anticipated to continue performing, depending on the measurement) within nominal limits.

- The DLP-6 channel provides an analog voltage measurement of the 12 VDC battery supply in the ADCP bay (that supplements the SV3 power provided for the MacMini).

  ⚖⚖⚖ *If the 12 VDC battery drops to 11 VDC or less, the mission should be terminated,* because the computer power supply may fail (the MacMini should be shut down).

- The DLP-7 channel is not presently in use and is reserved for future applications.

- The DLP-8 channel provides an analog voltage measurement, which is accurate to within 0.5%, of a high precision 2.5 VDC reference. The reference voltage is included in the design, because the ADC on the DLP-IO8 uses the 5 VDC supply on the USB port it is attached to as a voltage reference.

  ⚖ *If the voltage reading of the 2.5 VDC precision reference is out of the range of acceptable user tolerance, then the voltage reading of the precision reference can be used to scale all of the other analog readings to improve accuracy.*

  For example, if the 2.5 VDC reference is reported as 2.0 VDC by the DLP-IO8, then the other analog readings should be multiplied by the ratio 2.5/2.0 to improve their accuracy.

8.3.8 In-Water (Towed) Measurements

The TOW-FISH backplane is a modified version of the C-OPS with C-PrOPS accessory backplane (Chap. 2). The TOW-FISH backplane is bigger to accommodate the larger C-PHIRE instruments and the digital thrusters are positioned for vertical thrust in mounts that can be rotated clockwise or counterclockwise for canted thrust. The TOW-FISH backplane with the instruments attached is 36.5 in (92.7 cm) wide, 16.3 in (41.4 cm) deep, and 20.1 in (51.1 cm) high, wherein the width is considered to be the long axis shown in Fig. 78. The corresponding dimensions for a C-OPS with the C-PrOPS accessory backplane are 27.8 in (70.6 cm) wide, 12.8 in (32.5 cm) deep, and 15 in (38.1 cm) high.

The fully assembled TOW-FISH backplane weighs 59 lb (26.8 kg), which is 32.8 lb (14.9 kg) more than a fully assembled C-OPS with C-PrOPS accessory backplane. The extra weight is due to the increased size and, thus weight, of the principal components, as follows: a) the C-PHIRE radiometers, b) the ERP electronics module, c) the perforated backplane plate, and d) the thruster mounting system. An isometric drawing of the backplane is presented in Fig. 84 (compare to Figs. 16 and 17).

Table 9. A summary of the HARPOONS field campaigns, environment type (with water type and depth or atmosphere type and altitude), deployment platform, starting date for data collection in the field (with the number of days), plus the number of observational sequences (or casts) obtained for the instrument systems or subsystems, including hardware and software. The CVR codes indicate the science application of the data, i.e., vicarious calibration (C), algorithm validation (V), or baseline research (R). Water depths for open-ocean (case-1) campaigns were typically greater than 1 km and frequently greater than 4 km, whereas for case-2 waters they were much shallower (less than 20 m).

Environment and Topography	CVR Codes	Deployment Platform	Field Sampling Start Date (days)	Observational Sequences (Casts)		
				TOW-FISH	C-OPS§	C-OSPREy
Case-2 8 m	R	R/V *Hakuho Maru*	5 Mar. 2015 (1)	9†		
Case-1 >1 km	V	R/V *Hakuho Maru*	4 Nov. 2015 (20)		34	37‡
Case-1 146 m	V	R/V *Po'okela*	19 Aug. 2016 (6)	23		
Case-1 81 m¶	$C\,V$	R/V *Huki Pono*	28 Aug. 2016 (2)	36	20	
Case-2 52 m	$V\,R$	R/V *John Martin*	26 Oct. 2016 (1)	10	6	
Case-1 >1 km	V	R/V *Hakuho Maru*	6 Dec. 2016 (20)		15	
Case-1 <1 km	$C\,V$	R/V *Sultana*	18 Jan. 2017 (8)	83	46	402
Case-2 19 m	$V\,R$	R/V *Hobson's Choice*	15 Jun. 2017 (1)	22		
Eclipse Sea Level	$V\,R$	BSI Rooftop	21 Aug. 2017 (1)			40
Alpine 1,800 m	$C\,V$	Mount Laguna (CA)	4 Oct. 2017 (1)			52
Case-1 >1 km	R	R/V *Hakuho Maru*	17 Oct. 2017 (24)		25	
Case-2 15 m	$C\,V$	R/V *Hobson's Choice*	14 Dec. 2017 (2)	22		

§ C-OPS S/N 21 with C-PrOPS † C-HyR with C-PrOPS. ‡ Solar reference only. ¶ 387 m at station near MOBy site.
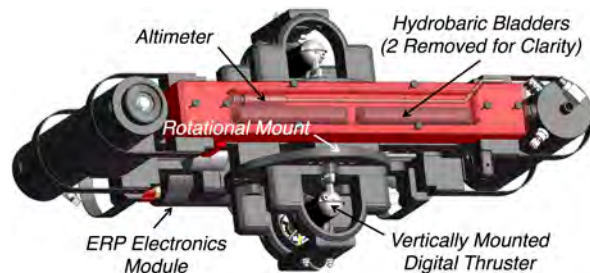
Fig. 84. An isometric view of the TOW-FISH backplane with the instrumentation affixed (E_d and L_u C-PHIRE radiometers on the left and right, respectively). The transparent top shows the altimeter inside the hydrobaric buoyancy chamber (two of four compressible bladders are omitted, because they would obscure the altimeter).

The thruster mounts allow each thruster to be positioned in a vertical orientation or in a number of canted angles with respect to vertical. The tow point is through the center of mass to ensure the cyclical towing forces act exclusively along the long axis with little or no forces in the other two dimensions. This means a canted ascent angle to provide slack in the tow cable to smooth out towing forces during the shallowest near-surface sampling is not a requirement. The ability to rotate the thrusters to set cant angles is retained, however, to allow deployment of the backplane from a ship, wherein the thrusters must be canted to drive the backplane away from the vessel.

In addition to short-term tests during the day (e.g., BSI rooftop trials for C-OSPREy), a sequence of field campaigns (Table 9) provided the opportunities to deploy the HARPOONS above- and in-water instrument to advance the TRL values of subsystems in relevant end-to-end environments and ultimately the entire system in an operational environment. The principal instruments that were deployed in increasingly more complete configurations were the TOW-FISH and C-OSPREy sensor suites, wherein C-OPS serial number (S/N) 21 with the C-PrOPS accessory was the primary validation system.

During the first deployments of the TOW-FISH off Kawaihae Harbor in Hawaii (19–25 August 2016), the dynamical response of the TOW-FISH during ascent and descent was investigated as a function of thruster orientation. The trials confirmed a vertical orientation of the thrusters was the superior configuration, because all of the thrust force was used in moving the instrument package to the surface, and was, thus, the most energy efficient.

During initial design planning regarding towing an instrument package similar to the C-OPS with C-PrOPS accessory from the SV3 Float, concerns emerged from engineers experienced in SV3 tow operations that a fairing to streamline the package would be needed. These concerns were based primarily on towing a device from the Sub, wherein the device was not subjected to near-surface wave effects. The fairing for the TOW-FISH is substantially comprised of four large rigid plates of ultra-high molecular weight polyethylene (PE) and two sheets of polypropylene (PP). Two plates are secured in multiple locations to blocks on each side of the TOW-FISH backplane and to the landing pads used to mount the thrusters. The blocks used are already present on the backplane; mounting holes and notches were designed into them in anticipation of the

requirement for testing the system both with and without a fairing in field trials.

PE retainers were designed to secure the plate to the landing pad, and to connect adjacent plates, utilizing existing hole patterns. The PP sheets are wrapped around the leading and trailing edges of the standard backplane bumpers and secured into both the plates and the blocks through an overlapping hole pattern. Each plate has a small cutout to permit the routing of the thruster cables into the enclosed areas of the fairing, which provides additional protection for the cables and other normally exposed components. The fairing is designed to be modular, such that not all parts need be used simultaneously, i.e., the plates or the sheets can conceivably be used independently, allowing different evaluation approaches to be explored. A drawing of the TOW-FISH backplane with the fairing attached is presented in Fig. 85.
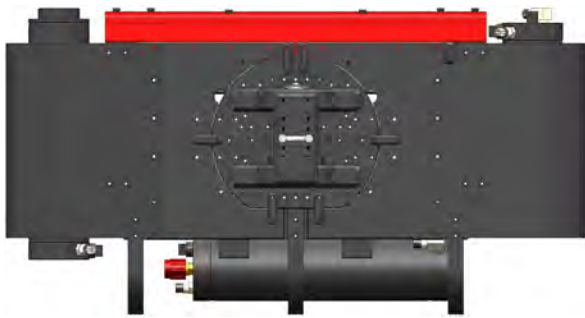
Fig. 85. A drawing of the TOW-FISH backplane with the fairing attached, which results in a profiling package with predominantly large flat sides and curved edges (not shown) plus an exposed electronics module on the bottom.

During the second deployments of the TOW-FISH off the island of Lana'i in August 2016, the dynamical response of the TOW-FISH during ascent and descent was investigated with and without a fairing (Fig. 85). The use of a fairing did not improve the overall tow dynamics. The larger flat surface area of the backplane with the fairing installed resulted in larger vertical tilts when the TOW-FISH was at the surface and subject to wave effects. Without the fairing installed, the somewhat open design of the backplane made the instrument package more transparent to swell, which resulted in smaller vertical tilts when the backplane was near the sea surface.

The sea cable used with the TOW-FISH is the same cable developed to deploy the C-HyR profiler (Table 4 and Fig. 28) except that the strength member is terminated for TOW-FISH profiling. The strength member was not terminated for C-HyR profiling, because C-HyR was only deployed as a handheld system. The strength-member is terminated to a machined adapter that is integral to the stainless steel connectors at each end of the sea cable. The termination procedure is proprietary and is not disclosed.

To remove the necessarily periodic (and herky-jerky) motions imparted to the backplane during towing, four

isolation segments are attached to the sea cable a short distance from the backplane Kellems grip. More complete details are presented in Sect. 9.3.7, so only summary information is provided here. Each isolation segment is constructed by creating a semicircular loop in the sea cable and spanning the widest opening with lengths of shock (*bungee*) cord. When fully brought under tension, the stretched shock cord were approximately the same length as the sea cable loop brought under tension. Each of the four isolation segments had different degrees of elasticity ranging from easily stretched to difficult to stretch. The scale of elasticity ensures most of the tow motions can be absorbed by the isolation segments.

8.3.9 Above-Water (Float) Measurements

The solar reference with shadow band, GPS, and PAR sensor all operate on SV3 power. No performance issues for any of the above-water (Float) instruments were detected during field tests, field commissioning, or operational demonstrations (Sect. 8.8.1–8.8.11). Power consumption of the instruments was within nominal limits (Sect. 8.9).

8.3.10 Near-Proximity Atmospheric Data

The C-OSPREy with quad detector and solar reference (Chap. 10) underwent field testing in a limited configuration, wherein the filter wheel was set to the ND 3.0 filter for sun pointing trials, and is described in Sect. 8.8.7.11. Detailed testing of the refinements made to the solar tracking capabilities as a result of the first field tests occurred during the solar eclipse on 21 August 2017; the results are described in Sect. 8.8.9.

The filter wheel capability was upgraded after the first field tests as described in Sect. 10.3.3. The final field testing of the upgraded C-OSPREy instrument system, including a Langley calibration, was performed on Mount Laguna in San Diego County (California) on 4 October 2017, and is described in Sect. 8.8.10. Summary results obtained with the C-OSPREy instrumentation are presented in Sect. 10.4.

8.3.11 Laboratory Instruments

Two instruments useful to laboratory exercises were built as part of the HARPOONS project. The CXR in a radiance embodiment (CXL) is based on the C-PHIRE instrument design and is described in Chap. 11 with additional aspects of the design clarified in Chap. 9. The principal purpose of the CXL is to contribute to the long-term traceability and short-term evaluation of the BSI calibration facility.

Another instrument useful to laboratory exercises that was built as part of the HARPOONS project is the CQM. The CQM is a portable source based on LED and other

COTS technologies and is designed to be used in the laboratory or field as part of assessing the long- and short-term performance and long-term stability of optical instruments. The CQM is described in Chap. 12.

8.4 Instrument Calibrations

The BSI optical calibrations used for the HARPOONS project strictly adhere to the standard calibration method described in the Protocols and in Appendix I of the NASA Technical Memorandum documenting the OSPREy System (Hooker et al. 2012a). The calibration methodology is straightforward to implement and requires a standard lamp that is traceable to the NIST Facility for Automated Spectroradiometric Calibrations (FASCAL) scale of spectral irradiance.

The objective of the standard calibration method is to determine the responsivity (including the immersion factor for in-water instruments) for the microradiometer and spectrograph components of C-PHIRE and C-OSPREy field instruments. Irradiance and radiance calibrations are performed on permanently dedicated optical benches, respectively. Once the responsivity has been established, immersion factors determined (by a laboratory experiment for irradiance and a calculation for radiance), and dark currents recorded, the measurements obtained for each channel (SiP) or pixel (CGS) can be converted to calibrated geophysical units.

8.4.1 Laboratory Facilities

The BSI lamp library was established as part of the OSPREy development activity (Hooker et al. 2012a). To populate the library, 21 tungsten-halogen 1,000 W FEL lamps were obtained. Nine lamps were calibrated by NIST, and the rest were uncalibrated, but seasoned lamps (by the supplier). To assess the stability of each lamp, they were operated for periods ranging from 4–35 h. Changes in brightness were typically ±0.02% per hour with a few lamps exhibiting slightly larger drifts, which were seasoned for an additional 8–30 h to improve their stability.

The calibration facility at BSI was upgraded to operate lamps of the OSPREy lamp library at the highest level of accuracy achievable. Upgrades included a new system for powering the lamps, which allows regulation of the lamp current to within a precision of 50 μA (or 0.0006% for a target amperage of 8.2 A). Other facilities required for accurate lamp transfers were also upgraded to reduce uncertainties caused by stray light, misalignment, and temperature variations.

The BSI calibration facility has three radiometers for calibration activities and maintaining optical standards: the OSPREy transfer radiometer (OXR) in an irradiance embodiment (OXE), the new CXL based on the C-PHIRE technology, plus a transfer radiometer built using the BSI ground-based UV (GUV) class of radiometers and called the XGUV. The older OSPREy transfer radiometer in a radiance configuration (OXL) was retired during the HARPOONS activity and replaced by the CXL for routine calibration operations. A summary of the field and laboratory instruments associated with the HARPOONS activity, along with the transfer radiometers used in the calibration process, are presented in Table 10.

8.4.2 Irradiance Bench Calibrations

The responsivity of an irradiance sensor is defined as the ratio of the average net light signal, derived from repeated measurements of the spectral irradiance from a standard lamp at a nominal wavelength and at a calibration distance of 50 cm as outlined in the Protocols, to the established irradiance of the source. Standard lamps issued by FASCAL are 1,000 W tungsten halogen FEL lamps.

The net signal is the difference between the signal when exposed to the lamp and the average dark signal that is obtained by either covering the sensor aperture with an opaque cap or by placing an occulting device between the sensor and the FEL lamp. The difference between the two darkening methods changes the net signals typically by less than 0.1% in the UV and visible (VIS) wavelength domains, and by less than 0.2% at short-wave infrared (SWIR) wavelengths.

Once the responsivity has been calculated, the spectral irradiance can be derived as the ratio of the field observation, after dark correction using a dark measurement obtained in the field, to the responsivity at the nominal wavelength (with the immersion factor included for in-water instruments).

8.4.3 Radiance Bench Calibrations

The standard calibration method for radiance sensors is similar to that described for irradiance sensors, except that the spectral irradiance of the standard lamp is replaced by the radiance of the calibration source. For radiance, the source is typically a standard reflectance plaque made of Spectralon and illuminated by a standard FEL lamp, and the instrument to be calibrated is facing the center of the plaque at an angle of 45°.

In addition to the reference and centerline distance between the plaque and the lamp, the radiance responsivity must take into account the spectral reflectance factor of the plaque for an incidence angle of 0° and a viewing angle of 45°. Once the source radiance is determined, the responsivity is calculated similarly to irradiance, i.e., as the ratio of the average net signal to the radiance of the source.

Given the spectral responsivity, the spectral radiance is derived as the ratio of the field signal from a natural target, after dark correction using a dark measurement in the field, to the responsivity at the nominal wavelength (with the immersion factor included for in-water instruments).

Table 10. A summary of the field and laboratory instruments (or instrument suites) built for, or associated with, the HARPOONS activity presented as a function of the fixed wavelength (e.g., microradiometer) detectors and corresponding nominal wavelengths (in nanometers). Hyperspectral spectrograph (HSG) units appear at the end of the detector lists, if present. For the TOW-FISH, C-AERO, and C-OPS instrument systems, all the radiometers, including the solar references, are spectrally identical. The C-OSPREy solar reference has three more microradiometers than the radiance instrument, as shown by the detector list to the right of the nominal wavelengths, and the C-HyR profiler has a separate L_u HSG positioned to measure very close to the sea surface when profiling commences (Fig. 26). Instruments built or modified for HARPOONS are shown in slanted typeface; the instruments in plain typeface supported HARPOONS objectives. The number of radiometers and their type are shown with E for irradiance and L for radiance.

TOW-FISH 1L,2E		C-OSPREy 1L,1E			C-AERO 2L,1E		C-HyR 2L,2E		C-OPS 1L,2E		OXE 1E		CXL 1L		XGUV 1E	
															1	290
															2	300
															3	313
							1	313	1	313						
1	320	1	320	1	1	320	2	320	2	320	1	320	1	320	4	320
2	340		340	2	2	340	3	340	3	340	2	340	2	340	5	340
3	380	2	380	3	3	380	4	380	4	380	3	380	3	380	6	380
4	395						5	395	5	395						
5	412		412	4	4	412	6	412	6	412	4	412	4	412		
6	443	3	443	5	5	443	7	443	7	443	5	443	5	443	7	443
							8	465	8	465						
7	490	4	490	6	6	490	9	490	9	490	6	490	6	490	8	490
8	510				7	510	10	510	10	510	7	510	7	510		
9	532		532	7	8	532	11	532	11	532	8	532				
10	555	5	555	8	9	555	12	555	12	555	9	555	8	555	9	555
11	589	6	589	9	10	589	13	589	13	589			9	589		
12	625	7	625	10	11	625	14	625	14	625	10	625	10	625		
											11	665			10	665
13	670	8	670	11	12	670	15	670	15	670			11	670		
14	683				13	683	16	683	16	683	12	683	12	683		
15	710	9	710	12	14	710	17	710	17	710	13	710	13	710		
16	780	10	780	13	15	780	18	780	18	780	14	780	14	780	11	780
17	820	11	820	14												
18	875	12	875	15	16	875	19	875	19	875	15	875	15	875	12	875
		13	1,020	16	17	1,020					16	1,020	16	1,020		
		14	1,245	17	18	1,245					17	1,245	17	1,245		
		15	1,640	18	19	1,640					18	1,640	18	1,640		
19	HSG	16	HSG	19†	20	HSG‡					19	HSG§	19	HSG		

† C-OSPREy reference does not have a filter wheel.   ‡ C-HyR has a separate L_u HSG.   § OXE HSG has 256 pixels.

8.4.4 Solar Calibrations

In addition to a standard reflectance plaque (radiance) calibration, the C-OSPREy radiance instrument was also calibrated using the Langley technique for solar observations of the direct solar irradiance. Field commissioning data obtained for the C-OSPREy instrument suite included contemporaneous observations with a MicroTops II sun photometer that was also calibrated using the Langley technique (Sect. 8.8.10).

The C-OSPREy calibration via the Langley technique (Slusser et al. 2000) involves observations of the direct solar irradiance at different solar zenith angles. Because of the need for varying solar zenith angles, which also varies the amount of atmosphere attenuating the solar illumination, the measurements are obtained for a cloud-free sky in the morning or afternoon, i.e., after sunrise or before sunset, respectively. From these measurements, the hypothetical signal amplitude, F_0, that the instrument would measure outside Earth atmosphere is calculated using an extrapolation technique. Because the Sun is a stable source (variations in the solar output between 300–1,600 nm are less than 0.1%), the instrument responsivity can be determined from F_0 and the known extraterrestrial spectrum of the Sun.

S.B. Hooker, R.N. Lind, J.H. Morrow, J.W. Brown, R.M. Kudela, H.F. Houskeeper, and K. Suzuki

A stable atmosphere (i.e., constant aerosol loading) during the period of data acquisition is a prerequisite for accurate Langley calibrations. High mountains above the boundary layer and away from pollution sources are considered ideal locations, e.g., Mount Laguna (San Diego, California). For the instruments used by Schmid et al. (1995 and 1999), the uncertainty of F_0 was between 0.6–1.6%, depending on wavelength, for all channels unaffected by gaseous absorbers (e.g., ozone and water vapor). A similar uncertainty can be achieved for the C-OSPREy instrument. The extraterrestrial solar spectrum is known only to within an uncertainty of 1–3% (Gueymard 2003), and the total uncertainty achievable with the Langley technique is limited to about the same range.

8.4.5 Calibration Monitoring

Controlling instrument calibration uncertainties over time is an important goal for maintaining the ability of radiometric instrument suites to obtain high quality data. Changes in the output of working standards caused by aging can be assessed by comparing these standards in regular (e.g., yearly) intervals with a NIST Standard of Spectral Irradiance (e.g., NIST lamp F-616). In addition, newly calibrated instruments are used to compare working standards monthly. Greater than a 0.5% difference is sufficient to trigger a deeper investigation into the behavior of an apparently outlying lamp.

Working standards are also compared with other lamps of the OSPREy Lamp Library following the hierarchical approach outlined in Sect. 6.8 of Hooker et al. (2012a). For quality control, the time that a lamp is powered is recorded by the operator in a metrology notebook located in the darkroom. The so-called burn times are reviewed annually during the lamp assessment. Aged lamps are retired and new lamps are seasoned in preparation for transferring the calibration information.

Standard lamps are not the only part of the calibration trail that must be maintained. High precision shunts and multimeters must be used to ensure that the lamps are run with the correct current. NIST traceability for to these devices is maintained using periodic (e.g. as recommended, or bi-annually for multimeters) recalibration at known laboratories. As a result of the OSPREy project (Hooker et al. 2012a), two moderate-bandwidth transfer radiometers are also available and maintained, the XGUV and the OXL, which are used to monitor lamps during use and especially during lamp calibration transfers to working standard lamps.

8.5 Instrument Characterizations

The following characterizations or analyses were performed for the new radiometers built for the HARPOONS project (Table 10) with only a subset documented in detail, because some are either already well documented

within the BSI calibration environment or are not significant contributors to the final uncertainty budget for the principal data products derived from the optical measurements:

- Directional Irradiance Response;
- Directional Radiance Response;
- Immersion Factor;
- CGS Pixel-to-Wavelength Function;
- CGS Slit Scattering Function;
- Stray Light Effects;
- Filter Spectral Response;
- Filter Center Wavelength;
- Calibration Measurement;
- Temperature Effects;
- Nonlinearity Effects;
- Lamp Irradiance;
- Radiance Plaque Reflectance;
- Detector and Aperture Fouling; and
- Polarization Sensitivity.

The first eight of these are considered in this section and the latter seven are considered as part of presenting the initial aspects of the uncertainty budget in Sects. 8.6.1–8.6.8.

8.5.1 Directional Response

The directional response of a C-PHIRE irradiance instrument was characterized using the BSI Directional Response Tester (DRT). The DRT is equipped with a computer controlled rotary table and hardware to mount the instrument. The generalized setup is shown in Fig. 86, wherein the required baffling to minimize stray light contamination at the instrument aperture is not shown for brevity and clarity. The axis of rotation is tangent to the instrument front surface, which is defined by the rim of the instrument end cap. The rim of the end cap also serves as the outer shadow ring, and the center (tip) of the sensor diffuser is in the same plane defined by the rim.
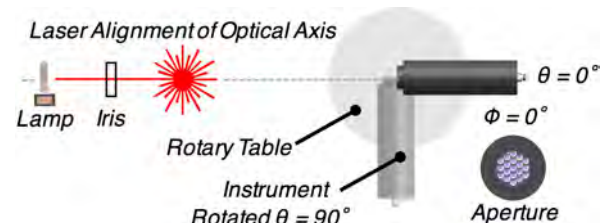
Fig. 86. A schematic of the DRT, wherein the alignment of all components along the optical axis (gray dashed line) is done with a laser. Rotations around the long axis of the instrument are indicated by ϕ. Baffling components are not shown for clarity.

The rotation angle, θ, of the table is zero when the instrument is pointed directly at the light source, in which case the instrument aperture is aligned perpendicular to the light source. The DRT mounting hardware allows the manual rotation of the test instrument around the center optical axis to characterize the directional response as a function of the azimuth angle, ϕ. An FEL lamp with a limiting aperture (iris) serves as the light source, which is mounted 165 cm from the diffuser. The limiting aperture ensures only the diffuser on the instrument is illuminated and baffling that is part of the DRT apparatus ensures only the beam of collimated light through the limiting aperture reaches the diffuser.

Prior to measuring the directional response, the instrument is aligned with a laser. The laser is mounted behind the lamp and its beam is aligned such that it is collinear with the optical axis, which is defined by the center of the lamp filament and the center of the test instrument. By holding a mirror flush against the rim of the instrument end cap and observing the retroflection of the laser beam, it is ensured that the instrument is aligned perpendicular to the optical axis when the rotary table is in the $\theta = 0°$ position. The uncertainty of the 0° position is 0.10°.

The DRT apparatus is enclosed with black baffles (curtains) specifically selected for low reflectivity. A black wall is installed approximately halfway between lamp and the test instrument. The wall has an aperture where it intersects the optical axis. The diameter of the aperture is selected such that the complete diffuser of irradiance is illuminated under all conditions, but yet small enough to reduce stray light in the test compartment to a negligible amount, i.e., less than 0.1%.

After the test instrument is properly aligned, the FEL lamp is powered up and allowed to stabilize. The rotary table is then moved from $-110°$ to $+110°$ in 1° steps. The average of measurements at angles smaller than $-98°$ are used to determine the dark current of the test instrument, which is subtracted from measurements at all of the other angles. DRT measurements are carried out in two azimuth orientations, 0° and 90°. The first measurement is performed at $\phi = 0$ with the index mark (indentation in end cap) facing up.

8.5.1.1 Directional Irradiance Response

The cosine error $\epsilon(\lambda, \theta, \phi)$ of a test instrument is calculated in accordance with CIE (1982) and Seckmeyer et al. (2001) and is defined as

$$\epsilon(\lambda, \theta, \phi) \;=\; \frac{T(\lambda, \theta, \phi)}{T(\lambda, 0, \phi)\cos(\theta)} \;-\; 1, \qquad (1)$$

where λ is wavelength, θ is the incidence angle of the radiation (equal to the angle of the rotary stage), ϕ is the azimuth angle of the instrument (Fig. 86), and T is the test instrument signal (voltage) with the dark current removed. The denominator is the ideal angular response,

that is, the reading of the radiometer is proportional to the $\cos(\theta)$. For an ideal instrument, ϵ is zero at all angles θ and ϕ.

In addition, the mean cosine error, $\bar{\epsilon}$, is calculated by averaging measurements performed at positive and negative incidence angles, i.e., $\bar{\epsilon} = 0.5\big[T(\lambda, \theta, \phi) + T(\lambda, -\theta, \phi)\big]$. The error in measuring irradiance for a uniform (isotropic) radiance distribution is defined as

$$\varepsilon(\lambda, \phi) \;=\; \frac{\int_0^{90} \big[\bar{\epsilon}(\lambda, \theta, \phi) + 1\big]\cos(\theta)\sin(\theta)d\theta}{\int_0^{90} \cos(\theta)\sin(\theta)d\theta}, \qquad (2)$$

wherein the two integrals are evaluated from the discrete data using the trapezoidal rule (i.e., approximating the region under the graph of the function as a trapezoid and calculating its area). The mean isotropic error, $\bar{\varepsilon}$, is calculated by averaging $\varepsilon(\lambda, 0)$ and $\varepsilon(\lambda, 90)$.

Average cosine errors for wavelengths less than 780 nm are typically less than 2% when $\theta < 65°$, and 10% or less for $65 < \theta < 80°$, which is in compliance with the Protocols. The analysis shows that cosine errors depend only slightly on azimuth angle for wavelengths up to 780 nm. For longer wavelengths, the ability of the secondary diffuser to remove azimuth asymmetries is reduced due to the declining diffuser scattering properties. As a result, cosine errors at longer wavelengths are larger, and may be slightly asymmetrical about $\phi = 0°$. The cosine error of the microradiometer 875 nm channel, however, depends only slightly on azimuth angle, because for C-PHIRE instruments it is mounted in the center of the array of 18 microradiometers.

The deviations between the measurement components for adherence to a cosine response is approximately 2% or less for wavelengths less than 780 nm, as shown in Table 11, which is compliant with the Protocols.

Table 11. The average isotropic cosine errors, $\bar{\varepsilon}$, in percent as a function of λ in nanometers.

λ	$\bar{\varepsilon}$	λ	$\bar{\varepsilon}$	λ	$\bar{\varepsilon}$
320	2.2	490	1.7	670	1.8
340	2.1	510	1.5	683	1.6
380	1.8	532	1.4	710	1.8
395	1.3	555	1.6	780	3.1
412	1.4	589	1.8	820	4.4
443	1.5	625	1.8	875	6.9

For the 780 nm wavelength and longer, *the increase in $\bar{\varepsilon}$ is not understood and is being investigated.*

8.5.1.2 Directional Radiance Response

The directional characterization of a radiance radiometer is performed in a darkroom using the DRT apparatus and is used principally to determine the instrument

field of view (FOV). Because the array of microradiometer (SiP) channels within an EAL instrument are not collocated (Fig. 2), the most accurate directional response measurements of all channels using this method requires an optical alignment of each channel individually (a very tedious and time consuming procedure).

For the characterization described here, the only ideally aligned channel is 625 nm, because it is in the center of the microradiometer array. All other channels are laterally displaced, and the directional response profiles of off-axis channels are directionally shifted to within less than 1°, depending on location (these shifts partially cancel when calculating the average of measurements at positive and negative angles).

The results of the directional characterization of the CXL show an average directional response $\epsilon(\lambda, \theta, 0)$ of 15° full width at half maximum (FWHM) or a half angle FOV, hereafter half view angle (HVA), of 7.5°.

The 7.5° HVA result is compliant with the Protocols, which require a HVA that is less than 10°, *but it is slightly less than the nominal 9° HVA that has been cited in past descriptions of the radiance FOV.*

Consequently, an investigation of the calibration and characterization history of this design was made in an attempt to discern when the disparity occurred.

The investigation revealed that the original two-gain microradiometer had a roughly 9° half angle, but subsequent improvements in the electronic circuitry to include an additional gain stage and other changes resulted in a narrowing of the FOV to approximately 7.5° HVA, (Hooker et al. 2012a). With the exception of radiance sensors designed for above-water radiometry, all modern microradiometer systems use microradiometers having a HVA of 7.5° and three gain stages (yielding 10 decades of dynamic range).

Directional features outside an 11° half angle of incidence appear in the CXL SWIR channels that are not apparent in observations obtained at shorter wavelengths.

Although not confirmed by the tests, *a likely explanation is that the anomalous directional features result from reflections internal to the design wherein the black anodization is not sufficiently black in the SWIR domain.*

Evidence supporting this conjecture is that the standard microradiometer detector for wavelengths shorter than the SWIR is a Hamamatsu S1226, which features silicon suppression in the IR domain. The photodetectors used for the 1,020, 1,245, and 1,640 nm channels are designed not to suppress the IR sensitivity and are enhanced for use in this application. The SWIR shoulders are likely not stray light inside the DRT test chamber, because they do not appear in the 875 nm waveband, nor in others in the visible region of the spectrum.

For characterizing the spectrograph component of the CXL, the instrument was aligned such that the spectrograph fiber entrance was collinear with the optical axis, thus precluding geometric artifacts resulting from the fixture apparatus.

While remaining compliant with the Protocols at 8.5°, the HVA of the spectrograph component is approximately 1° larger than the microradiometer HVA. This results from uncertainties involved in optimizing the pairing of an optical fiber collector with microradiometer collectors in a hybridspectral instrument. The maximum aperture of the collector itself is defined by the numeric aperture of the bundle, convolved with the subminiature version A (SMA) connector FOV restrictions. In practical use, the bundle with the mating SMA is potted to constrain micro-bending variations that develop when the bundle is flexed, which must be minimized. It is this potted assembly that is installed into the bottom of a Gershun tube which defines the actual FOV.

Recognizing that there are benefits to matching the microradiometer FOV with the spectrograph FOV, *an improvement planned for a future revision will attempt to modify the mechanical assemblies to more closely match the FOV of each subsystem.*

Near-angle features are apparent in the spectrograph FOV analysis. While these are not completely understood, a likely explanation is that they result from light reflecting from the surface edge of the spiral anti-reflection helix that is used to define the Gershun tube.

8.5.2 Immersion Factor

The immersion factor is a necessary part of the characterization of an in-water instrument, because it corrects the instrument calibration, which is performed in air, to account for changes in transmissivity at the sensor aperture (glass or diffuser) when in water, i.e., it corrects for the change in medium between the calibration process and the use of an-water instrument in the field.

For a radiance instrument, the immersion factor is calculated rather than measured, for which the in-water responsivity is smaller than in air for two reasons:

- Air and water have different refractive indices, and the transmission through the interface between air and the quartz radiance window is different than the transmission through the interface between water and the window; and

- The solid angle (or field of view) of the radiometer is smaller in water than in air.

The immersion factor for radiance, $F_L(\lambda)$, is calculated in accordance with the Protocols using the formulation

$$F_L(\lambda) = \frac{n_w(\lambda)\big[n_w(\lambda) + n_g(\lambda)\big]^2}{\big[1 + n_g(\lambda)\big]^2}, \qquad (3)$$

where $n_w(\lambda)$ is the refractive index of seawater, and $n_g(\lambda)$ is the refractive index of the radiance glass (i.e., quartz)

window. The $n_w(\lambda)$ term in (3) is parameterized as a function of wavelength using

$$n_w(\lambda) \;=\; 1.31891 \;+\; \frac{6.31446}{\lambda - 139.596}, \qquad (4)$$

which is a fit to measurements of the refractive index of pure water measured by Austin and Halikas (1976). The front window is made of quartz glass and $n_g(\lambda)$ is parameterized with

$$\begin{aligned} n_g(\lambda) \;=\; & 1.7395 \;+\; 12.121\lambda^{-1} \;-\; 1{,}865.6\lambda^{-2} \\ & +\; 771{,}416\lambda^{-3}. \end{aligned} \qquad (5)$$

For an irradiance sensor, the immersion factor cannot be calculated and must be measured with a laboratory apparatus.

There is no absolute truth in characterizing the immersion factor of an irradiance diffuser, i.e., there is nothing that can be purchased from a standards laboratory that will allow a comparison of the experimental results with a set of known values; *the immersion factor is achieved experimentally by following an accepted protocol as accurately as possible.*

The spectral immersion factors for the C-PHIRE in-water irradiance instrument were determined with an apparatus patterned after the Compact Portable Advanced Characterization Tank (ComPACT) introduced by Hooker and Zibordi (2005). The apparatus consists of a cylindrical water vessel with an inner diameter of 23.5 cm and a height of 50 cm. A light source consisting of a small 1,000 W tungsten halogen lamp (approximating a point source) and powered by a stabilized power supply is mounted 62 cm above the top of the vessel, which has an aperture with an inner diameter of approximately 45 mm. Three knife-edge baffles with a diameter of approximately 16 cm are installed inside the vessel to minimize reflections and stray light contributions.

The test instrument is inserted through a water-tight flange from the bottom of the vessel. The vessel is filled with distilled water and any contamination such as dust floating at the surface is carefully removed with a syringe. A long pipette is used to remove air bubbles clinging to the collector or the vessel. A high-accuracy pressure gauge is used to measure the water level in the vessel with an accuracy of 1 mm. A BSI single-channel irradiance sensor with sensitivity between 400–600 nm is mounted 60 cm away from the lamp and is used to monitor the lamp output during the test.

Test measurements consist of *wet* readings of the test instrument at different water levels and *dry* readings of the instrument with no water in the vessel. Dry readings are performed before and after the wet test and the two results are averaged. Before the commencement of dry readings, the irradiance diffuser of the test instrument is cleaned with alcohol.

Wet measurements are performed at water levels between 3–30 cm, as measured from the top of the irradiance diffuser. Water is slowly drained from the vessel, while readings of the test instrument, the pressure gauge, and the monitor detector are recorded. A typical sequence of wet measurements lasts 14–15 min, resulting in approximately 13,000 data points for microradiometers and about 4,300 data points for the spectrograph. Dark measurements are also performed by placing an opaque cap above the opening of the vessel.

Immersion factors are calculated from these measurements according to the procedure outlined by Mueller et al. (2003). Corrections are applied to adjust for the following:

1. The attenuation of the lamp radiation at the air-water interface;

2. The attenuation over the water path length, which is a function of depth and wavelength; and

3. The change in solid angle of the radiation from the light source that arrives at the diffuser that is caused by the change in direction of light rays at the air-water interface, and which varies with wavelength and water depth.

Variations of the lamp output are corrected using measurements of the monitor detector. The refractive index of water, $n_w(\lambda)$, which is required for the first and third corrections, is parameterized in (4).

The complete derivation is given in Petzold and Austin (1988), so only a brief summary is provided herein. By using the Fresnel reflectance equations, the transmittance through the water surface, T_s, is

$$T_s(\lambda) \;=\; \frac{4n_w(\lambda)}{\left[1 + n_w(\lambda)\right]^2}. \qquad (6)$$

The transmittance through the water path, T_p, is given by

$$T_p(\lambda) \;=\; \mathrm{e}^{-K_d(z,\lambda)}, \qquad (7)$$

where z is the path length.

The change with water depth z of the refracted solid angle subtended by the collector, W, as viewed from the lamp filament, is given by the factor

$$W(z,\lambda) \;=\; \left[1 \;-\; \frac{z}{d}\left(1 \;-\; \frac{1}{n_w(\lambda)}\right)\right]^{-2}, \qquad (8)$$

where d is the distance of the lamp source from the collector surface. The immersion correction factor for irradiance, $F_E(\lambda)$, is then calculated for each depth z as

$$F_E(\lambda) \;=\; \frac{E_a(\lambda)}{E_w(z,\lambda)}\, T_a(\lambda)\, T_p(\lambda)\, W(z,\lambda), \qquad (9)$$

where $E_a(\lambda)$ and $E_w(z,\lambda)$ are the measured irradiance in air and the measured irradiance in (usually pure) water at depth z, respectively.

8.5.3 CGS Pixel-to-Wavelength Function

The pixel-to-wavelength mapping function of the CGS spectrograph internal to a C-PHIRE radiance radiometer was determined by using the spectrograph to measure the irradiance of a low-pressure mercury-argon (HgAr) discharge lamp. The resulting spectrum is recorded as a function of pixel number of the spectrograph array sensor and is parsed into several spectral segments with one distinct spectral line from the HgAr source per segment. Gaussian functions of the type similar to (10) are fitted to each segment and the center pixel number of the fit function is determined,

$$G(\lambda_s) \;=\; a \exp\left[\frac{(\lambda_s \,-\, b)^2}{2\,c^2}\right], \qquad (10)$$

where λ_s denotes the spectral segment, and a, b, and c are fit parameters. The parameter b is interpreted as the center wavelength of the spectral line for the chosen segment. The fitted value is generally a rational number, while the pixel number of the array sensor is an integer.

The nominal wavelengths of the spectral lines (Lide 1993) are plotted against the pixel numbers determined from the Gaussian fits. Then, a third-degree polynomial of the type

$$\lambda_f(p) \;=\; C_0 \;+\; C_1\,p \;+\; C_2, p^2 \;+\; C_3\,p^3, \qquad (11)$$

is fitted to the data, where λ_f is the fitted wavelength, and C_0, C_1, C_2, and C_3 are fit coefficients. The residuals of the typical fits, calculated as the difference between the nominal wavelengths and the fitted wavelengths, λ_f, derived from spectrograph data, are to within 0.3 nm. The small size of the residuals indicates that a third-degree polynomial provides adequate accuracy to specify the pixel-to-wavelength mapping function for this spectrograph type.

8.5.4 CGS Slit-Scattering Function

The slit-scattering function (SSF), also known as the slit function or the bandpass function, of a spectrograph is defined as the spectrum measured by a spectrograph when illuminated with a narrow-band light source. It can be described either as a function of wavelength or as a function of the pixel number for the spectrograph array detector.

The stray light correction procedure for each spectrograph requires a measurement of the spectrograph SSF over the entire wavelength range, whereby a stray light correction matrix is determined using a method similar to that suggested by Kreuter and Blumthaler (2009) and applied to spectra that have been corrected using the dark signal data.

The SSF for the CGS spectrographs used in the HARPOONS project was determined using a single helium-neon (HeNe) laser line (632.8 nm) in the BSI laboratory.

The laser provides a strong spectral line source whose line width is very narrow, so this measurement directly describes the SSF.

The test apparatus includes the laser, a diffraction grating, the spectrograph, and a narrow slit. The laser beam is directed at the grating and the slit is positioned such that the first diffraction order falls on the slit. The beam passing the slit falls on a diffuser made of polytetrafluoroethylene (PTFE), also known as Teflon™ when manufactured by the Chemours Company (Wilmington, Delaware), that is mounted in front of the entrance optics of the instrument being tested. By using a grating, any potential side modes of the laser are removed from the laser beam.

To extend the dynamic range of the test, spectrograph measurements were performed at four different integration times (5, 100, 200, 1,000 ms), and the four measurements were combined manually. For example, a short integration time (5 ms) is needed to describe the region spectrally near the peak of the laser line to avoid saturation, while a longer integration time (200 or 1,000 ms) is required away from the peak to describe out-of-band and stray light characteristics. A plot of the SSF for CGS spectrograph serial number 004 is shown in Fig. 87.
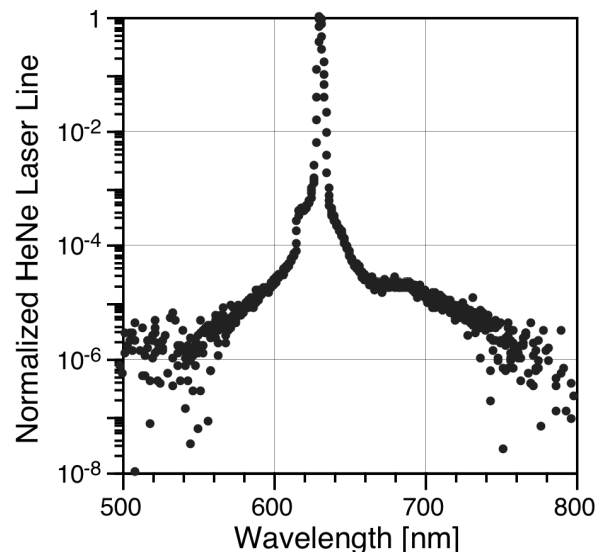
Fig. 87. A spectrum of the slit-scattering function for CGS spectrograph serial number 004 using a HeNe laser line (632.8 nm). The original resolution of the data is discernible and shows how well the peak is discriminated.

8.5.5 Stray Light Effects

The stray light correction matrix is used to remove stray light contributions from the spectrograph data and is derived from the slit-scattering function described in Sect. 8.5.4. The method of setting up the matrix and the associated stray light correction is based on the procedure developed by Kreuter and Blumthaler (2009). According

to this method, the spectrum measured by the spectrograph can be written as

$$\begin{aligned} \vec{S} &= \vec{S}_{\text{IB}} + \vec{S}_{\text{SL}} \\ &= \vec{S}_{\text{IB}} + \mathbb{D}\,\vec{S}_{\text{IB}} \\ &= \left[\mathbb{I} + \mathbb{D}\right]\vec{S}_{\text{IB}}, \end{aligned} \quad (12)$$

where $\vec{S}$ is the column vector of the measured net (dark corrected) signal, $\vec{S}_{\text{IB}}$ is the contribution of the net spectrograph signal from the *in band* (subscript IB) response, $\vec{S}_{\text{SL}}$ is the contribution from stray light (subscript SL), $\mathbb{I}$ is the identity matrix, and $\mathbb{D}$ is the stray light distribution matrix.

The purpose of the stray light correction is to find $\vec{S}_{\text{IB}}$. Rearranging the terms in (12) and applying matrix operations results in

$$\begin{aligned} \vec{S}_{\text{IB}} &= \left[\mathbb{I} + \mathbb{D}\right]^{-1}\cdot \vec{S} \\ &= \mathbb{C}\cdot \vec{S} \end{aligned} \quad (13)$$

where $\mathbb{C}$ is the stray light correction matrix.

The stray light distribution matrix $\mathbb{D}$ is a square matrix equal to the number of pixels of the spectrograph array sensor. The matrix element $d_{i,j}$ of $\mathbb{D}$ (with i and j indicating row and column, respectively) can be written as

$$\begin{aligned} d_{i,j} &= t_3 + t_2|i-j|^{-t_1} & \text{if } |i-j| \text{ iń IB,} \\ d_{i,j} &= 0 & \text{if } |i-j| \text{ in IB,} \end{aligned} \quad (14)$$

where iń indicates $|i-j|$ is outside IB (i.e., not in). The parameters t_1 and t_2 are determined by fitting a function of the type $f(\Delta p) = t_2|\Delta p|^{-1}$ to the slit-scattering function (Sect. 8.5.4).

According to Kreuter and Blumthaler (2009), the value of the t_3 parameter is determined such that when the signal that is corrected for stray light, the signal then fluctuates about zero for those wavelengths wherein the actual signal should be zero. For the solar spectrum, this is the case for wavelengths below 290 nm due to ozone absorption in the Earth atmosphere.

Note that the t_3 variable cannot generally be determined from measurements of the slit-scatting function, because stray light can originate from photons with wavelengths outside the spectral range of the spectrograph. The method by Kreuter and Blumthaler (2009) provides a simple method to account for these photons by adjusting parameter t_3.

When applying the aforementioned method to a spectrograph measurement used by a radiance instrument, it was discovered that the stray light contribution cannot be sufficiently reduced to acceptable levels for calibration and validation activities. The reason is that the stray light contribution generally increases towards shorter wavelengths, which cannot be explained by the shape of the slit-scattering function.

To apply a correction for this problem, an alternative stray light distribution matrix $\mathbb{D}$ is used with $d_{i,j}$ defined as:

$$\begin{aligned} d_{i,j} &= t_3 + t_2|i-j|^{-t_1} + t_4|i-j| & \text{if } |i-j| \text{ iń IB,} \\ d_{i,j} &= 0 & \text{if } |i-j| \text{ in IB,} \end{aligned} \quad (15)$$

following the nomenclature established in (14). Once the stray light distribution matrix is established, the stray light correction matrix $\mathbb{C}$ is calculated, and measured spectra $\vec{S}$ are corrected for stray light according to (13). The results are tested by measuring the spectrum of an FEL lamp, attenuated with one of several long-pass filters. The transmission of these filters increases exponentially over a range of approximately 50 nm from virtually zero to almost one.

Additional experience obtained with the CGS spectrographs has revealed that the average value of the net signals measured from 179–246 nm at each at each integration time can be subtracted from measurements at all wavelengths to correct for stray light. Ideally, stray light corrected spectra should vary about zero for wavelengths below 250 nm. This approach assumes that the actual output of the calibration lamp is negligible in this wavelength range, which is an agreeable assumption for the calibration lamps used by BSI, which are 1,000 W FELs (either NIST standards or working standards).

8.5.6 Microradiometer Spectral Response

The spectral response functions of the microradiometer channels are characterized with the BSI Spectral Response Tester (SRT). The SRT apparatus consists of a 1,000 W xenon arc lamp and a grating double monochromator with prism predisperser, designed and built by BSI. The two single monochromators that make up the Czerny-Turner double monochromator are stacked vertically and share a common shaft to which the gratings are mounted. This design ensures that the two single monochromators are always synchronized. Each of the two monochromators is equipped with three diffraction gratings designed for different wavelength ranges.

The intensity of radiation exiting the monochromator is characterized as a function of the monochromator wavelength setting with photodiodes that have a responsivity calibration traceable to NIST. The current produced by these reference detectors is measured with a Keithley Instruments Inc. (Cleveland, Ohio) model 6485 picoammeter. For determining the wavelength mapping of the monochromator, a mercury-argon (HgAr) discharge lamp is mounted in front of the entrance slit of the monochromator. Table 12 presents an overview of the monochromator specifications of the SRT.

Table 12. The monochromator specifications for the BSI SRT.

Parameter	Specification
Focal Length	500 mm
Focal Ratio	f/5
Configuration	Grating 1: 2,400 grooves/mm
	Grating 2: 1,200 grooves/mm
	Grating 3: 300 grooves/mm
Dispersion	Grating 1: 0.35 nm/mm
	Grating 2: 0.69 nm/mm
	Grating 3: 2.80 nm/mm
λ Range	Grating 1: 200–600 nm
	Grating 2: 600–1,100 nm
	Grating 3: 1,100–2,000 nm
λ Accuracy	Grating 1: ±0.1 nm
	Grating 2: ±0.2 nm
	Grating 3: ±0.8 nm

To characterize the spectral response of an irradiance instrument, the radiometer is placed directly behind the exit slit of the monochromator with the beam exiting the monochromator centered on the radiometer diffuser. To characterize a radiance radiometer, the beam exiting the monochromator is directed into an integrating sphere with a 25 cm diameter and the radiometer is mounted at the exit port of the sphere. The data acquisition entails at least three measurements:

1. The test instrument signal $\widetilde{T}_i(\lambda_s)$ for the light observed at each channel i as a function of SRT wavelength λ_s using the xenon lamp as the light source;

2. The monitor detector signal $\widetilde{M}_X(\lambda_s)$ for the light observed using the xenon lamp (subscript X); and

3. The monitor detector signal $\widetilde{M}_D(\lambda_s)$ for the light observed using the discharge lamp, i.e., HgAr wavelength standard, (subscript D).

Because some instruments have wavelengths spanning the UV–SWIR domains (e.g., C-OSPREy), the sequence is performed with all three SRT gratings. The scans are used to compare the net signals of the test instrument with the net signals of the monitor detectors to calculate spectral response functions. The procedure takes the finite bandwidth of the SRT and potential wavelengths misalignment errors into account.

UV measurements starting at a wavelength λ_s less than 150 nm, where no detectable radiation exists, are used as dark signals to correct the light measurements, which produce the net signals $T_i(\lambda_s)$, $M_X(\lambda_s)$, and $M_D(\lambda_s)$ for the three measurement sequences above, respectively.

The wavelength reported by the SRT may deviate from the true wavelength, λ. The difference, $\Delta\lambda \equiv \lambda_s - \lambda$ depends on wavelength and is determined by analyzing the spectrum of the HgAr lamp. In brief, $M_D(\lambda_s)$ is parsed into segments that are centered at the following spectral lines of mercury and argon spanning (approximately) 250–1,650 nm, which fully encompasses the spectral range for HARPOONS instruments:

- 253.652 nm, 289.36 nm, 296.728 nm,
- 302.150 nm, 334.148 nm,
- 404.656 nm, 435.835 nm,
- 546.074 nm, 576.959 nm,
- 696.543 nm,
- 763.511 nm,
- 826.452 nm,
- 912.297 nm, 965.779 nm,
- 1,013.975 nm, 1,047.005 nm,
- 1,128.74 nm, 1,295.6659 nm,
- 1,529.582 nm, and 1,651.986 nm.

A Gaussian function $G(\lambda_s)$ of the type in (10) is applied to determine the a, b, and c fit parameters, wherein b is interpreted as the center wavelength of the spectral line for the chosen segment. Wavelength shifts, $\Delta\lambda$, are calculated for all segments as the difference between the fit parameter b and the true wavelength of the spectral line taken from Lide (1993). A wavelength correction function $\Delta\lambda(\lambda)$ for the wavelength range of interest is determined by linear interpolation, and the net signals $T_i(\lambda_s)$ and $M_X(\lambda_s)$ are corrected accordingly resulting in new wavelength-corrected functions $T_i'(\lambda_s)$ and $M_X'(\lambda_s)$.

The *relative spectral response function*, γ, for channel i is calculated as

$$\gamma_i(\lambda) = \frac{T_i'(\lambda_s)}{M_X'(\lambda_s)} \Gamma(\lambda), \qquad (16)$$

where $\Gamma(\lambda)$ is the NIST-traceable responsivity of the monitor detector provided by the manufacturer, Newport Corporation (Irvine, California).

The γ_i values are normalized by the maximum spectral value, resulting in the normalized relative spectral response function, $\widehat{\gamma}_i(\lambda)$. The $\widehat{\gamma}_i(\lambda)$ function is artificially smoothed due to the finite bandwidth of the monochromator (Table 12). This smoothing effect is reduced with a deconvolution algorithm that is based on the following approximation:

$$\frac{\gamma_i^d(\lambda)}{\widehat{\gamma}_i(\lambda)} \approx \frac{\widehat{\gamma}_i(\lambda)}{\gamma_i^c(\lambda)}, \qquad (17)$$

where $\gamma_i^d(\lambda)$ is the deconvolved relative spectral response function, which is ideally the true response function, and $\gamma_i^c(\lambda)$ is the convolution of $\widehat{\gamma}_i(\lambda)$ with the slit function $\psi(\lambda)$ of the monochromator

$$\gamma_i^c(\lambda) = \frac{\int \widehat{\gamma}_i(\tau)\,\psi(\lambda-\tau)\,d\tau}{\psi(\tau)\,d\tau}, \qquad (18)$$

where τ is used to create the shift in λ for the convolution and the denominator is a normalization that scales
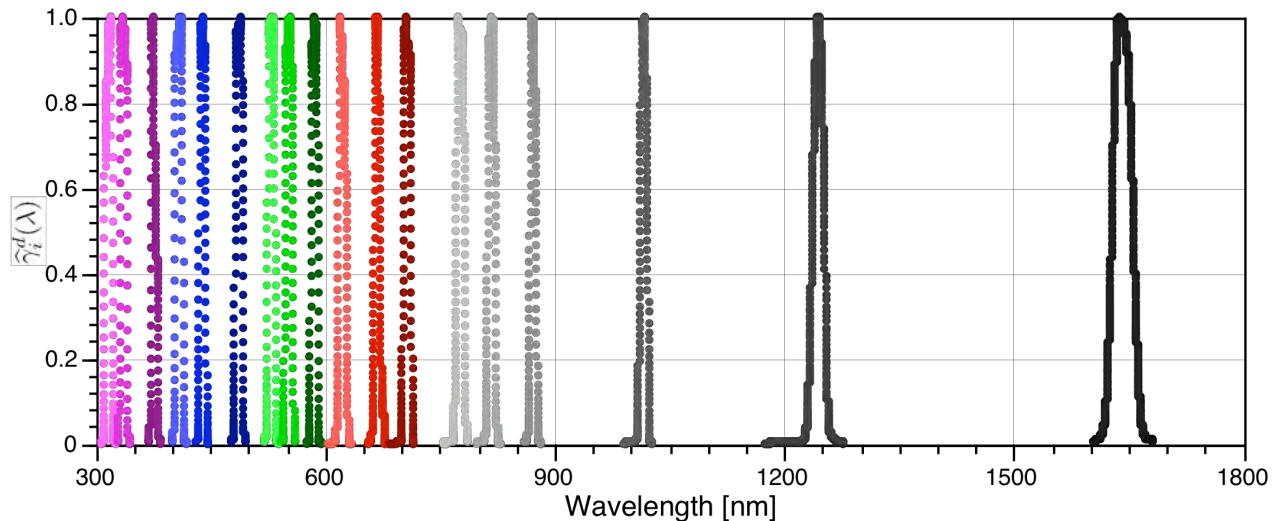
Fig. 88. The normalized deconvolved relative spectral response function, $\widehat{\gamma}_i^d(\lambda)$, of an EPIC (C-PHIRE) above-water irradiance (EAE) instrument. The original resolution of the data is discernible and shows how well the peaks are discriminated.

the convolution such that wavelength integrals of differing resolution and the convolved spectra become equal.

Given $\widehat{\gamma}_i(\lambda)$, $\gamma_i^d(\lambda)$ can be estimated using (18) and by rearranging (17). The resulting deconvolved spectral response is somewhat affected by noise in the measurement. In order to reduce this effect, $\widehat{\gamma}_i(\lambda)$ is set to 0.0001 if the normalized response is smaller than 0.0001. The deconvolved result is limited to four orders of magnitude because of this restriction.

As a final step, $\gamma_i^d(\lambda)$ is normalized, resulting in a normalized deconvolved relative spectral response function $\widehat{\gamma}_i^d(\lambda)$. These functions are shown in Fig. 88 for an EAE test instrument. For each channel of the test instrument, the centroid wavelength for each λ_c is calculated from

$$\lambda_c \;=\; \frac{\int \lambda\, \widehat{\gamma}_i^d(\lambda)\, d\lambda}{\int \widehat{\gamma}_i^d(\lambda)\, d\lambda}, \tag{19}$$

which is provided for completeness.

8.6 Estimation of Uncertainties

The methods used herein to calculate and express uncertainties are based on International Organization for Standardization (ISO) procedures (ISO 1993), which were adopted by NIST (Taylor and Kuyatt 1994). In brief, uncertainty components are grouped into two categories, denoted *Type A* and *Type B* standard uncertainties. Type A uncertainties are evaluated by statistical methods, whereas Type B uncertainties are evaluated by other means. The combined standard uncertainty is calculated from the individual components and represents the estimated standard deviation of the results. The result is multiplied with a

coverage factor of $k = 2$, resulting in an expanded uncertainty with a 95% confidence level.

The uncertainty estimates discussed herein are valid when instruments are characterized and operated with attention to detail, i.e., the Protocols must be strictly applied. Sources of uncertainty resulting from improper handling and operation are not considered. For example, an inaccurate measurement of the distance between a radiometer and calibration target, or improper installation of the radiometers in the field (e.g., failure to level and clean the instruments, selection of a location whereby near-proximity objects may cast a shadow or a reflection on an instrument aperture, etc.) are not considered and will negatively impact the uncertainty budget.

A comprehensive uncertainty analysis was conducted during the development of the OSPREy sun photometer showed the use of moderate-bandwidth radiometers, such as the XGUV and OXL, are suitable to transfer calibrations of FEL lamps (Hooker et al. 2012a). Uncertainties related to the relatively large bandwidth of these instruments are on the order of 0.3%.

8.6.1 Calibration Measurement

To estimate the combined uncertainty of the net calibration signals of field sensors, the following components are considered: a) lamp current, b) distance scaling, c) lamp alignment, d) laboratory stray light, e) photon and electronic noise, plus f) the aging of working standards.

The lamp current is determined by measuring the voltage across a $0.0100042\,\Omega$ precision shunt with a high quality digital multimeter (Agilent model 34401A, Santa Clara, California). The former has a NIST traceable calibration by Davis Inotek (Irwindale, California) and the latter has a NIST traceable calibration by Keysight Calibration

(Irvine, California). The accuracy of the current is dominated by the calibration uncertainty of the shunt, which is 0.002%. The percentage change in the spectral irradiance of FEL lamps is approximately $5 \times (600/\lambda)$, with λ in nanometers (Kostkowski 1997). Using this formula, the current measurement of the spectral irradiance has an uncertainty of 0.02% at 300 nm and 0.01% at 600 nm.

The distance between the calibration standard and the front of the diffuser of an irradiance sensor is measured with an aluminum rod that is accurately machined to a length of 500±0.1 mm. Calibration of irradiance sensors requires scaling according to the inverse square law. The uncertainty of the distance measurement using this rod is approximately 0.5 mm, which translates into an irradiance uncertainty of 0.2%. Sperling et al. (1996) investigated the effect of alignment errors for FEL lamps with respect to lateral displacement and rotation. For the alignment accuracy that can be achieved with the laser alignment system used for the calibration of radiance instruments, e.g., Sect. 6.3.2.1 in Hooker et al. (2012a), the standard uncertainty in spectral irradiance that is caused by these alignment uncertainties is 0.1%.

The radiance calibration requires a scaling of the spectral irradiance from the reference distance, $l_r = 500$ mm, to the typical lamp-to-plaque calibration distance of $l_c = 1{,}219$ mm. By setting the uncertainty (u) terms $u(l_r) = 0.5$ mm, $u(\Delta l) = 1.0$ mm, and $u((l_c) = 1.0$ mm, the relative standard uncertainty of the irradiance scaling equates to 0.35%. Calibration of irradiance EAL sensors requires scaling according to the inverse square law. By setting the distance between the EAL aperture and the front of the lamp post, l_p to 2,461 mm and the absolute uncertainty of this distance $u(l_p)$ to 1 mm, the relative standard uncertainty of the irradiance scaling calculates to 0.38%.

The contribution of stray light to the total spectral irradiance at the diffuser of irradiance sensors was determined by comparing light signals with dark signals that were either measured by capping the collector or by using an occulting device. The stray light contribution to the light signal is less than 0.2% at all wavelengths and typically less than 0.1% at wavelengths in the visible. When calibrating irradiance sensors, the dark signal is measured with the occulting device. A large fraction of the stray light, therefore, affects both light and dark measurements equally and is subtracted when the net signal is calculated. The relative standard uncertainty of the net signal caused by stray light is, therefore, only 0.05%.

Stray light is an important factor for radiance measurements because the calibration approach requires the illumination of a relatively large target. Radiation reflected off the target that is intercepted by radiance bench components is partially reflected onto the target and contributes to the plaque brightness. This stray light was quantified by measuring the irradiance at the center of the plaque with and without the plaque being covered by black baffling material. For the large plaque, the stray light contribution is approximately 0.6%, and for the small plaque,

it is 0.1%. The latter value was used for calculating the combined uncertainties presented below (Sect. 8.6.9).

Radiance radiometers are calibrated by measuring the dark and light signals of the calibration target for one minute. The sampling rate for the microradiometer component is set to 10 Hz and spectrographs are sampled with multiple integration times, ranging from 10–1,625 ms depending on the intended use of the instrument. From these measurements, the relative standard error of the net calibration signals are determined. For the microradiometer component of irradiance sensors, the contribution of noise to the average net signal is less than 0.01% for all channels. For the spectrograph component, the contribution is 1% at 300 nm, 0.5% at 350 nm, 0.1% at 400 nm, and below 0.03% for wavelengths greater than 450 nm. For radiance sensors that are calibrated for radiance, the noise contribution is 0.06% for UV channels and less than 0.01% for visible and SWIR channels. For radiance sensors calibrated for irradiance, the noise contribution is 0.01% for all microradiometer channels.

Changes in the flux output of working standards caused by aging is assessed by comparing lamp standards in regular (e.g., annual) intervals with a designated primary standard (e.g., lamp F-616). To limit usage of the primary standard, working standards are also compared with other lamps in the OSPREy Lamp Library following the hierarchical approach outlined in Sect. 6.8 of Hooker et al. (2012a). With this approach, the uncertainties caused by the output of working standards is limited to 0.5%.

8.6.2 Temperature Effects

Short-term (e.g., 1 min to 1 h) changes in dark current are predominantly a function of instrument temperature. For the microradiometers, the uncertainty caused by changes in the dark signal due to temperature variability was estimated from the following parameters: a) the temperature stability of the microradiometer component of the instruments; b) the change in dark current as a function of temperature; c) the change in dark current in relationship to the noise in the dark current, which defines the detection limit; and d) the difference between the detection limit and the spectral irradiance of relevant targets (e.g., calibration sources or spectral global irradiance).

For irradiance radiometers, the spectral irradiance of relevant targets is typically more than a factor of 3,000 times larger than the detection limit, expressed as noise equivalent irradiance as documented in Sect. 8.9.3. by Hooker et al. (2012a). From the parameters introduced above, the standard uncertainty in measurements of spectral irradiance calculates to 0.01% in the visible range. Channels that use InGaAs photodiodes (e.g., measurements at 1,245 and 1,640 nm) have a larger uncertainty of 0.1% because of the larger temperature coefficient of these detectors compared to the SiP channels.

For radiance instruments calibrated to measure radiance, the spectral radiance of relevant targets is typically

a factor of 600 times larger than the detection limit. The standard uncertainty is 0.02% in the visible range and approximately 0.5% for channels using InGaAs detectors. For radiance sensors measuring the direct solar irradiance (C-OSPREy), variations in the dark current are insignificant because the spectral irradiance of the Sun is a factor of 1,000,000,000 times larger than the detection limit.

According to specifications provided by the photodiode manufacturer, Hamamatsu Photonics (Hamamatsu City, Japan), the change in sensitivity of the silicon photodiodes in microradiometers is less than 0.01% per °C for wavelengths between 190–600 nm over the operational temperature range 5.5–35.5°C. This equates to a standard uncertainty of 0.08%. The uncertainty increases with wavelength and is 0.05% at 700 nm over the same temperature range, which translates to a standard uncertainty of 0.43%. The temperature coefficients of InGaAs photodiodes are considerably larger than that of silicon detectors, and increases with wavelength. For the 1,640 nm channel, the standard uncertainty is approximately 0.1%.

The dark current of miniature spectrographs is generally very sensitive to temperature, as documented in Sect. 7.4.5 of Hooker et al. (2012a). For the Carl Zeiss Monolithic Miniature-Spectrometer (MMS) UV-VIS II spectrograph, a 1°C change in temperature at 30°C typically leads to a change in the dark current by 10–20 digital counts, which is 0.03–0.06% of the saturation signal of 32,768 digital counts. The CGS is comparable to this, or slightly better, when corrected for its greater sensitivity. While these variations are small, changes in dark current can nonetheless lead to important uncertainties when the difference between light and dark signals is small.

The change in spectrograph sensitivity as a function of temperature is not specified by the manufacturer. An uncertainty of 0.03% for sensitivity drift per °C is valid for the CGS between 400–700 nm. The uncertainty rises to 0.1% per °C at 800 nm, and dips back down to 0.08% per °C at 850 nm.

8.6.3 Nonlinearity Effects

The nonlinearity of a microradiometer is primarily a consequence of gain changes combined with offset drifts. Uncertainties caused by offset drifts are minimized in the C-PHIRE radiometers deployed on the SV3 (solar reference) or towed behind it (TOW-FISH) through the use of high resolution temperature sensors on the photodetector array and automated measurements of the nighttime dark current. For C-OSPREy, dark current characterization is obtained by capping the instrument before and after field measurement time periods, and in between if the time periods span more than 4 h.

Linearity testing of microradiometers are discussed in Sect. 2.3 in Hooker et al. (2012a). Results indicate that microradiometers are linear to within 0.7% between photodiode currents of 20 nA and 160 mA (the high value is close to the saturation current). The resulting standard uncertainty is 0.4%.

Nonlinearity of the spectrograph component mostly arises from the fact that different integration times have to be used for calibration scans and field measurements because of the large difference between the irradiance (or radiance) of the calibration target and the natural target. During the OSPREy activity (Hooker et al. 2012a), nonlinearities of the Zeiss MMS spectrographs were tested by setting up the instruments in front of an FEL lamp and measuring spectra with several integration times ranging between 5 ms and signal saturation (typically 500 ms).

Dark measurements were performed at each integration time within 2 min of the *light* measurements to ensure that the results were not affected by dark signal drifts. The derived net signals were divided by the integration time. For integration times between 50–500 ms (i.e., the range typically used for field measurements), normalized spectra were linear to within 1% for wavelengths between 350–785 nm. Below 350 nm, interference with stray light and noise makes an assessment difficult. Additional analyses with normalized spectra for the Zeiss spectrographs used in OSPREy sensors showed linearity to within 1% for wavelengths between 330–1,080 nm. Preliminary testing with the CGS spectrographs show superior performance, but to allow a safety margin for incomplete analyses, the standard uncertainty associated with nonlinearity of spectrograph measurements is retained at 1%.

8.6.4 Lamp Irradiance

When the BSI lamp library was established, the inventory of NIST lamps were intercompared and agreed to within ±2% (Hooker et al. 2012a), which is a very good result considering that some lamps were rather old and were calibrated using different NIST scales of spectral irradiance. A protocol on the usage of the lamp library was developed with the goal of preserving the spectral irradiance scale over a timescale of 15 y or more.

8.6.5 Radiance Plaque Reflectance
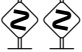
BSI radiance calibrations use two reflectance standard plaques, as follows: a) a large $60.7{\times}60.7\,cm^2$ plaque, and b) a small $25.4{\times}25.4\,cm^2$ plaque. Both of the plaques were procured from Labsphere, Inc. (North Sutton, NH). The large plaque was calibrated by Labsphere and the reflectance factor expanded ($k = 2$) uncertainty is 1.8% between 380–410 nm, 1.5% for 410–700 nm and 1.8% between 700–780 nm. The small plaque was calibrated by the NIST Spectral Trifunction Automated Reference Reflectometer (STARR), and the reflectance factor expanded ($k = 2$) uncertainty is 1% for 280–290 nm, 0.88% for 300–400 nm, and 0.87% for 410–1,700 nm.

Because of its small size, *there are FOV issues associated with transferring the small plaque SWIR calibration to the large plaque, because the device involved needs to also support in-water (larger FOV) instruments.*

S.B. Hooker, R.N. Lind, J.H. Morrow, J.W. Brown, R.M. Kudela, H.F. Houskeeper, and K. Suzuki

These issues are being addressed, and the small plaque calibration scale will be used for future calibrations. The uncertainty of this plaque was used to calculate the combined uncertainties (Sect. 8.6.9).

8.6.6 Detector and Aperture Fouling

Changes in responsivity resulting from detector contamination are principally caused by how components are stored and handled, particularly during instrument assembly or during maintenance and repair operations. For example, the polarization filters sourced from Moxtek (North Orem, Utah) for the C-OSPREy sun photometer provide multiple benefits (i.e., broadband transmission and square edges for accurate orientation), but they also present a number of technical challenges to prevent their contamination.

⬦⬦ The Moxtek filters are so delicate that *the surfaces cannot be touched during installation, may only be handled by the edges with clean tweezers, and the polarizing surface may not be cleaned once contaminated.*

The small size and low mass of Moxtek filters require that they are carefully manipulated, and they must only be exposed to environments that mitigate the potential for contamination (e.g., a laminar flow cabinet).

To prevent contamination as part of building or servicing an instrument, filters and other optics (e.g., lenses) are stored in a dedicated area with restricted access. All but the most critical optical components are sorted, cleaned, and assembled in this dedicated area at a workstation used solely for this purpose. The handling and installation of the most critical optical components (e.g., Moxtek polarization filters) is performed in an Air Science (Fort Meyers, Florida) laminar flow cabinet designed to protect materials from particulate contamination. Room air passes into the cabinet through a high efficiency particulate air (HEPA) filter and exits uniformly by laminar flow to prevent the introduction of airborne particulates during assembly.

In addition to industry-standard static control measures (i.e., active monitoring of grounded operators and assembly surfaces), the critical electronics assembly area at BSI utilizes a bench top air ionizer to remove static charges from non-conductive objects and surfaces prior to assembling or servicing an instrument. As a final measure to prevent and remove sources of contamination, and to discourage accelerated degradation of optical and electronic assemblies, all EPIC and Expandable Technologies for Radiometric Applications (XTRA) instruments have the residual air evacuated from the environmentally sealed housings with a vacuum pump and are backfilled with ultra-high purity nitrogen gas.

Changes in responsivity resulting from aperture contamination (e.g., particle deposition, pollutants, biofouling, etc.) in the field are hard to quantify, because they depend on the platform location, position of the sensors on the platform, and environmental conditions around the platform. Biofouling of above-water irradiance radiometers is minimized by using a diffuser made of PTFE, an inert material that is easily cleaned by rain and wind. The solar reference on the SV3 is almost always in motion, so wind effects minimize permanent particle deposition. For in-water radiometers, HARPOONS missions are much shorter than the time period by which biofouling reaches the few percent level, which is about 21 d for a properly cleaned aperture (McLean et al. 1997).

A recurring source of uncertainty is direct sun light that is scattered by particles on the aperture, especially the glass aperture of radiance instruments when measuring sky radiance. For the TOW-FISH, the radiance aperture is pointed downwards, so particle deposition is unlikely, and the backplane is in motion, which significantly minimizes permanent deposition. Because sunlight is about six to seven orders of magnitude brighter than the sky, even a small amount of contamination on an above-water radiance aperture can lead to large systematic uncertainties if sunlight reaches the aperture. To avoid the problem sunlight can create during sky viewing, C-OSPREy is equipped with a shroud that prevents direct sunlight from reaching the aperture except when the radiance instrument is purposely pointed at the Sun.

Because C-PHIRE instruments are hybridspectral and consist of more than one detector technology, comparison of data products is a primary *in situ* tool to detect contamination. Because data with discrepancies larger than a few percent can be detected and flagged as abnormal, a standard data product uncertainty of 5% is assumed as a comparison threshold.

8.6.7 Filter Contributions to Uncertainties

The capability of C-OSPREy radiance radiometer is enhanced by a filter-wheel assembly, which has nine positions and is mounted in line with the spectrograph fiber. The filter wheel and can be custom populated, but in the standard configuration, permits hyperspectral measurements in the following nine positions as follows:

1 Improved stray light correction with a 395 nm cut-on filter;

2–4 Polarimetry with three polarized filters (0°, 45°, and 90°, respectively);

5 Dark currents with an opaque disk (also, the filter-wheel assembly is sufficiently light tight that dark currents can be measured by moving the filter wheel to the half-way point between the filters);

6–7 Bright targets with two neutral density (ND) filters (3.0 and 1.5);

8 Dim targets with an open aperture; and

9 A home position (a half-way point).

Additional details about the C-OSPREy filter wheel and the installation of an encoder to improve performance are presented in Sects. 10.3.2 and 10.3.3, respectively.

The filters used in the C-OSPREy filter-wheel assembly are not independently characterized. The specifications from the selected manufacturers are used to determine if the filters meet the requirements for C-OSPREy observations. The filters used with the array of 15 microradiometers, as will all microradiometers, are characterized, as documented in Sect. 8.5.6.

The uncertainty associated with the transmission of filters for the filter-wheel assembly used in the C-OSPREy spectrograph component is estimated from the characterization procedure described in Sect. 8.5.6. The largest uncertainty component is the nonlinearity of the spectrograph measurements. Nonlinearity is particularly an issue for the ND 3.0 filter because signals measured with and without the filter are different by a factor of 1,000. The standard uncertainty of filter transmission was set to 1.0% based on the discussion of spectrograph nonlinearity in Sect. 8.6.3.

8.6.8 Polarization Sensitivity

The direct component of sunlight is essentially unpolarized (measurements include a negligible polarization due to atmospheric effects). In contrast, the indirect skylight component is polarized by transmission through the atmosphere (which is easily demonstrated with polarizing sunglasses, wherein skylight is no longer uniformly colored), and again at the dielectric interface of the sea surface. The impact of polarization is negligible for EPIC (C-PHIRE) above- and in-water profiling irradiance instruments, denoted EAE and EPE, respectively, wherein the double Teflon diffuser removes polarization of the light. The above- and in-water profiling radiance instruments, denoted EAL and EPL, respectively, are influenced by polarization sensitivity. Because C-PHIRE instruments are hybridspectral and consist of more than one detector technology, the microradiometer component and the spectrograph component must be characterized for polarization effects.

To test the sensitivity of the filter channels to polarization orientation, an external polarizer was placed in front of the microradiometer array and mechanically rotated while the microradiometer array sampled at 5 Hz.

The size of the polarizer in its holder was smaller than the array, and only a subset of filters were tested, specifically those at 490, 510, 589, and 625 nm.

The observed variation was within ±1%, which equates to an estimated uncertainty of 0.46%. A larger polarizer will be obtained so that in the future all microradiometers can be sampled simultaneously.

Ideally, the sensitivity of the spectrograph component should not depend on whether or not the light to be measured is polarized, or on the orientation of the polarization.

The degree of spectrograph sensitivity to polarization was measured by setting an external polarizer to different angles. For these tests, the instrument was placed facing a Spectralon reflectance plaque on the radiance optical bench. A handheld polarizer was used to visually determine that the radiance source produced unpolarized light. During the test, the external polarizer was set to 0, 45, 90, and 135°. The spectrograph component was least sensitive when the polarizer was set to 90°. The polarization sensitivity was strongest at 800 nm, and the results were consistent to within the measurement uncertainty. The testing revealed that the spectrograph signal in the visible varies by ±1.5% as a function of polarization, which equates to approximately a 0.86% uncertainty.

The spectrograph polarization characterizations presented above were performed with a Zeiss MMS UV-VIS II device, which is an earlier embodiment of the CGS device used for C-PHIRE instruments.

A decade of experience with a number of small Zeiss spectrographs suggests a C-PHIRE instrument likely has a similar or improved performance, but this assumption requires confirmation.

8.6.9 Combined Uncertainties

The expanded ($k = 2$) uncertainty of standards issued by FASCAL is 1.56% at 250 nm, 1.12% at 350 nm, 0.63% at 655 nm, 0.47% at 900 nm, and 0.33% at 1,600 nm (Yoon et al. 2002). The cited uncertainties are only guaranteed by NIST for the time of the lamp calibration. Uncertainties in the transfer of the FASCAL scale represented by standard lamp F-616 to working standards include uncertainties of the calibration method, stray light in the laboratory, and uncertainties in lamp alignment and lamp current.

The standard uncertainty of the method to interpolate values of spectral irradiance tabulated in the NIST certificate of lamp F-616 is 0.1%. The method of scale transfer has an uncertainty of 0.15%. Uncertainties arising from stray light in the laboratory are considered insignificant (less than 0.05%) for two reasons:

1. The contribution of stray light to the total spectral irradiance at the diffuser of the transfer radiometer is less than 0.2% at all wavelengths; and

2. The light paths for the reference standard (i.e., lamp F-616) and the working standard are identical and any stray light contribution cancels when performing the transfer.

The reference and working standards, as well as the two transfer radiometers, are held in place with kinematic mounts. Even though the distance between the lamp and a transfer radiometer may have an uncertainty as large as 0.5 mm, the effect on the transfer measurement is negligible, because both standards are similarly affected and the associated uncertainties cancel. The lamp power system can control the lamp current to within 0.006%. Any

systematic uncertainties in setting the lamp current (e.g., a systematic uncertainty in the shunt value used to calculate the current) would also cancel. The combined uncertainty of the scale transfer is calculated to be approximately 0.18%.

Table 13 presents the combined uncertainties for the sources identified and discussed in this section. The tabulated uncertainties refer to the visible and SWIR wavelength ranges. Some uncertainties (e.g., the noise contribution for the spectrograph component) increase towards shorter wavelengths in the UV, but the combined uncertainty is considered properly assessed with the information presented.

Table 13. The sources of uncertainty in percent affecting the measurement of the calibration signal of field irradiance (E) and radiance instruments, with the latter calibrated for radiance or irradiance (L_L and L_E, respectively).

Source and Type		E	L_L	L_E
Lamp Current	B	0.01	0.01	0.01
Lamp Alignment	B	0.10	0.10	0.10
Lamp Output Drift	B	0.50	0.50	0.50
Distance	B	0.20	0.35	0.38
Stray Light	B	0.05	0.10	0.05
SiP Noise	A	0.01	0.01	0.01
CGS Noise	A	0.03	0.06	0.03
Unexplained Variability	B			0.60
SiP Combined Uncertainty		0.55	0.63	0.88
CGS Combined Uncertainty		0.55	0.63	0.88

8.7 Data Acquisition and Processing

The overall software design for acquiring and processing all above- and in-water HARPOONS data is presented in Sect. 8.3.3. Data acquisition is accomplished using the DACPRO environment, and the data products derived from those observations are produced using PROSIT. An international DACPRO and PROSIT user community of research scientists, students, and technicians ensures both software environments are routinely evaluated to discover problems in the applications or documentation. The user community also recommends useful new features.

DACPRO and PROSIT workshops are held approximately on an annual basis (Table 14) and emphasize the linkages between acquisition and subsequent processing. The workshops and training sessions are also conducted at sea aboard ships, so hands-on experience is acquired. A principal objective is to establish an awareness that what is learned in data processing can be applied to improve data acquisition and vice versa. To ensure participants experienced thruster-assisted profiling with the new TOW-FISH backplane, a C-OPS with C-PrOPS accessory provided at-sea simulation of new capabilities.

Table 14. A summary of the workshops emphasizing three types of training: DACPRO (D) and PROSIT (P) software, plus at-sea hardware (H) training (including the C-OPS with C-PrOPS accessory, which is rather similar to the TOW-FISH instrument system in terms of the protocols used).

Start Date (days)	Location	Type
14 Oct. 2014 (3)	Akkeshi, Japan†	D H P
26 Aug. 2015 (2)	San Francisco, CA	D
19 Jan. 2016 (1)	Tokyo, Japan	D P
28 Oct. 2016 (1)	Santa Cruz, CA	D P
4 Dec. 2016 (1)	Tokyo, Japan	D P
16 Jan. 2017 (10)	La Parguera, PR	D H P
15 Jun. 2017 (1)	San Diego, CA	D H
6 Oct. 2017 (27)	Tokyo, Japan‡	D H P

† And TR/V *Misago Maru*   ‡ And R/V *Hakuho Maru*

8.7.1 DACPRO Software

LabVIEW was chosen for the DACPRO development environment, because LabVIEW enables use of measurement and control hardware in a single development environment, as well as offering seamless integration across multiple types of instruments, buses, and sensors. The NI Instrument Driver Network provides over 10,000 instrument drivers for connecting to third-party instruments.

LabVIEW has similarities to *traditional* software development tools (e.g., RealBasic, XCode, and Metroworks) in that code is written (but in a two-dimensional graphical approach), then it is debugged, and deployed. The integrated LabVIEW development environment is designed for engineers and scientists. Native to LabVIEW is a graphical programming language (G) that uses a data-flow model instead of sequential lines of text, thereby allowing the creation of functional code using a visual layout.

LabVIEW was selected as the runtime environment because LabVIEW provides standard libraries, analysis toolkits, and an open architecture that enables integration of any hardware device and any software approach. Use of these libraries and toolkits means the OSs can be different, and change over time, but the user will always be able to utilize the LabVIEW code without the developer having to rewrite and recompile on a regular basis.

The DACPRO software for the TOW-FISH with solar reference and accessories includes manual (operator enabled) and unattended (autonomous) operation modes. The latter capabilities include a system preference file for mission configuration, a daily schedule file describing when and how to collect data, power management of subsystems, management of data collection subsystems, plus periodic reporting of data collection activities and status. Subsystems are powered on when required and otherwise stay powered off to conserve battery power.

Data collection subsystems are started when required and otherwise are left off to minimize computer overhead

and memory usage. Data collected with DACPRO can be processed and visualized using PROSIT.

A light cast occurs at a user-specified interval set in a preferences file that establishes the sampling parameters, which is typically 30 min. The maximum number of light casts per day is also set by the user in the preferences file, and is usually set to 20.

⚠ Whether or not a light or dark cast is initiated and executed depends on the PAR sensor data, *wherein clear-sky conditions are required for a light cast and no measurable light is required for a dark cast*; if threshold requirements are not satisfied, a cast is not executed.

A light cast begins based on the user-specified options within the preferences file. Casts can start automatically based on time, or they can be controlled by sky conditions evaluated by the PAR sensor. For the latter, if the PAR sensor determines the prior 5 min history of observations established clear-sky conditions, a cast will be executed; otherwise it will not.

Once a cast is established as being executed, the subsequent sequence of steps in a light cast are as follows:

1. The light cast is initiated by powering on the solar reference and profiler instruments that had been turned off after the last cast, and activating data recording.

2. The thrusters are turned on using the user-selected thrust levels set in the preferences file.

3. After the backplane reaches the surface, which is determined by the pressure transducer and altimeter, the thrusters are turned off, unless the thrust-assisted descent option has been set in the preferences file. If the thrusters are used during descent, the thruster levels are set in the preferences file.

⚠⚠ *Using the thrusters during descent consumes more power from the payload batteries,* and shortens the nominal mission lifetime.

4. Data recording continues as the backplane slowly sinks vertically in the water column and is towed horizontally by the Float. When the backplane reaches the user-specified maximum recording depth or time during descent, whichever occurs first, the profiler instruments are all turned off.

5. The shadow band is turned on, and a fast hemispherical sweep is followed by a slower hemispherical sweep, which takes a total of about 90 s.

6. Data recording is terminated, and all equipment is turned off except the MacMini and the PAR sensor.

All data are recorded as American Standard Code for Information Interchange (ASCII) text using a format compliant with the SeaWiFS Bio-Optical Archive and Storage System (SeaBASS) architecture (Hooker et al. 1994).

A dark cast is rather similar to a light cast except the thrusters are not used, i.e., the profiler data are obtained at the TOW-FISH resting depth (typically about 5–6 m). The cast is initiated, and then data are recorded sequentially at all three microradiometer gain stages. A dark cast collects 70 s of data (i.e., approximately 450 samples) at each gain stage. The time needed to collect the dark data is approximately 4 min, which is about the same as a light cast.

It is also possible to collect shadow band observations outside the time period established for in-water profiling with the TOW-FISH. This capability allows for extra data for Langley calibrations (Sect. 8.8.10), and the resulting schedule is set in the preferences file. This option does not activate any of the in-water instrumentation, so it does not consume any power from the payload batteries; all power consumption is from the SV3 power system (CCU, APU, and solar panels), except for some losses to the MacMini back-up battery if interrupts occur.

The acquisition software maintains a cast history log. The user can select an option in the preferences file to safeguard against a defective PAR sensor. If the `OverridePAR` boolean is set to `true`, and if the immediately prior cast was not executed, the present cast is executed regardless of the PAR threshold logic. This prevents a significant loss of data due to a defective PAR sensor, while still saving battery energy. This is also follows from the reasonable expectation that the fair-weather mission perspective of HARPOONS sampling will result in at least 50% of the casts being executed.

8.7.2 PROSIT Software

The prototype PROSIT application was developed using the Adobe Flex programming environment and deployed using Adobe Integrated Runtime (AIR). The main PROSIT computational module leverages the proven functionalities of the original GSFC processor, while employing a newly designed intuitive GUI. Adobe Flex was chosen for the development environment for the following reasons: a) Flex is an open source framework for developing and maintaining a Rich Internet Application (RIA); and b) Flex is designed to consistently deploy with all the major browsers, desktops, and operating systems.

Flex is very similar to *traditional* software development environments, like RealBasic, XCode, Metroworks, etc., in that the programmer writes line-by-line code, debugs it, and deploys the application. These traditional development tools, however, only leverage a single technology, are mostly proprietary, and require multiple builds to make the application available to the various OSs, and usually require recompiling for OS updates. Flex on the other hand combines multiple proven technologies, such as, ActionScript (AS) 3.0, Extensible Markup Language (XML), and Cascading Style Sheets (CSS). Flex also leverages Hypertext Markup Language (HTML), Flash Player, and AIR as the runtime environment. Use of these runtime environments means the OSs can be different, and

change over time, but if the end-user has the latest version of the AIR runtime, they will always be able to utilize the PROSIT application, without the developer having to rewrite and recompile on a regular basis.

AS 3.0 is an object-oriented programming language and follows European Computer Manufacturers Association (ECMA) specifications, i.e., ECMA-262. AS is very similar to Javascript, which could be used in a Flex application with no issues. The RealBasic code used for visualizations in the original GSFC processor was converted to AS. AS is a sophisticated language with the needed properties, methods, and functions to perform high-order mathematics. AS is also used for the GUI navigation logic.

XML is a generalized specification. Its major purpose is to aid in sharing commonly understood structured data within multiple information systems. It is recommended by W3C, and is an open standard that specifies lexical grammar and parsing requirements. XML, actually Maximum Experience Markup Language (MXML), was used in the layout of all the UI components. The MXML components communicate directly with AS, because the MXML components are converted to AS during compilation.

CSS is a style-sheet language that uses XML to describe how to present a document or, in this case, the UI. It is typically used to set global and sometimes local style rules (color, font, and size). In the case of Flex and the PROSIT application, it is used to define common fonts and styles across multiple graphical elements and to set the graphical icons for buttons. CSS is a standardized language that is understood across all major browsers.

Adobe AIR is the runtime environment, because AIR is a free download. AIR enables developers to package AIR applications into native apps for Windows and Mac OS. AIR applications can be developed using Flex, Ajax, and Flash, and then deployed directly to the desktop instead of having to use an HTML page and a browser for display. Consequently, what used to be considered a Web application can now be deployed as a stand-alone application that uses web technologies, but more importantly, with access to a local drive. Such access was not possible with prior Web applications because of security issues.

Flex programs executing in the Flash runtime environment can connect to servers and databases, but not the local machine. Flex programs that use AIR can connect to the local drives and make calls to remote servers. Flex communicates with *back-end* technologies using a number of *middleware* languages, e.g., HTML, Active Server Page (ASP), Hypertext Preprocessor (PHP), and Coldfusion Markup Language (CFML).

PROSIT uses Perl in the form of common gateway interface (CGI) scripts during the steps of uploading the data to the server, pre-processing the data, loading and sending of all data (both in the plot and in populating all the user interface components), the processing phase, and retrieving the analysis results. CGI is also used to communicate between the Flex application and the database

residing on servers that archive all of the uploaded data and results from the user community.

There is no need for a browser to use the PROSIT application. A browser is required to register as a user, change the user password, download the software from an exchange server, and access updates. The serverclient environment can be hosted on a single computer, which is how the application is built and tested (which allows the entire PROSIT environment to be taken into the field). The usual architecture is anticipated to be a user located at a site far removed from the shared server.

The primary data product PROSIT is designed to derive from AOP observations is $L_W(\lambda)$ from both above- and in-water instrument suites, e.g., airborne radiance radiometers and free-fall profilers, both with a solar reference (the former is not of immediate interest for HARPOONS, although C-OSPREy is capable of making above-water measurements of the sea surface if the proper viewing geometry is available, as follows:

1. The governing equation used for HARPOONS data products is

$$L_W(\lambda) \;=\; 0.54\,L_u(0^-,\lambda), \qquad (20)$$

where $L_u(0^-)$ is the upwelling radiance at null depth $z = 0^-$, wherein the 0.54 constant accurately transmits $L_u(0^-)$ through the sea surface (Mobley 1999).

2. The needed measurements are geolocation (typically from GPS) and Coordinated Universal Time (UTC); $L_u(z,\lambda,t)$, $E_d(z,\lambda,t)$, and $E_s(\lambda,t)$, with the latter needed for the normalized forms; the vertical tilt for all instruments; water temperature and salinity, if possible; plus IOPs or proxies (e.g., the chlorophyll concentration); and the diffuse solar irradiance, $E_i(0^+,\lambda,t)$, where $z = 0^+$ is immediately above the water surface, for the self-shading correction (Gordon and Ding 1992), which is obtained herein with the BioSHADE accessory to the solar reference.

3. Corrections include, but are not limited to, dark current subtraction at all gain stages, normalization of slow changes in solar illumination (e.g., solar zenith transit), aperture offsets with respect to the pressure transducer, and self-shading.

4. Constraints are vertical tilt filtering to within $5°$ and $E_d(0^-,\lambda)$ from the extrapolation interval to within 5% of $E_s(0^-,\lambda)$, i.e., $E_s(\lambda)$ transmitted through the surface to null depth.

5. Laboratory characterizations are a) NIST-traceable calibrations (Sect. 8.4), b) immersion factors for E_d (requires an immersion tank) and L_u (computed) as documented in Sect. 8.5.2, and c) many other characterizations that depend on the detector technology (Sects. 8.5 and 8.6).

6. Field characterizations are principally dark current measurements at all gain stages.

The principal publications to consult regarding the above are Hooker et al. (2013), Hooker (2014), and the Protocols.

The principal PROSIT data products derived from the above- and in-water AOP observations associated with hybridspectral in-water profiling instrument suites (i.e., the TOW-FISH with solar reference), wherein λ_Σ indicates both the 2,048 pixels of the CGS and the 18 SiP microradiometers, are as follows (wherein λ_Σ indicates the combination of the SiP and CGS spectral domains):

- Geolocation and solar geometry parameters (e.g., solar zenith angle, solar azimuth angle, etc.);
- $E_s(\lambda_\Sigma)$, $L_u(0^-, \lambda_\Sigma)$, and $E_d(0^-, \lambda_\Sigma)$;
- $E_i(0^+, \lambda_\Sigma)$ from shadow band data;
- E_d and L_u diffuse attenuation coefficients, $K_d(\lambda_\Sigma)$ and $K_{L_u}(\lambda_\Sigma)$, respectively, based on the in-water extrapolation interval;
- $L_W(\lambda_\Sigma)$ and $R_{\rm rs}(\lambda_\Sigma)$, plus normalized, $\left[L_W(\lambda_\Sigma)\right]_{\rm N}$, and exact forms, $\left[L_W(\lambda_\Sigma)\right]_{\rm N}^{\rm ex}$;
- Surface and underwater PAR parameters (e.g., euphotic depths, percent light levels, etc.);
- Fluorescence products, e.g., the depth of the chlorophyll and fluorescence maximums and fluorescence line height (FLH) parameters; and
- Common ocean color (OC) algorithm products (e.g., OC4, OC3M, etc.).

Additional products are derived if an upward irradiance, $E_u(\lambda_\Sigma)$, instrument is used, plus a variety of diagnostic parameters are provided to understand the details of the data products, e.g., the diffuse attenuation coefficient for pure water, $K_w(\lambda_\Sigma)$, bidirectional terms, etc.

8.8 Results

The results obtained during the HARPOONS project are organized chronologically based on the most significant field campaigns to test, commission, operationally demonstrate—and then refine or augment—the hardware, firmware, and software technologies that were developed (Table 9). Both sea and land campaigns were conducted as part of developing the TOW-FISH and C-OSPREy instrument suites, respectively. Although joint TOW-FISH and C-OSPREy deployments are anticipated (Fig. 71), the two systems are stand-alone capabilities that do not require interoperability—they can be deployed and evaluated independently.

8.8.1 R/V *Hakuho Maru* (March 2015)

The first HARPOONS field campaign was the KH-15-1 expedition along the coast of Japan aboard the R/V *Hakuho Maru*. The principal HARPOONS objective of this deployment was to test the CGS spectrograph to be used with C-PHIRE instruments, as well as the altimeter, gyro, and HyPower (hyperspectral power, data, and

telemetry) box, which were all included as part of the C-HyR profiler design (Chap. 3). The C-HyR accessory was shipped with a C-OPS equipped with a C-PrOPS accessory to Tokyo (Japan). The profiling system was assembled on the ship and deployed into Tokyo harbor. The C-HyR profiler is described in Chap. 3, and the results obtained in Tokyo Harbor are presented in Sect. 3.4.

The successes achieved with the C-HyR trials confirmed the following: a) the functionality of the Zeiss and tec5USA 2,048 pixel CGS spectrograph selected for HARPOONS; b) the ability to mount a spectrograph as an accessory with the optical fiber restrained in a rigid radiance collector assembly (RCA); and c) the capability to safely deploy an enlarged backplane into the ocean and control it with thrusters. Because of the vulnerability of the RCA to ship strikes, the thrusters ensured the backplane could be quickly maneuvered away from the ship after the instrumentation was lowered into the water. Similarly, during recovery, the thrusters allowed the backplane to held in a position wherein the RCA is safely pointed away from the ship.

The purpose of the RCA is to immobilize the optical fiber to prevent motion-induced perturbations to light transmission and to extend the L_u aperture beyond the perturbation field of the profiler backplane to allow observations with negligible shading contamination. Two variants for also immobilizing an irradiance optical fiber while being mounted on a profiler backplane were created and are presented in Fig. 89a. Another design variant for immobilizing the spectrograph optical fiber, wherein the fiber is fixed in a rigid tube that replaces a microradiometer in a 19-channel cluster, is shown in Fig. 89b. This latter variant was selected for the C-PHIRE instruments (Chaps. 9–11).
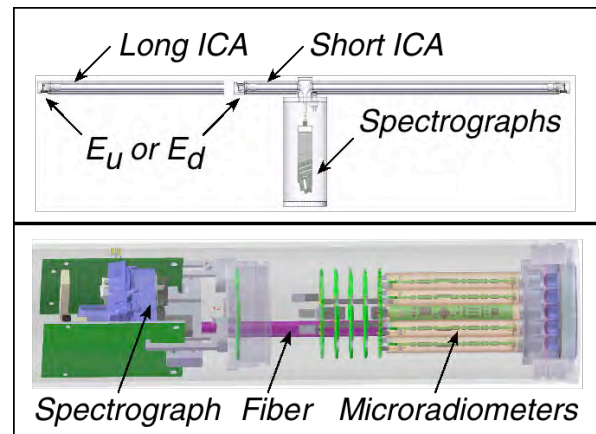
Fig. 89. Design variants for immobilizing the optical fiber in an instrument while being mounted on a profiler backplane (top and bottom, respectively): **a)** matching short (E_d) or long (E_u) irradiance collector assembly (ICA), with the latter lengthened to avoid shading perturbations; and **b)** a partial instrument rendering (no end cap), which was the basis for the C-PHIRE instrument design.

For the combined RCA and ICA designs, individual microradiometer instruments can be omitted or included. Omitting them reduces the overall weight and bulkiness of the profiler backplane, but the ability to intercompare two detector systems is lost. Three basic profiler designs using the concepts shown in Fig. 89 are possible:

1. A hyperspectral only instrument suite ($\lambda_{2,048}$) with configuration options to measure E_d and L_u; b) E_d and E_u; or c) E_u and L_u.

2. A separated hybridspectral instrument suite, wherein the ICA and RCA apertures (both $\lambda_{2,048}$) are paired with microradiometer instruments (both λ_{19}), for example, E_d and L_u for the former and E_u and L_u for the latter.

3. An integrated hybridspectral instrument suite with the spectrograph fiber ($\lambda_{2,048}$) replacing one of the 19 microradiometers (λ_{18}) in a radiance or irradiance radiometer (i.e., a configuration that follows the C-PHIRE design).

All three of the above profiler configurations require an accompanying instrument with matching wavelengths to measure the global solar irradiance, which should also preferably be equipped with GPS and shadow band accessories.

A conceptual drawing of what one version of a separated hyperspectral profiler might look like is shown in Fig. 90, wherein the hyperspectral capability is added as an accessory to the backplane used for the C-HyR instrumentation. The design permits both E_d and L_u hyperspectral observations very close to the sea surface while also allowing E_u and L_u microradiometer measurements to derive the Q-function (Morel and Gentili 1991, 1993, and 1996). To ensure coincident planar observations, the L_u instrument could be moved downwards, so the L_u microradiometer aperture matches the depth offset of the E_u microradiometer aperture with respect to the pressure transducer or high-precision altimeter.
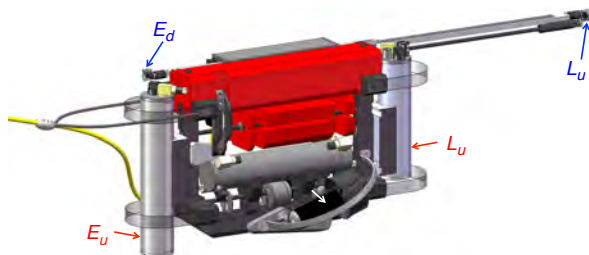
Fig. 90. A separated hybridspectral profiler concept drawing with the 19-channel microradiometer instruments labeled in red and the hyperspectral apertures in blue.

An instrument with only hyperspectral components would support the derivation of the Q-function and could be built by removing the microradiometer instruments in Fig. 90, and changing the E_d aperture to measure E_u. This configuration would require a long ICA to ensure

the E_u measurements were not perturbed by the profiler backplane. The approach of making the hyperspectral capability an accessory permits observations very close to the sea surface and straightforward configuration options, but the external collector assemblies make the hyperspectral apertures more vulnerable to deployment and recovery mishaps.

An autonomous system requires minimization of all vulnerabilities, because the principal operational mode is based on an operator not being able to intervene if a vulnerability rises to a threat level requiring an immediate intervention. Consequently, an integrated hybridspectral design was used for the C-PHIRE instrument suite (Chap. 9) that was developed for the HARPOONS activity.

8.8.2 R/V *Hakuho Maru* (November 2015)

The second field campaign was the KH-15-4 expedition to the Kuroshio Current (Japan) aboard the R/V *Hakuho Maru*. This deployment tested the first C-PHIRE radiometer, which was the solar reference for the C-OSPREy instrument suite. The solar reference was shipped approximately halfway around the world, set up, and then deployed much as it would during a HARPOONS mission. The field campaign involved the deployment of a C-OPS instrument suite, so some of the wavelengths in the new C-OSPREy solar reference were changed to match the C-OPS solar reference to maximize intercomparison opportunities. To test as many components as possible for the HARPOONS project, the C-OSPREy solar reference was deployed with shadow band and GPS accessories.

The first instrument built and evaluated in the field was an irradiance radiometer, because an irradiance instrument is more difficult to build than a radiance instrument (except for the C-OSPREy sun photometer, which is the most complex of the HARPOONS instruments, because it requires an internal filter-wheel assembly).

To acquire data from the new C-PHIRE instrument, the DACPRO LabVIEW environment needed to be ported to a PC to run on the Windows version of the LabVIEW software, because *Zeiss and tec5USA do not directly support the CGS on the Macintosh operating system with a device driver and DLL.*

This significant recoding exercise allowed the existing CGS device driver and DLL supplied by tec5USA for the Windows operating system to be used with DACPRO, so the new C-PHIRE instrument could be properly commanded and the data acquired.

To field test the first C-PHIRE solar reference, the instrumentation was mounted on a Telescoping Mount for Advanced Solar Technologies (T-MAST) and positioned next to a C-OPS solar reference (Fig. 91). A T-MAST can accommodate multiple instruments and the telescoping ability allows the instrument apertures to be raised

above any nearby obstructions that can cause light perturbations (Hooker 2010), i.e., reflections and shading, and to be lowered for easy access and safe stowage when data is not being recorded.
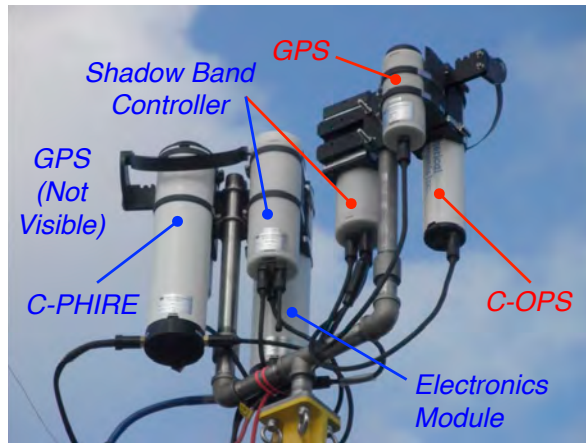
Fig. 91. The C-PHIRE solar reference (blue) next to a C-OPS solar reference (red) revealing the larger size of the former with respect to the latter. Both instrument systems had a GPS and a shadow band (the C-PHIRE GPS is behind the C-PHIRE instrument and is not visible).

The instruments mounts used with the T-MAST are specifically designed to make the positioning and leveling of multiple cosine collectors a straightforward exercise, thereby ensuring one instrument system is not a source of perturbations to a neighboring instrument system. The microradiometer arrays in the two references were almost spectrally identical (17 channels were the same), while remembering that the C-PHIRE instrument necessarily had one fewer microradiometer, because the spectrograph fiber replaced one microradiometer in the usual array of 19 microradiometers.

Because the spectrograph and the microradiometers have different bandwidths (i.e., approximately 0.4 nm for the former and 10 nm for the latter), the spectrograph data are binned to form equivalent 10 nm bandwidths to match the microradiometers. The inter- and intra-comparison of the various detector systems for the instrumentation shown in Fig. 91 are as follows:

a) The C-PHIRE spectrograph and C-PHIRE microradiometers agree to within 0.4–1.7%;

b) The C-PHIRE spectrograph and C-OPS microradiometers agree to within 2.3–3.4%; and

c) The C-PHIRE microradiometers and C-OPS microradiometers agree to within 2.9–4.1%.

The intracomparison of the C-PHIRE spectrograph and C-PHIRE microradiometers should exhibit the best agreement, because the two detector systems have the same temperature and are synchronized to exactly the same time base. All the results are to within 5%, which means all instruments performed to within nominal expectations.

8.8.3 R/V *Po'okela* (August 2016)

The third field campaign was in the coastal ocean near the LRI Wave Glider training facility located in Kawaihae Harbor (Hawaii). The SV3 and C-PHIRE instrument suites were air shipped to the facility, whereupon the SV3 was assembled at the facility, the optical equipment mobilized, and the combined SV3 and C-PHIRE instrumentation deployed from the R/V *Po'okela*. The principal objectives of the campaign were as follows: a) participate in SV3 at-sea launch and recovery training including time in the classroom to learn how to use the WGMS software; b) deployment of the completed C-PHIRE instrumentation system operating in manual and automated modes within an operational environment; and c) verification of data processing capabilities for the acquired data.

The LRI training began with classroom instruction followed by learning how to launch and recover an LRI Wave Glider. After the HARPOONS team achieved sufficient competency with the latter, continued expertise was obtained launching and recovering the NASA SV3. Evaluation of the capabilities of the TOW-FISH started with deploying it into the water while the SV3 was still on the deck of the R/V *Po'okela*. This simplified the operational environment and facilitated in-water access by the scientific team to observe the functioning of the sea cable with attached floats and compressible bladders, isolation segments, and the backplane.

The manual trials and swimmer observations confirmed the efficacy of the overall design and no significant deficiencies were detected. As a precaution, because of the presence of multiple swimmers documenting the in-water functions, an external strength member was added to the sea cable. This would ensure that if a swimmer were to bring the sea cable under an unanticipated load, the external strength member would protect the tow apparatus and attached equipment. This addition was retained for all subsequent SV3 deployments, because in each case, swimmers were present to document the functionality of the entire system.

The water depths off Kawaihae were 137–155 m. After the first deployment of the SV3 system in Hawaii, the distribution of floats and compressible bladders attached to the sea cable was refined. In addition, the elasticity of the isolation segments was tuned to match the oceanic swell. A cascade of elasticity was established as a sequence of shock cords attached between a series of sea cable loops, such that increasing tension was absorbed by sequentially longer lengths of shock cord. This allowed light to strong cable tension to be absorbed as the isolation segments progressively absorbed increasing tension on the sea cable.

The original design for obtaining vertical profiles with the TOW-FISH was based on the handheld procedures used with C-OPS equipped with the C-PrOPS accessory (Fig. 20) and C-HyR (Fig. 26). For handheld operations, the sea cable harness is attached to the irradiance instrument side of the backplane, the thrusters are canted to

drive the backplane away from the operator holding the sea cable, the radiance end cap, which contains the pressure transducer port, is elevated above the water surface, and only down casts are usually recorded (favorable currents can occasionally result in high quality up casts as measured by vertical tilts being less than 5°).

Trials after the start of the first SV3 field campaign confirmed the TOW-FISH could be trimmed to rise mostly vertically through the water column and the harness could be positioned very close to the center of mass. The latter suggested that the TOW-FISH could ascend and descend rather stably while being towed without a need for canted thrust to generate slack in the sea cable, so there was potentially no need for canted thrusters. Consequently, the end of the first field campaign did not use canted thrusters and relied on vertically oriented thrusters, although the cable harness point on the irradiance side of the backplane was retained. Figure 92 shows the TOW-FISH being towed by a barely visible SV3 in the clear blue waters off Kawaihae Harbor. The isolation segments appear as loops in the yellow sea cable.
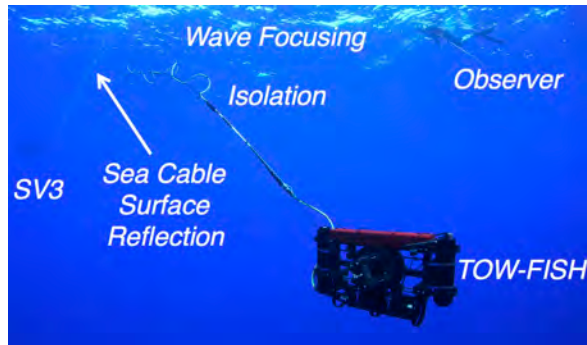
Fig. 92. The ascending TOW-FISH attached to the SV3 in the clear coastal waters near Kawaihae Harbor early in the first SV3 field campaign. The black SV3 is barely visible.

The field trials during the first field campaign primarily obtained data during down casts. To ensure the sea cable and harness sank below the aperture plate of the irradiance cosine collector, the shackle point was weighted.

Once the backplane reached the nominal resting depth of 5–6 m, *the sea cable catenary resulted in the harness and cable being above the cosine collector.*

This was not deemed a problem at the time, because up casts were usually not recorded, although 5 casts were recorded on the last day to understand the full dynamics of the TOW-FISH during towing. A total of 28 optical casts were obtained during the first field campaign.

8.8.4 R/V *Huki Pono* (August 2016)

The fourth field campaign was the second deployment of the SV3 system in the oceanic coastal waters off the island of Lana'i (Hawaii), which is the same geographical area where the Marine Optical Buoy (MOBy) site is located. The SV3 and TOW-FISH were air shipped to Lana'i City and trucked to the port of Manela. The SV3 was assembled outside next to a parking lot with shade, while the optical equipment was mobilized. The SV3 was then rolled down a driveway onto the dock, and the instrumentation was installed and secured aboard the R/V *Huki Pono.* The mobilization of the entire SV3 system outdoors demonstrated the portability of the instrumentation.

The principal objective of the fourth field campaign was to field commission the overnight autonomous capabilities of the SV3 system. To exploit the opportunity to collect up casts, the harness point for the TOW-FISH was changed to the radiance side of the backplane (Fig. 93) to allow up casts to be recorded without perturbations. To ensure the harness shackle point and sea cable did not fall under the radiance aperture, a small float was attached to the shackle point to make it neutrally buoyant. Swimmer observations during the first deployment of the TOW-FISH confirmed the sea cable and harness were not obstructing the radiance aperture.

Fig. 93. The TOW-FISH in the water with the harness and cable connection on the radiance side of the backplane with the SV3 readied for launch (left).

The SV3 could not be deployed at the MOBy site due to worsening sea state and wind from approaching typhoon Madeline, so the SV3 was deployed at the nearest safe location within the much quieter near-shore lee of Lana'i. Although close to the coast, the water depth was nonetheless quite deep (837 m). Intercomparisons of the remote sensing reflectance, $R_{rs}(\lambda)$, near the MOBy site (approximately 7 nmi away) show the C-OPS and C-PHIRE microradiometers agree to within the following: 3.0% UV; 2.4% blue; 3.3% green; 4.0% red; and 24.3% NIR (Fig. 94). The usable part of the lee was sufficiently close to the island that overnight autonomous operations were not considered safe. The water depths off Lana'i were 76–387 m.
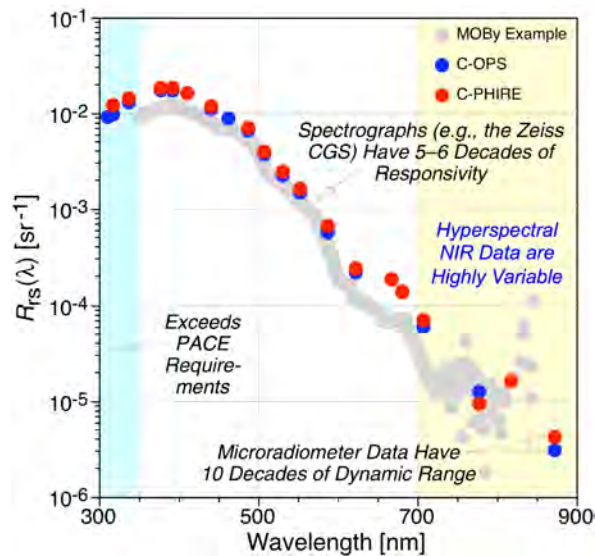
Fig. 94. An intercomparison of microradiometer R_{rs} data obtained with the C-PHIRE instruments on the TOW-FISH and the C-OPS validation instrument close to the MOBy site.

The MOBy example data shown in Fig. 94 are obtained nearby, but from a different time and from different extrapolation depths than C-OPS and C-PHIRE validation data, and are only provided to show the general shape of the R_{rs} spectrum offshore.

The NIR disagreement in the C-OPS and C-PHIRE intercomparison is a consequence of the low signal level and coarser C-OPS vertical resolution. The University of California Santa Cruz (UCSC) C-OPS was used to facilitate the training of UCSC team members, and did not have the C-PrOPS accessory. The larger difference in the NIR is almost the same as obtained in the C-OPS with C-PrOPS system 21 intercomparison to C-OPS system 34 without C-OPS (Table 3), which was 25.1% in the NIR. The better agreement in the UV–VIS domains with the C-OPS and C-PHIRE intercomparison is due to the enhanced homogeneity in the clearer waters off Lana'i.

The deployments of the SV3 off the coast of Lana'i were terminated early, because of the approach of typhoon Lester. Despite the abbreviated schedule, 20 C-OPS validation casts and 36 TOW-FISH autonomous casts were obtained. In addition, the first attempts to collect up casts proved encouraging. The early termination of the field campaign did not permit the full development of thruster-assisted profiling during up casts.

8.8.5 R/V *John Martin* (October 2016)

The fifth field campaign was opportunistically scheduled to demonstrate overnight autonomous operations and to complete thruster-assisted profiling during up casts, both of which were not possible during the fourth field campaign due to severe weather from typhoons Madeline

and Lester. The fifth field campaign took place in the turbid coastal waters off the Pajaro River mouth in Monterey Bay close to Moss Landing (California). The sampling area was experiencing a red tide event, so the campaign also demonstrated the ability of the SV3 to collect research data in a phenomenon that tends to be surface intensified.

The SV3 with sea cable and above-water instrumentation was assembled at BSI (San Diego, California) and trucked mostly assembled (the Sub fins were not attached), along with the TOW-FISH and support gear, to the Moss Landing Marine Laboratories (MLML) facility at Moss Landing harbor. Like the Lana'i campaign (Sect. 8.8.4), this deployment demonstrated the portability of the entire SV3 system. Final mobilization of the equipment occurred inside the MLML port facility, and the instrumentation was loaded and secured aboard the R/V *John Martin*. The water depth in the red tide was about 52 m.

A picture of the C-OPS validation instrument with the C-PrOPS accessory deployed within the red tide is shown in Fig. 95 (compare to the clear Lana'i offshore waters in Fig. 92). Despite the turbidity, wave focusing effects are nonetheless visible on the red hydrobaric flotation chamber. In addition, the neon green sea cable appears blurry due to brightening caused by the enhanced scattering from the bloom conditions within the red tide.

Fig. 95. The C-OPS with C-PrOPS slowly sinking in the red-brown waters of a red tide off the Pajaro River mouth in Monterey Bay.

The field team included new participants from UCSC who had not participated in the third and fourth campaigns in Hawaii, so the original plan included extra time for training before the SV3 was launched. The original deployment plan was to have the SV3 with TOW-FISH operate overnight from 26–28 October 2016. Unfortunately, remnants of hurricane Seymour threatened the operational area before the field campaign commenced, and the weather forecast included small-boat advisories and rain. Consequently, the SV3 was recovered at the end of the day on 26 October. The remaining scheduled deployment time was used for training and documentation requirements to advance TRL values.

Another misfortune demonstrated the strength of the SV3 Float, Umbilical, and Sub units. During the first deployment attempt, the release mechanism stuck and the Sub would not release properly. The captain refused to recover the SV3 attached to the deployment cradle, and instead insisted on releasing the Sub. Unknown at the time, the Umbilical had come loose and washed out from within the cradle and over the fins. When the Sub finally was released and descended it got tangled in the fins, and then the Sub flipped upside down and rotated 180°. Consequently, the Float was moving backwards onto the TOW-FISH as the latter was executing its programmed autonomous sampling.

The Float, plus inverted and rotated Sub, were recovered, but there was minor damage to the thrudder (one broken propeller, but the propeller was not going to be used, because of the developed sea state from the approaching remnants of hurricane Seymour). The release mechanism plus other damage to the SV3 was fixed or mitigated, and the entire SV3 was relaunched into the red tide without incident.

A total of 10 optical casts were obtained with the TOW-FISH, as well as 6 validation casts using the C-OPS with C-PrOPS instrument. The latter included new trials using the thrusters to further slow the descent of the profiler after the TOW-FISH ascended to the surface, and these trials were successful. In all cases, the application of low thrust levels (15%) improved stability and vertical resolution. Unfortunately, the weather forecast would not allow the system to stay out overnight, because it seemed unlikely the SV3 could be safely recovered in the anticipated high winds and sea state.

Another misfortune was that the aft 3-MPU dry box cracked prior to being transported to MLML, because it was inadvertently exposed to a vacuum during the N_2 purge. The crack was stabilized with a two-part epoxy and did not subsequently leak. In addition, the WiFi on the ship was not working properly (it was rebooted three times with intermittent levels of success), so communications with the SV3 were restricted to cellular WiFi, which made a difficult operation even more difficult.

8.8.6 R/V *Hakuho Maru* (December 2016)

The sixth field campaign was in the Kuroshio Current (Japan) and tested new software for controlling the descent of a profiling backplane with thrusters, which are not usually used during descent. Given the successful testing in Monterey Bay of thruster-assisted profiling, the ability of C-PrOPS to improve data quality by using thrust to overcome a tilt bias and to slow the descent rate of a profiler was evaluated more rigorously during the KH-16-7 campaign aboard the R/V *Hakuho Maru*. For these trials, a C-OPS with C-PrOPS was used to simulate the TOW-FISH, which is rather similar (but larger) in size.

On a windy day with a well-developed sea state, one cast was executed wherein the thruster was off during profiler descent, which is the normal practice. This cast was noted during acquisition, per the DACPRO near surface vertical tilt summaries, as having a tilt bias. The bias was close to, but typically within, the ±5° maximum tilt threshold used for data processing rejection and was principally in the long axis of the backplane, i.e., in the same axis that the thrust is applied to the backplane. During the second cast, the thrusters were not turned completely off; instead, they were reduced to a 15% thrust level to compensate for the pitch bias.

The two casts are compared in Fig. 96. The cast with no thrust during descent (blue) is usually close to the −5° vertical tilt limit and occasionally spikes to values beyond the −5° threshold. The cast with a 15% thrust level applied during descent (red) is rarely above the ±5° vertical tilt limit and rarely spikes to values beyond the −5° threshold. Both profilers show a *lively* response near the surface in the active wave field, but with a large amount of data to within ±5° because of enhanced surface loitering from the hydrobaric bladders.
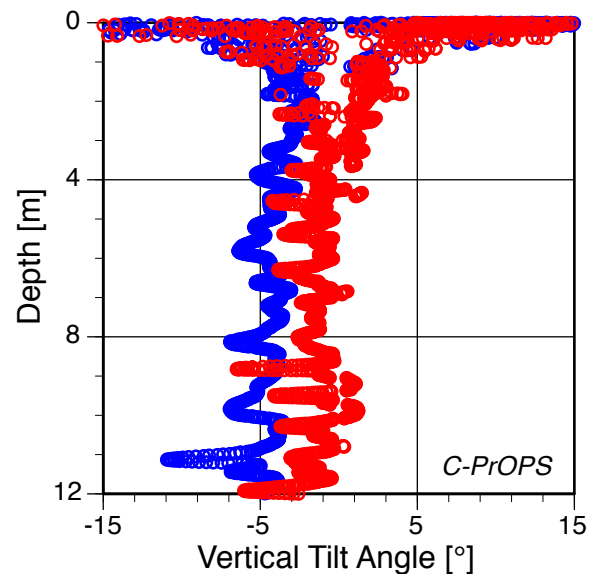
Fig. 96. The intercomparison of two C-OPS system 21 with C-PrOPS casts, wherein the profiler descended in rough conditions with no thrust applied during descent (blue) and with 15% thrust applied (red) to compensate for a pitch bias.

The application of thrust in the second cast also slowed profiler descent, so a principal difference between the two profiles in Fig. 96 is the number of samples (N_s) obtained by a particular depth z, which establishes the vertical resolution (V_r) of the water column above z, i.e., $V_r(z) = z/N_s(z)$. By 12 m, the profile with no thrust applied during descent obtained 1,797 observations, whereas the profile with thrust applied during descent obtained 2,083. This corresponds to nominal $V_r(12)$ values of 0.7 cm and

49

0.6 cm, respectively. The number of observations obtained with thrust applied is greater, but the $V_r(12)$ values are rather similar.

The number of observations in the upper 12 m with vertical tilt angles to within $\pm 5°$, however, is significantly different for the two profiles. After tilt filtering, for the profile with no thrust applied $N_s(12) = 929$ and for the profile with thrust applied during descent $N_s(12) = 1,653$. This corresponds to $V_r(12)$ values of 1.3 cm and 0.7 cm, respectively, which is about a factor of two improvement in the vertical resolution for the profile with thrust applied.

At the conclusion of a down cast, the thrusters are turned on to maximum safe thrust (approximately 50%) and the operator starts hauling in cable as quickly as possible. The operator slows the rate when the tension on the cable indicates the backplane is resisting the effort to haul in cable, and then stops hauling in cable once the mark on the cable identifying 35 m of cable are in the water is reached. If the backplane is not on the surface at that time, the thrusters bring the backplane to the surface. The combined effort brings the backplane to the surface in the shortest time possible, thereby minimizing the time intervals between sequential casts.

The use of thrusters to minimize the cycle time between casts is dependent on environmental conditions, e.g., local currents. In some cases, currents can return the profiler to the vicinity of the deployment platform. In these cases extra caution is required to ensure the profiler location is known before it is allowed to surface. The concern is to avoid any damage to the irradiance cosine collector if the profiler surfaces under the deployment platform or very close to it (although the bumpers on the profiler mitigate the likelihood of damage).

When the operator hauls in cable, the irradiance end of the backplane is pulled upwards and the radiance end is pushed downwards. The cable hauling imparts a *herky-jerky* motion to the backplane that exacerbates tilting. Normally the up cast is not recorded, because the resulting vertical tilts usually exceed the allowed $\pm 5°$ threshold for data processing. If the cable hauling is slower and smoother, the negative aspects of returning the profiler to the surface can be significantly reduced.

It is possible to work carefully during an upcast and obtain useful data, because of the kite-shaped dynamics of the backplane. It is not unusual, however, for there to be multiple contributing conditions (e.g., currents, variable cloudiness, unknown bottom features, etc.) that can make the attempt less productive than simply getting to the surface as quickly as possible, waiting for optimal conditions, and starting anew. In situations wherein clouds are actively forming and not just being transported by winds aloft, forecasting when to start a cast is particularly difficult.

In the case of the TOW-FISH, it is appealing to get the most out of every watt spent on sampling, because power is a precious resource. Consequently, understanding the

parameters that are important to improving an up cast is a useful investigation. The differences in the TOW-FISH backplane (e.g., it is larger, always being towed, and the thrusters are oriented vertically) might require additional refinements or changes, but addressing the problem with some amount of experience is preferable to having none.

An important practical consideration is that deploying C-OPS with the C-OPS accessory to gain experience with thruster-assisted profiling is easier than deploying an SV3 with TOW-FISH attached. To overcome the latter disadvantage, a ship-based configuration for deploying the TOW-FISH and solar reference was developed and is described below (Sect. 8.8.8). In addition, the lessons learned from C-OPS with C-PrOPS trials are useful to other researchers deploying C-OPS with the C-PrOPS accessory and, thus, to the validation measurements collected to evaluate the data obtained with the TOW-FISH.

Figure 97, presents the vertical tilt angle for a down cast (blue) and the up cast (red) executed immediately thereafter, wherein both casts had manual thrust control applied. For the down cast, the thrust level upon release of slack cable into the water at the start of the cast was set to 19%. For the up cast, the thrust level was set to 35% at the bottom of the cast, and then to 15% for the last 2 m of the up cast.
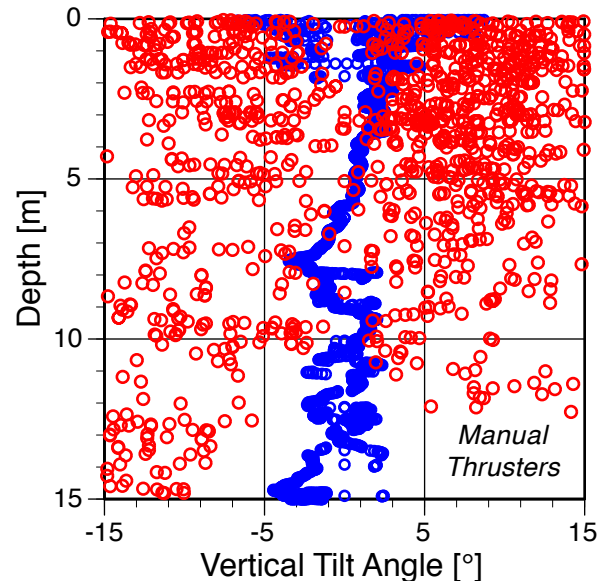

Fig. 97. The vertical tilt angles obtained for a down cast (blue) and the immediately following up cast (red), wherein manual thruster control was applied throughout both the up and down casts.

The down cast in Fig. 97 is characterized by vertical tilt angles usually to within $\pm 5°$. The $N_s(15)$ value is 2,348 of which 1,955 are tilt compliant, yielding $V_r(15) = 0.8$ cm, i.e., the vertical resolution is less than 1 cm. For the companion up cast, there is significantly more variability in the vertical tilt data with continuous oscillations back and forth through zero, which are caused by the operator pulling on the cable to create a tilt in one direction

and then the thrusters working to compensate in the other direction.

For the up cast in Fig. 97, $N_s(15) = 1{,}713$, 309 samples are tilt compliant, and $V_r(15) = 3.2$ cm. The data are not evenly distributed, however, with no compliant data below approximately 11 m. If the top 1.5 m of the water column is considered—which is where the extrapolation intervals must be selected to ensure data products across the entire wavelength domain of 313–875 nm—105 samples are tilt compliant and $V_r(1.5) = 1.4$ cm.

With a resolution approaching 1 cm, the up cast in Fig. 97 is expected to yield an extrapolation interval that closely matches the down cast, and data products that are rather similar. Figure 98 provides a summary of the $E_d(\lambda)$ values for the up cast shown in Fig. 96 and they are in keeping with profiling resolution associated with down casts, thereby demonstrating that active thrust control can improve vertical profiling. This suggests, adaptive thrust control, i.e., computer controlled application of thrust, could significantly improve up cast data quality.
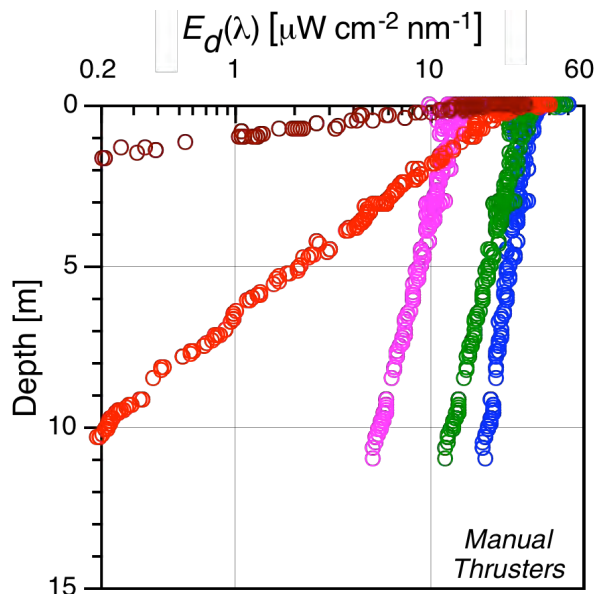
Fig. 98. A summary of $E_d(\lambda)$ values for the up cast shown in Fig. 97, wherein the colors correspond to the spectral domain from the UV (magenta) to the NIR (dark red).

8.8.7 R/V *Sultana* (January 2017)

The seventh field campaign was in the oceanic coastal waters near La Parguera, Puerto Rico. The principal objectives of the campaign, with some results documented in other sections as indicated, were as follows:

1. Continued logistical demonstration of shipping the SV3 by air with GPS package tracking (Sect. 8.10);

2. Rapid SV3 mobilization in a remote location;

3. Review and training of SV3 launch protocols, which had been revised to minimize the chance the release latch could stick;

4. Operational demonstration of autonomous SV3 sampling over an extended time period (i.e., 5–10 d) with clear skies and fair seas;

5. Demonstration of at-sea risk mitigation, e.g., recovery from software faults using remote desktop over WiFi to log in to the MacMini;

6. *In situ* optical and laboratory characterization of coastal source waters within adjacent bays, coves, and lagoons;

7. At-sea demonstration of fine tuning TOW-FISH profiling;

8. At-sea demonstration of maintenance (e.g., cleaning an optical aperture);

9. Training and verification of protocols associated with the SV3 instrumentation hardware plus PROSIT and DACPRO software (Table 14);

10. Demonstration of validating TOW-FISH data products with contemporaneous C-OPS vertical profiles (Sect. 9.4);

11. Rooftop field trials of the C-OSPREy instrument suite in coordination with Pandora spectrophotometer observations (Sect. 10.4);

8.8.7.1. SV3 transportation logistics were successfully demonstrated by shipping the SV3, TOW-FISH, C-OSPREy, C-OPS system 21 with the C-PrOPS accessory, with spares and ancillary equipment (e.g., cables) as air cargo from San Diego to La Parguera, Puerto Rico. The rubber seal that was added to the three SV3 wooden crates when the exteriors were coated with a two-part marine epoxy prevented the ingress of any water (Sect. 8.10). All SV3 components, including the GPS package trackers, arrived in proper working condition for staging and daily operations conducted out of the University of Puerto Rico (UPR) *Isla Magueyes* campus in La Parguera.

8.8.7.2. Rapid SV3 mobilization in a remote location, wherein the SV3 was assembled outside during the day of 16 January 2017, and then rolled into a small outbuilding to complete the installation of the HARPOONS instrumentation during the night. Unpacking and assembly was completed in approximately 12 h, thereby demonstrating the SV3 can be rapidly deployed, if circumstances warrant. Testing was completed during 17 January, and the combined SV3 and C-PHIRE instrumentation plus C-OPS validation instrumentation was mobilized aboard the R/V *Sultana* and readied for deployment on 18 January.

8.8.7.3. SV3 launch protocols were reviewed and revised prior to deploying the SV3. The principal revision was to ensure the positioning of the latch mechanism allowed the release lanyard to function over the largest range of angles possible. The release mechanism was tested repeatedly to ensure the latch opened when the lanyard was

pulled over a variety of geometries. No failure modes were discovered, and the SV3 was launched without incident on 18 January 2017.

8.8.7.4. Autonomous SV3 sampling was demonstrated for an approximately one-week time period from 18–25 January 2017, inclusive. The SV3 was launched and recovered within a weather forecast providing a satisfactory test of operational mission requirements, i.e., clear skies and fair seas were anticipated for approximately 10 d. The autonomous data sampling was controlled by a daily scheduler that set the types of scenarios that would be executed. The scenarios included multiple variations in thruster-assisted profiling trials to improve data collection during up and down casts.

After deployment (Fig. 99), approximately daily visits to the SV3 with a fast small boat from the nearby UPR Magueyes Island campus were used to obtain validation data in near-proximity to the SV3 using C-OPS with the C-PrOPS accessory. The SV3 visits were also used to simulate aspects of a rapid recovery capability, including at-sea risk mitigation, fine tuning of profiling scenarios, and at-sea maintenance.

Fig. 99. The SV3 shortly after being deployed for operational demonstration off the coast of La Parguera (Puerto Rico).

8.8.7.5. At-sea risk mitigation was demonstrated by visiting the SV3 on almost a daily basis and logging on to the MacMini within the SV3 to look for fault conditions and clearing them as appropriate. The autonomous profiling software had evolved since the prior deployments in Hawaii and Monterey Bay, so an exhaustive test of possible fault conditions triggered by operational performance in the field had not been possible.

An example of at-sea mitigation, wherein mission operations revealed heretofore unanticipated problems, had to do with the WiFi network interface and how to configure the Macintosh OS so it would not request a non-existent operator to click within a window to clear a fault condition. The ability to mitigate these kinds of risks to mission success at sea while the system was operating limited the gaps in data collection created by the faults as they emerged. One of the reasons the sampling scenarios

were altered daily during the Puerto Rico campaign was to ensure the greatest diversity of operational parameters were exercised, so fault conditions could be discovered and cleared, with subsequent revisions to the autonomous sampling software.

8.8.7.6. Coastal source waters along the La Parguera coast were sampled optically using C-OPS system 21 with C-PrOPS (Fig. 100) and a seawater sample was obtained for laboratory analysis of water constituents. Much of the shoreline is populated with mangroves, which are a significant source of CDOM. The source waters were sampled to provide an understanding of the dynamic range in water properties in near vicinity of the offshore vicarious calibration activities.

Fig. 100. The C-OPS with C-PrOPS accessory being deployed in a coastal bay heavily populated with mangroves.

Severe weather events can transport source waters far offshore. The ability to subsequently exclude offshore sites that could be impacted by source waters with unsuitable properties for vicarious calibration will increase the likelihood of a positive outcome during field campaigns conducted after severe weather events.

8.8.7.7. At-sea fine tuning of the SV3 instrumentation suite can be accomplished with swimmers. The SV3 moves relatively slowly through the water (1–2 kt), so swimmers can swim over to it rather easily from a small boat positioned in near proximity. The swimmers can hold onto the SV3 or sea cable for stability without significantly impacting SV3 operations. During the Puerto Rico campaign, the wind field decreased significantly after the SV3 was launched. Consequently, on the third day at sea, the TOW-FISH resting depth was deeper than nominal.

The deeper resting depth required extra thrust to bring the backplane to the surface, *which negatively impacted the power budget for the thruster batteries.*

During the daily visit to the SV3 with a fast small boat, swimmers swam over over to the SV3 and waited for the TOW-FISH to ascend to the surface. Additional small yellow floats were then attached to the sea cable to ensure the TOW-FISH resting depth was nominal. This could be confirmed from the small boat by remotely logging on to the MacMini using WiFi and reading the TOW-FISH depth display. After a few days, the wind freshened and the floats were removed.

8.8.7.8. At-sea maintenance was demonstrated by visiting the SV3 on the second and third days of the Puerto Rico deployment to inspect the instrument suite and clean the solar reference and PAR diffusers. The first cleaning session was video recorded for detailed observations of the cosine collector, and the moving parts of the shadow band assembly (Fig. 101). Both of these components can be damaged or fouled by birds landing on, resting upon, or taking flight from, the solar reference.

Fig. 101. The at-sea cleaning of the C-PHIRE solar reference on the SV3, which is recorded for detailed observations.

Mitigation strategies to prevent birds from roosting on the above-water instrument components were restricted to deterrence from the shadow band sweep and daily inspections with a fast small boat, because the HARPOONS activity focused primarily on short-term development goals and not on long-term operational requirements.

8.8.7.9. Training and verification of SV3 hardware and software components were conducted during the Puerto Rico campaign to the greatest extent practicable (Table 14). DACPRO and PROSIT were the most significant components of the software training, with the former facilitated by communicating with the MacMini over WiFi. These activities involved substantial amounts of time, because the WiFi capability was improved and upgraded during the field campaign to make it more reliable.

Hardware training was not restricted to just the above- and in-water optical instrumentation. The rooftop field tests of the C-OSPREy instrument suite included training and verification of performance, e.g., sun tracking. The assembly, launch, recovery, and subsequent disassembly of the SV3 allowed training during all phases of the operation, including demobilization and packing, plus use of the GPS trackers.

8.8.7.10. Validation of SV3 data products was accomplished by visiting the SV3 in a small boat and deploying the system 21 C-OPS with the C-PrOPS accessory. The latter allows the C-OPS to be steered towards the path of the moving SV3 when the TOW-FISH is executing a profile (Fig. 102). The functioning of the TOW-FISH is monitored by remotely logging on to the MacMini using WiFi, once the small boat was in proximity. Three vertical casts with the C-OPS instrumentation plus a surface water sample for laboratory analyses were obtained during each validation exercise.

Fig. 102. The system 21 C-OPS with C-PrOPS accessory (foreground) being steered with digital thrusters towards the SV3 (background).

As part of the Puerto Rico deployment, UCSC team members collected contemporaneous IOP measurements and near-surface water samples for validation data. IOP measurements included a winch-operated profiling package equipped as follows: a) an ac-s instrument manufactured by Western Environmental Technology Laboratories (WETLabs), Inc. (Philomath, Oregon) and configured for whole-water measurements; b) a HydroSCAT-6 backscatter instrument built by Hydro-Optics, Biology, and Instrumentation (HOBI) Laboratories, Inc. (formerly Tucson, Arizona); and c) a SeaBird Electronics (SBE) integrated conductivity, temperature, and depth (CTD) SBE-49 instrument (Bellevue, Washington).

There were plans to also deploy the UPR HyperPro II radiometer package manufactured by Satlantic Inc. (Halifax, Nova Scotia), *but the HyperPro II was not functional during the field campaign.*

At all stations where the C-OPS with C-PrOPS was deployed, discrete surface water samples were collected for high performance liquid chromatography (HPLC) pigment and colored dissolved organic material (CDOM) absorption analyses. Samples were processed at the field station (within a few hours of collection) after being stored in a cooler in the dark.

Pigment filters were flash-frozen in liquid nitrogen and transferred to UCSC in a dry-shipper. CDOM samples were filtered at UPR, stored in pre-combusted glass amber vials at $4°C$, and hand-carried to UCSC for analysis in a container with freezer packs. CDOM samples were measured using a Cary 50 spectrometer built by

Agilent Technologies (Santa Clara, California) equipped with a 10 cm cell, as well as an UltraPath liquid core wave guide (200 cm) system manufactured by World Precision Instruments (Sarasota, Florida). Pigments were processed following SeaWiFS HPLC Analysis Round-Robin Experiment (SeaHARRE) protocols (Hooker et al. 2012b) using an Agilent Technologies 1200 (Wilmington, Delaware) equipped with a diode array detector.

8.8.7.11. C-OSPREy Field Tests took place on the rooftop of a UPR building at the Magueyes Island campus. The rooftop had sufficiently unobstructed views of the sky to test he system in an operational environment and ensure useful data could be obtained for the majority of the day. The C-OSPREy system was deployed from 21–25 January 2017, inclusive, which included short-duration tropical rain events with no discernible negative effects.

Only sun tracking measurements were collected with the filter wheel in the ND 3.0 position. A total of 402 observational sequences were recorded, with a portion of these obtained under variable cloudiness to confirm the operational limits of the quad detector. The daily data were analyzed in near-real time to improve the sun-tracking software and other aspects of instrument performance, as follows: a) automated start up, b) acquisition of high (temporal) frequency solar observations during sunrise, c) hourly observations through the day, and d) high frequency solar observations during sunset.

Despite generally poor atmospheric conditions over the land during the periods when SV3 data were collected, the C-OSPREy instrument suite performed within the nominal limits established for the field testing scenarios.

Tracker hardware and software problems emerged during the deployment, and *updated software was successfully deployed in the field to fix the issues, thereby demonstrating sustainability and field maintenance.*

8.8.8 R/V *Hobson's Choice* (June 2017)

The eighth field campaign was a field test of a prototype configuration for deploying the TOW-FISH profiler with solar reference from a small boat. The boat was trailered to Miramar Reservoir (San Diego, California), the optical equipment mobilized onto the boat in the parking lot, and then the boat was launched into the lake for optical profiling trials. Like the deployments in Lana'i (Sect. 8.8.4) and Monterey Bay (Sect. 8.8.5), this deployment demonstrated the portability of the SV3 system with an added emphasis on versatility.

The principal campaign objectives, all of which were accomplished, were as follows:

1. Test the control of spectrograph integration time using new software procedures;

2. Test new software associated with the execution of down and up casts;

3. Manually establish an optimal thrust level for up casts, wherein the backplane rises as slow and stably as possible; and

4. Continue the training of BSI personnel in the use of DACPRO, especially new features designed for the campaign.

8.8.9 Solar Eclipse (August 2017)

After software refinement trials on the BSI rooftop in March 2017, the C-OSPREy instrument suite was set up on the BSI rooftop on 21 August 2017 with an unobstructed view of the sky during the time period of the solar eclipse (Fig. 103). The objective of the deployment was to test the sun-tracking capabilities of the DACPRO software created for C-OSPREy. At the height of the eclipse, approximately 60% occlusion of the Sun was expected in San Diego. The minimum tracking value of the quad detector is about 15% less than the anticipated direct beam from the Sun at 60% occlusion. The DACPRO software successfully tracked the Sun during all phases of the solar eclipse.

Fig. 103. The C-OSPREy radiance instrument (right) mounted on the PTU-D300 with the ERA and quad detector (left) tracking the Sun as part of observing the August 2017 solar eclipse.

8.8.10 Mount Laguna (October 2017)

The C-OSPREy validation instrument is the UCSC MicroTops II sun photometer manufactured by Solar Light Company, (Glenside, Pennsylvania). The MicroTops II is calibrated annually (last calibration August 2017) and provides the aerosol optical depth (AOD) at 440, 500, 675, 870, 936 nm (as well as the corresponding radiance values), column water vapor, and the standard deviation for the solar measurements.

UCSC configured the MicroTops II to obtain 32 scans per measurement and to calculate the mean and standard deviation for the five highest signal scans. Ten sets of scans for each time point are selected and the lowest AOD values from those scans are retained. The instrument is synchronized directly to a GPS which provides time and location. The MicroTops II has a built-in pressure sensor, and uses pressure, time, location, and the calibration coefficients to calculate AOD and column water vapor.

On 4 October 2017, the C-OSPREy instrument suite was transported to Mount Laguna (San Diego County, California) and mobilized at an elevation of approximately 1,570 m (5,151 ft).

The proximity of the Mount Laguna site to a large industrialized and heavily populated urban environment means it is not ideal for Langley calibrations, but it was the closest site within a reasonable distance of BSI that was suitable for field commissioning.

All of the equipment was powered from an uninterruptible power supply (UPS) connected to a portable generator placed far from the data acquisition computer and support electronics (Fig. 104). The purpose of the deployment was as follows: a) verify the functionality of the new filter wheel with encoder; b) perform a Langley calibration of the C-OSPREy radiance instrument; and c) intercompare the results obtained with C-OSPREy to a MicroTops II handheld sun photometer provided by UCSC.

Fig. 104. The C-OSPREy instrument suite mobilized on Mount Laguna for a Langley calibration. Power is supplied by a generator (red) connected to a small UPS below the table supporting the acquisition computer and a HyPower box with two cable ports (HyPower2) and advanced capabilities denoted the HyPower2+ (orange).

For optimal results, the Langley calibration must be performed during clear-sky conditions. The BioWheel accessory in the EAL is used to position a ND 3.0 filter in front of the spectrograph aperture to prevent saturation of the spectrograph during the direct measurements of the solar disk that are required for sun photometry.

The Mount Laguna site had a clear eastern view of the rising sun at an elevation anticipated to reduce the negative impact of lower-elevation atmospheric effects (e.g., the marine boundary layer). The C-OSPREy instrument suite was assembled before dawn and confirmed to be operational just after sunrise. The sky was clear, completely cloud free, with the exception of a haze visible on the southeastern horizon which persisted throughout the activity.

Solar disk observations commenced at 1410 UTC (0710 local) with observations recorded at 10 min intervals within 100 min of sunrise to improve data density at large solar zenith angles, and at 15 min intervals for the remainder of the observation period. In total, 52 measurements of the Sun were obtained, and the activity concluded at 1937 UTC (1237 local). A Microtops II sun photometer was used to collect a contemporaneous data set. A MicroTops II measurement was collected concurrently with each C-OSPREy sun observation.

8.8.11 R/V *Hobson's Choice* (December 2017)

A CGS can be operated in multi-pinned phase (MPP) mode. The advantage of this mode is that it is supposed to increase the sensitivity of the instrument, which is an advantage for spectral domains with low light levels, e.g., the L_u NIR observations in clear waters. The disadvantage is the structure of the dark currents must be characterized separately and the calibration must be repeated.

To test the extra sensitivity of MPP mode, the CGS L_u spectrograph was configured for MPP mode, calibrated, and then deployed as part of the TOW-FISH in Lake Murray (San Diego, California) on 14–15 December 2017 (Fig. 105). After anchoring in approximately 15 m water depth, the first day was used to trim the TOW-FISH to have a terminal velocity of approximately 30 cm s^{-1} while maintaining the vertical tilt of the backplane to within 5°. The weights were distributed so that incremental removals would result in terminal velocities of 20, 10, and 5 cm s^{-1}, without causing the vertical tilt to exceed to within 5°.

Fig. 105. The TOW-FISH being deployed in Lake Murray (San Diego, California) as part of MPP mode testing.

The second day was cloud free, with a few near-horizon wispy clouds, and a slight haze on the horizon. The wind was calm and the lake surface was flat (Fig. 105). A series of triple casts were obtained for each of the four terminal velocities, wherein the spectrograph integration time was set based on the maximum of the following: a) the overall signal, b) the 700 nm signal, and c) the 800 nm signal. At the end of the last sequence of casts, two additional casts were obtained with spectrograph integration time based on the maximum of the 600 and 750 nm signals.

8.9 Power Budget

The overall hardware design for the SV3 is based on acquiring high quality in-water optical profiles using the TOW-FISH backplane with contemporaneous solar reference measurements (Fig. 78). The architecture naturally divides the hardware into an above- and in-water pair of systems, i.e., Float and Sub, respectively. The former includes the Mac-Mini computer (with inverter, WiFi router, etc.), HyControl electronics, solar reference with shadow band, GPS, and PAR sensor, while the latter includes the instruments mounted on the TOW-FISH backplane.

The power provided to the above- and in-water systems are distinctly different. The above-water instrument suite receives power from the SV3 power system, i.e., the CCU and APU batteries with charging from solar panels as part of the SV3 AMPS domain (Sect. 8.3.6), except the MacMini has a PCA with a back-up battery (Sect. 8.3.6). The PCA and back-up battery are designed for the following: a) remote control for powering the MacMini on and off using WGMS (Sect. 8.3.6); b) ensuring instantaneous current is available (the SV3 power system does not provide instantaneous current, like a battery, and functions more like a power supply); and c) preventing power transients from interrupting MacMini operations, especially during data collection. Power transients are not considered likely, because of the sophistication of the SV3 power system.

The in-water system, i.e., the TOW-FISH backplane, receives power from the 48 VDC payload batteries located in the aft 3-MPU dry box (Sect. 8.3.5).

The four 300 W h payload batteries plus the 120 W h MacMini back-up battery cannot be recharged during the at-sea mission, so these power sources are limited to the energy stored when charging the batteries prior to the mission (usually the night before launching the SV3).

A summary of the above- and in-water power budgets in terms of rated wattages plus daily and mission (10 d) consumption are presented in Table 15. The Table 15 entries are separated into reference (above water) and profiler (in water) instrumentation values, wherein the former are connected to SV3 AMPS domain (APU and CCU batteries with solar panel charging) and the latter are connected to the 48 VDC payload batteries in the aft 3-MPU dry box. The instruments that are always on during a mission appear as part of the reference entries, i.e., the MacMini with inverter, WiFi router, and back-up battery, plus the PAR sensor, and the HyControl electronics.

The rated, daily, and mission power usage values for payload reference devices appear in lines 1–4 in Table 15. The power requirements for executing light and dark casts for the reference and profiler systems are given in lines 7–16 and 19–26, respectively. Power usage values for 20 light casts and 4 dark casts for the reference and profiler systems, as well as the total for the 24 casts for both, are presented in lines 29–34 in Table 15.

Summary totals in Table 15 allow for an evaluation of power margins on a rated, daily, and mission basis. The summary totals for the MacMini and SV3 hotel load, which both use SV3 power, are presented in lines 5 and 6, respectively. These values are comparable and represent the largest power requirements, which is why the MacMini is on SV3 power (but with a back-up battery to mitigate risk and improve reliability).

The power requirements for a 10 d mission executing 20 light casts and 4 dark casts per day with both the reference and profiler systems are given in lines 35 and 36, respectively. Although, the largest rated power usage is by the (in-water) profiler, it is powered on for relatively short periods of time, so the largest daily and mission power usage is by the (above-water) reference devices that are always on and relying on SV3 power (which includes the MacMini with inverter and WiFi router, HyControl electronics, PAR sensor, and the SV3 hotel load).

From the perspective of daily and mission power margins, the daily reference power consumption is 745.6 W h and the mission value is 7,456.2 W h.

The SV3 hotel load is unverified, but the experience from multiple deployments of the SV3 strongly indicates the rated value in Table 15 (line 6) is reasonable.

The amount of daily and mission power that is available to the reference subsystem is derived from the CCU and APU batteries plus the charging from the solar panels.

As noted at the bottom of Table 15, *solar panel charging efficiencies assume no faults or shading*, so 60% and 40% efficiencies are used to include inevitable degradations.

The sum of the initially charged SV3 batteries plus a conservative 60% efficiency for solar-powered SV3 battery charging (lines 37 and 39 in Table 15) provides 1,114 W h daily and 11,140 W h for the 10 d mission. The lower consumption than available power yields a 33% reference system safety margin. If halfway through a mission the SV3 battery charging efficiency degrades to 40% (line 40 in Table 15), the reference system power safety margin drops to 22%. A solar panel failure at the start of a mission is unlikely, because all solar panels are checked prior to deploying the SV3, but if it occurs, there is enough power at 40% charging efficiency to complete the mission (8,020 W h available versus 7,456.2 W h consumption).

Table 15. The power budget for the above-water reference (Ref.) and in-water profiler (Pro.) systems, which are deployed on, or towed by, respectively, the SV3 Float. Not all rated power values are confirmed; some have been approximated using laboratory and field data. The MacMini idle (no data collection) and busy (data acquired) power values are based on a daily maximum of 20 light casts and 4 dark casts, and include inverter plus WiFi router electronics. The "SV3 hotel load" is the power required for SV3 operations independent of the scientific payload (i.e., the in-water TOW-FISH, above-water instruments, etc.), and no use of the thrudder. Summary information is indicated by the open and solid right-pointing triangles, as follows: the black solid entries are the mission total values based on a 10 d deployment, the red solid entries provide the charged battery maximums when the SV3 is launched, and the green solid entries show two different solar panel charging efficiencies. The line numbers along the right edge are for referencing.

System, Equipment, and Event	Rated [W]	Daily [W h]	Mission [W h]	Explanatory Notes	
Ref. MacMini busy	15.0	53.8	538.0	Always on (SV3 power with back-up battery)	1
Ref. MacMini idle	9.4	225.6	2,256.0	Always on (SV3 power with back-up battery)	2
Ref. PAR sensor	0.7	16.8	168.0	Always on (SV3 power)	3
Ref. HyControl electronics	4.7	112.8	1,128.0	Always on (SV3 power)	4
Ref. ▷ _MacMini total_	_29.8_	_409.0_	_4,090.0_	_Ref. total MacMini (SV3 power)_	5
Ref. ▷ _SV3 hotel load_	_13.3_	_319.2_	_3,192.0_	_Ref. total SV3 hotel load (SV3 power)_	6
Ref. Start light cast	10.0	0.0	0.4	Power on devices (SV3 power)	7
Pro. Start light cast	19.2	0.1	0.8	Power on devices (payload batteries)	8
Ref. Equipment on	10.0	0.0	0.4	15 s on time (SV3 power)	9
Pro. Thrusters on	175.0	0.7	7.3	15 s on time (payload batteries)	10
Ref. Light sampling	10.0	0.3	2.5	90 s profile (SV3 power)	11
Pro. Light sampling	19.2	0.5	4.8	90 s profile (payload batteries)	12
Ref. Equipment on	10.0	0.0	0.4	15 s on time (SV3 power)	13
Pro. Equipment off	19.2	0.0	0.4	TOW-FISH off (payload batteries)	14
Ref. Shadow band cast	13.4	0.3	3.4	90 s sweep (SV3 power)	15
Ref. Equipment off	10.0	0.0	0.2	SV3 power	16
Ref. ▷ _One light cast_	_63.4_	_0.7_	_7.3_	_Ref. subtotal (SV3 power)_	17
Pro. ▷ _One light cast_	_232.6_	_1.3_	_13.3_	_Pro. subtotal (payload batteries)_	18
Ref. Start dark cast	10.0	0.0	0.4	Power on devices (SV3 power)	19
Pro. Start dark cast	19.2	0.1	0.8	Power on devices (payload batteries)	20
Ref. Dark sampling	10.0	0.3	2.5	90 s darks (SV3 power)	21
Pro. Dark sampling	19.2	0.5	4.8	90 s darks (payload batteries)	22
Ref. Equipment on	10.0	0.0	0.4	15 s on time (SV3 power)	23
Pro. Equipment off	19.2	0.0	0.4	TOW-FISH off (payload batteries)	24
Ref. Shadow band cast	13.4	0.3	3.4	90 s sweep confirms darkness (SV3 power)	25
Ref. Equipment off	10.0	0.0	0.2	SV3 power	26
Ref. ▷ _One dark cast_	_53.4_	_0.7_	_6.9_	_Ref. subtotal (SV3 power)_	27
Pro. ▷ _One dark cast_	_57.6_	_0.6_	_6.0_	_Pro. subtotal (payload batteries)_	28
Ref. 20 light casts	1,268.0	14.6	146.2	Clear sky from PAR sensor (SV3 power)	29
Pro. 20 light casts	4,652.0	26.6	266.0	Clear sky from PAR sensor (payload batteries)	30
Ref. 4 dark casts	213.6	2.8	28.0	No light from PAR sensor (SV3 power)	31
Pro. 4 dark casts	230.4	2.4	24.0	No light from PAR sensor (payload batteries)	32
Ref. 24 casts total	1,481.6	17.4	174.2	SV3 power	33
Pro. 24 casts total	4,882.4	29.0	290.0	Payload batteries	34
Ref. ▶ _Mission total casts_	_1,524.7_	_745.6_	_7,456.2_	_Ref. total (SV3 power)_	35
Pro. ▶ _Mission total casts_	_4,882.4_	_29.0_	_290.0_	_Pro. total (payload batteries)_	36
Ref. ▶ Charged SV3 batteries		178.0	1,780.0	CCU plus APU ($2 \times 890\,\mathrm{W\,h}$)	37
Pro. ▶ Charged payload batteries		120.0	1,200.0	Payload batteries ($4 \times 300\,\mathrm{W\,h}$)	38
Ref. ▶ SV3 battery charging	156.0	936.0	9,360.0	60% efficiency for 10 h period ($3 \times 52\,\mathrm{W} \times 6\,\mathrm{h}$)	39
Ref. ▶ SV3 battery charging	156.0	624.0	6,240.0	40% efficiency for 10 h period ($3 \times 52\,\mathrm{W} \times 4\,\mathrm{h}$)	40

⚷ The SV3 hotel load is unverified. ⚷⚷ Solar panel charging efficiencies assume no faults or shading. ⚷⚷⚷ Use of the thrudder significantly increases power consumption.

⌁ ⌁ ⌁ *Using the thrudder increases power consumption and likely erodes power safety margins*, thereby requiring modifications to daily operations.

The profiler power system does not have the added complexity of a charging circuit that could deteriorate and is always approximately 76%. Given that the 48 VDC payload batteries that are used can be thoroughly tested and replaced prior to a mission (they are COTS items), this safety margin is realistically achievable for every mission.

The power consequences of using the thrudder should not be construed as a purely negative effect, because the thrudder would only logically be used to avert a mission threat, e.g., overcome a current that is preventing the SV3 from maneuvering as desired, or changing course to ensure a nearby large vessel could not pose a threat, etc.

The longest SV3 deployment was in Puerto Rico (Table 9). This approximately one week deployment used less power and had greater battery reserves than the prorated power budget in Table 15 forecast. Part of the reason for this is each day was used for one test out of a variety of sampling scenarios to determine how thruster-assisted profiling could improve profiling parameters, like planar stability of the optical apertures and vertical sampling resolution. In some cases, faults occurred and the number of executed profiles was reduced and, thereby, used less power. Because the SV3 was visited approximately daily by a small vessel, WiFi communications were used to clear faults and restart the scheduler for another day of testing, so the fault conditions were temporary.

8.10 Shipping and Transportation

The SV3 is provided and shipped in crates made out of wood packaging material (WPM), which is defined as *hardwood and softwood packaging other than that comprised wholly of wood-based products such as plywood, particle board, oriented strand board, veneer, wood wool, etc., which has been created using glue, heat, and pressure or a combination thereof used in supporting, protecting or carrying a commodity (includes dunnage).*

The International Standards for Phytosanitary Measures (ISPM) guidelines for regulating WPM in international trade (ISPM15) is one of several standards adopted by the International Plant Protection Convention (IPPC).

⌁ *The IPPC is an international treaty to prevent the spread and introduction of pests of plants and plant products*, and to promote appropriate control measures.

Many countries base their WPM regulations on applying the ISPM15 standard.

The intent of the ISPM15 standard is that once the WPM is treated and officially marked, the treatment does not expire. For both heat treatment (HT) and methyl bromide (MB) fumigation programs, the quality and treatment mark consists of the following:

- The agency trademark which is the identifying symbol, logo, or name of the accredited agency;
- The Facility Identification which is the WPM product manufacturer name, brand or assigned facility number;
- The HT or MB mark;
- The two-letter ISO country code;
- The IPPC Approved international symbol for compliant wood packaging material; and
- The DUN mark if the intended use is for dunnage.

⌁ The WPM can be reused without requiring a new treatment (HT or MB) and remarking, *as long as the original marks are retained, i.e., visible.*

The three SV3 wooden crates were built by CalPack Crating (Union City, California). The crates are ISPM15 compliant, have two IPPC marks (Fig. 106), and can be shipped to Hawaii and Puerto Rico. The crates are coated with a clear (two-part) marine epoxy to preserve the credentials and weatherproof the crates for longevity. Each crate was fitted with a rubber gasket to minimize the ingress of water when the crate is outside.

Fig. 106. The IPPC mark on one of the SV3 shipping crates; all marks are preserved with two-part clear marine epoxy.

All containers with lithium-ion batteries, i.e., the SV3 CCU and APU, plus the SV3 wooden crates, contain an individual Trackinapack Advanced Plus GPS Tracker made by Global Tracking Technologies Ltd. (London, United Kingdom). Unlike other package trackers, the recurring cost of these package trackers is based on pay-per-use fees and there is no annual contract or automatic monthly charge. They are water resistant, compact, and can have a prolonged rechargeable battery life depending on the number of positions requested per day. The package trackers are permitted to be used globally (but with a few country-specific restrictions based on the available cellular technology) and the user is able to set a time for the tracker to be in airplane mode when needed.

An SV3 contains internal lithium-ion batteries in the CCU and APU (if used). In addition, the 3-MPU dry boxes used for payload purposes might contain lithium-ion batteries (e.g., the HARPOONS project uses lithium-ion batteries to supplement the SV3 power system and to provide back-up power for the MacMini).

❧ *Early in the planning process to ship an SV3, it is advisable to investigate the evolving regulations for shipping internal lithium-ion and lithium-metal/alloy batteries for the departure and arrival locations*, because the process may be detailed, time consuming, and require training or official certifications prior to shipment.

The required steps that must be followed for items that are controlled by Hazardous Material (HazMat) regulations, which include lithium-ion batteries, can depend on, but are not necessarily limited to, the following:

1. The mode of transport (e.g., truck, rail, or air);

2. The charge-density of the battery; and

3. The total weight of the batteries in one shipment.

The above factors determine the handling labels required, identification and Dangerous Goods Regulations (DGR) listings, and emergency contact information. There are also regulations controlling how long to keep the shipping documentation, and how often the shipper of record needs to be certified.

❧ *There are different (but recognizably similar) classification and packaging requirements for batteries that are packed alone* (e.g., shipped as spares).

8.11 Conclusions

The solicitation supporting the HARPOONS development activity stated that the recommended *in situ* vicarious calibration instrument systems to support ocean color science applications shall provide an *in situ* vicarious calibration capability for maintaining global climate quality ocean color remote sensing radiances and reflectances for a multi- or hyperspectral polar-orbiting ocean color sensor and include the features documented in the following Sects. 8.11.1–8.11.10.

The hardware and software associated with developing the SV3 with TOW-FISH and the C-OSPREy systems were deployed during seven field campaigns, as summarized in Table 9. The purpose of field campaigns were to first field commission significant hardware subsystems of the C-PHIRE system architecture, then to deploy the SV3 with TOW-FISH, then to make refinements in hardware or software in preparation for finally deploying the full system with C-OSPREy shore observations in Puerto Rico, i.e., fulfillment of Fig. 71.

An important aspect of the HARPOONS activity is to ensure the emergence of capabilities that can distinguish HARPOONS with respect to typical alternatives, e.g., a buoy system. At this point in time, the distinguishing elements that are being advanced include (but are not limited to) the following:

1. The hybridspectral (microradiometers plus spectrograph) approach improves data quality, because intracomparing the two detector systems verifies stability and detects anomalous performance and drift.

2. The hybridspectral detector systems in both instrument suites (TOW-FISH and C-OSPREy with solar references) exceed the PACE spectral domain requirements wherein the TOW-FISH and C-OSPREy include additional data from 300–350 nm, and the C-OSPREy includes data from 900–1,640 nm (the CGS spectral range is 190–1,000 nm and the spectral range for the microradiometers depends on the instrument system, i.e., 320–875 nm for TOW-FISH and 320–1,640 nm for C-OSPREy).

3. A harmonized instrument design is used for all of the C-PHIRE and C-OSPREy instrument versions. The same *chassis* parts are used for each, but the population of components for the chassis changes with the instrument type. Proven COTS components are used, so costs are reduced, maintenance is simplified, and spare parts inventories are not as burdensome. There are very few custom parts, and even those are made with substantially COTS components, e.g., the C-OSPREy filter-wheel assembly uses COTS filters, a COTS stepper motor, etc.

4. A diversity of contemporaneous atmospheric data products are produced from the C-OSPREy sun photometer observations (Sun, sky, and Moon), plus C-PHIRE and C-OSPREy solar irradiance shadow band observations.

5. Both the TOW-FISH and C-OSPREy solar references are equipped with shadow band accessories and can provide contemporaneous atmospheric data products to improve atmospheric correction.

6. The C-OSPREy is not colocated with the SV3, but the C-OSPREy shadow band Langley observations can be compared to the SV3 shadow band Langley observations to determine the applicability of applying C-OSPREy data to the SV3 sampling site.

7. The C-OSPREy instrument includes a nine-position filter wheel in front of the spectrograph fiber, which provides an index (home) position, improved stray light correction (cut-on filter), dark offset measurements (opaque disk), three-axis polarimetry, solar (bright target) viewing through the use of two ND filters (1.5 and 3.0), and an open position (for relatively dim targets, e.g., the Moon or sea surface, with respect to the Sun).

8. Because the atmosphere is opaque below 290 nm, spectrograph data from 245–290 nm can be used to monitor variations in the dark offset, which can then be used to correct every hyperspectral data record obtained with the spectrograph. This correction is possible because tests indicate that changes in the dark offset are nearly independent of the spectrograph pixel, which means that information from the 245–290 nm range can be used to correct measurements in the other wavelengths.

9. The unprecedented dynamic range of the SiP microradiometers (10 decades) permits data products under moonlight (Gibbous to Disseminating moon) for the C-OSPREy, TOW-FISH, and C-PHIRE solar references.

10. Because the SV3 is in motion and the profiler executes vertical profiling, the optical apertures are cleansed by the air or water flowing across them, so bio-fouling is reduced. Furthermore, the short-duration (10 d) missions ensure negligible bio-fouling of the optical apertures. The regularly scheduled shadow band data collection discourages birds from roosting on the solar reference.

11. The CQM is a portable light source and permits pre- and post-deployment analyses to detect anomalous instrument performance (e.g., drift) of the C-PHIRE and C-OSPREy instrument suites, as well as the build up bio-fouling on exposed instrument apertures.

12. The combination of the OSPREy lamp library and the CXR (designed following established OXR instruments) improves absolute calibrations and provides high quality long- and short-term monitoring of instruments.

13. Hydrobaric vertical profiling of AOPs increases the vertical resolution of the in-water data and, thus, the number of degrees of freedom to produce data products. All data products spanning 320–875 nm can be derived in the upper 1 m of the water column.

14. The use of a near-surface altimeter (top 10 m of the water column) improves the accuracy and precision of depth over legacy (strain gauge) devices during profiling, in part because the temperature sensitivity is more than an order of magnitude better.

15. Platform yaw provides the compass heading calculated from magnetic field sensors, which allows the profiler orientation with respect to the solar (and lunar) geometry to be computed and the subsequent improvement of the self-shading correction for the TOW-FISH data (not fully implemented).

16. Pitch and roll (vertical stability) measurements are corrected by rate gyros, which are then used to remove the effects of wave-driven accelerations (not fully implemented).

17. Thrusters on the TOW-FISH can be used to stabilize the backplane during ascent and descent, so the vertical stability during profiling is significantly improved, which allows data from both the up and down casts to be used to derive optical data products.

18. Adaptive thruster control can be used to slow the ascent and descent of the TOW-FISH during profiling, which can overcome tilt biases and increase the vertical resolution.

19. The SV3 is (almost) always in motion, so it is not an established FAD. Its location is not known to fisherman or recreational boaters, so vandalism, whether intended or accidental, is significantly minimized. The anticipated launch and recovery location is beyond the usual distance from shore for recreational boaters.

20. Use of the SV3 lowers launch and recovery costs by permitting such operations in shallow water with a comparatively small vessel.

21. Adaptive thruster-assisted profiling expands the response for spectral end-member observations, which is particularly important in the clear and turbid waters required for calibration or validation and research activities, respectively.

22. The SV3 permits an immediate response for severe weather or unanticipated instrument malfunctions, because the SV3 can be commanded to return to "port" and intercepted in the appropriate amount of time.

23. The SV3 with TOW-FISH is capable of supporting all CVR oceanic activities and has obtained vicarious calibration data in clear coastal waters (Lana'i, Hawaii) plus clear oceanic waters (Mayaguez, Puerto Rico), algorithm validation data in coastal waters (Kawaihae and Lana'i, Hawaii), as well as baseline research data in a red tide (Monterey, California).

24. The SV3 is air portable and was boxed up, shipped by air to Kawaihae and Lana'i (Hawaii) plus La Parguera (Puerto Rico), whereupon the system was assembled, deployed for sampling from a research vessel, demobilized, and returned to BSI by air.

25. SV3 mobilization requires modest facilities. For the Lana'i deployment, the SV3 was assembled outside next to a parking lot with shade while the optical equipment was mobilized. The SV3 was then rolled down a driveway onto a dock, and the instrumentation deployed from the R/V *Huki Pono*.

26. To reduce the time required for mobilization, the SV3 can be transported almost fully assembled. For the field campaign in Monterey Bay (California), the SV3 was assembled, secured inside a 16 ft box truck, driven to Moss Landing (California), mobilized, deployed from a research vessel, demobilized, and returned to BSI by truck almost fully assembled.

8.11.1 Spectral Range

The solicitation requires a spectral range from 350–900 nm at less than 3 nm resolution (ideally 1 nm).

The C-PHIRE and C-OSPREy instruments exceed this requirement, because the in-water spectral range is approximately 305–1,000 nm, and the above-water spectral range is approximately 305–1,640 nm. The spectral resolution within the required (PACE) spectral range is about 0.4–2.2 nm, which satisfies the solicitation requirements.

S.B. Hooker, R.N. Lind, J.H. Morrow, J.W. Brown, R.M. Kudela, H.F. Houskeeper, and K. Suzuki

Table 16. Estimated $k = 2$ percent uncertainties for C-PHIRE instruments during clear-sky observations with solar zenith angles less than 40° for the blue-green and red spectral domains as a function of the microradiometer (SiP) and CGS components. The standard versus direct solar irradiance observations for C-OSPREy is indicated by EAL(L) and EAL(E), respectively. Inapplicable uncertainty sources have empty cells and temperature uncertainties are per °C. Combined and expanded uncertainties that must be compliant with the solicitation are indicated in bold typeface.

Source of Blue-Green Domain Uncertainty Description	Type	EAE SiP	EAE CGS	EAL(E) SiP	EAL(E) CGS	EAL(L) SiP	EAL(L) CGS	EPE SiP	EPE CGS	EPL SiP	EPL CGS
NIST Scale of Spectral Irradiance	B	0.44	0.44			0.44	0.44	0.44	0.44	0.44	0.44
Reflectance Plaque Standard	B					0.44	0.44			0.44	0.44
Transfer of NIST Irradiance Scale	B	0.18	0.18			0.18	0.18	0.18	0.18	0.18	0.18
Extraterrestrial Irradiance Spectrum	B			1.50	1.50						
Measurement of Calibration Signals	A B	0.55	0.55	0.88	0.88	0.88	0.88	0.55	0.55	0.63	0.63
Filter Transmission	B	0.40		0.40	0.01	0.40		0.40		0.40	
Spectrograph Wavelength Mapping	B		0.30		0.30		0.30		0.30		0.30
Polarization Effect on Responsivity	B					0.46	0.86			0.46	0.86
Temperature Effect on Dark Current	B	0.01	0.05	0.02	0.05	0.02	0.05	0.01	0.05	0.02	0.05
Temperature Effect on Responsivity	B	0.09	0.03	0.09	0.03	0.09	0.03	0.09	0.03	0.09	0.03
Departure from Ideal Cosine Response	B	0.30	0.30					0.30	0.30		
Contamination of Instrument Aperture	B	0.50	0.50	0.50	0.50	0.50	0.50	0.50	0.50	0.50	0.50
Determination of Immersion Factor§	B							0.25	0.25	0.17	0.17
Nonlinearity Effects on Responsivity	B	0.40	1.00	0.40	1.00	0.40	1.00	0.40	1.00	0.40	1.00
Stray Light Effects	B	0.05	0.10	0.05	0.10	0.05	0.10	0.05	0.10	0.05	0.10
Source of Red Domain Uncertainty Description	Type	EAE SiP	EAE CGS	EAL(E) SiP	EAL(E) CGS	EAL(L) SiP	EAL(L) CGS	EPE SiP	EPE CGS	EPL SiP	EPL CGS
NIST Scale of Spectral Irradiance	B	0.47	0.47			0.47	0.47	0.47	0.47	0.47	0.47
Reflectance Plaque Standard	B					0.44	0.44			0.44	0.44
Transfer of NIST Irradiance Scale	B	0.18	0.18			0.18	0.18	0.18	0.18	0.18	0.18
Extraterrestrial Irradiance Spectrum	B			1.50	1.50						
Measurement of Calibration Signals	A B	0.55	0.55	0.88	0.88	0.88	0.88	0.55	0.55	0.63	0.63
Filter Transmission	B	0.40		0.40	0.01	0.40		0.40		0.40	
Spectrograph Wavelength Mapping	B		0.30		0.30		0.30		0.30		0.30
Polarization Effect on Responsivity	B					0.46	1.00			0.46	1.00
Temperature Effect on Dark Current	B	0.01	0.05	0.02	0.05	0.02	0.05	0.01	0.05	0.02	0.05
Temperature Effect on Responsivity	B	0.43	0.03	0.43	0.03	0.43	0.03	0.43	0.03	0.43	0.03
Departure from Ideal Cosine Response	B	0.30	0.30					0.30	0.30		
Contamination of Instrument Aperture	B	0.50	0.50	0.50	0.50	0.50	0.50	0.50	0.50	0.50	0.50
Determination of Immersion Factor	B							0.28	0.28	0.17	0.17
Nonlinearity Effects on Responsivity	B	0.40	1.00	0.40	1.00	0.40	1.00	0.40	1.00	0.40	1.00
Stray Light Effects	B	0.05	0.10	0.05	0.10	0.05	0.10	0.05	0.10	0.05	0.10
Combined Blue-Green Uncertainty		**1.09**	**1.40**	1.90	2.09	1.41	1.88	**1.12**	**1.43**	**1.28**	**1.79**
Expanded Blue-Green Uncertainty (k = 2)		**2.19**	**2.81**	3.80	4.18	2.82	3.77	**2.25**	**2.85**	**2.56**	**3.58**
Combined Red Uncertainty		**1.18**	**1.41**	1.94	2.09	1.48	1.89	**1.22**	**1.44**	**1.36**	**1.80**
Expanded Red Uncertainty (k = 2)		**2.37**	**2.83**	3.89	4.18	2.96	3.78	**2.43**	**2.88**	**2.71**	**3.59**

## 8.11.2 Radiometric Uncertainty

The solicitation requires spectral radiometric uncertainty lower than 4% in the blue-green spectral region and of approximately 5% in the red, combining uncertainty contributions from instrument absolute calibration, characterization (including at least spectral calibration, nonlinearity, stray light perturbation and polarization sensitivity, temperature dependence and, if applicable, geometrical and in-water response), environmental perturbation, and data processing with NIST traceability.

For the purposes of providing radiometric uncertainties, the blue-green spectral range is from 400–599 nm and the red spectral region is from 600-799 nm, i.e., the latter overlaps the NIR domain. The individual uncertainties for C-PHIRE instruments are presented in Table 16. The combined and expanded ($k = 2$) uncertainties that must be compliant with the solicitation are indicated in bold

typeface and all of these values satisfy the solicitation requirements.

A variety of improvements were made to the immersion tank apparatus (Fig. 107) to address the challenges of the expanded spectral domain (UV, NIR, and SWIR) required for next-generation missions, i.e., PACE. Among these is to use a more powerful lamp (1,000 W) and a C-PHIRE radiometer as a reference instrument to more carefully monitor the flux of light from the lamp, especially in the UV where variability is likely to be seen first.
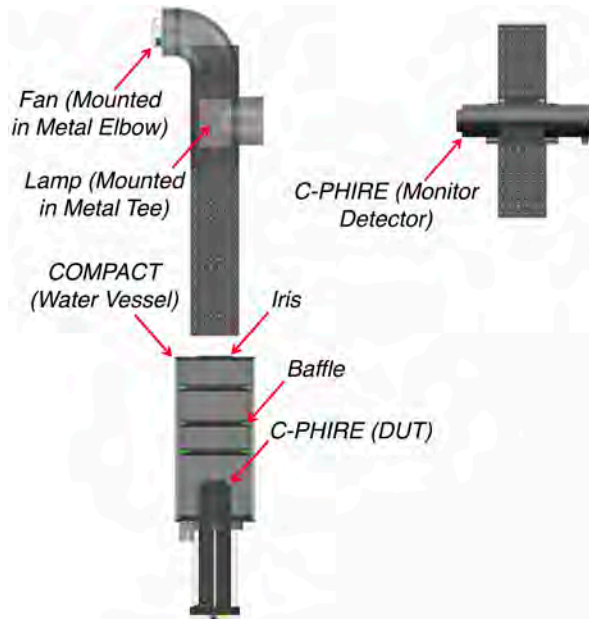
Fig. 107. The improved apparatus used to confirm irradiance immersion factors, wherein the device under test (DUT) and the monitor detector are both C-PHIRE radiometers, E_d and E_s, respectively. The green cross sections of the interior baffles shows the knife-edge design.

The original baffles inside the COMPACT water vessel had a flat underside and the top of the baffle closest to the wall of the water vessel had a small area that was flat allowing retention of a small volume of water. Changing the cross section so the top and bottom were both sloped substantially removed short-term surface disturbances that are caused when the water surface tension releases from the bottom of the baffle. The new design has a cross section that resembles an isosceles triangle with no flat surfaces to retain water. The knife edge of the old design resembled a right triangle with the hypotenuse facing up towards the top of the tank. Instead of continuously releasing the water inside the tank using gravity, which does not result in a constant rate of flow, a new magnetic pump is now used. The magnetic drive requires no seals, thereby eliminating the possibility of fluid leaks and contamination of the water in the vessel with a lubricant that some pump designs require. A new surface cleaning protocol allows the tank to be overfilled, rinsing away surface debris too small to be seen inside the apparatus.

The field data obtained from the EPE was calibrated using legacy immersion factors determined by a linear fit of microradiometer immersion characterization data from four C-OPS irradiance instruments. Linear interpolations and extrapolations of the legacy microradiometer immersion factors were used for the spectrograph component of the EPE. Subsequently, EPE immersion factors were characterized in the immersion test apparatus. There was good agreement of the measured immersion factor between the EPE microradiometers and spectrograph in the 380–910 nm wavelength range (the average RPD was less 0.2%), and a pixel-by-pixel examination of the spectrograph data indicated there was no unexpected spectral structure to the measured immersion factors. Additionally, the immersion factor for the microradiometers was found to vary linearly with wavelength with a coefficient of determination of 0.9996, indicating that the linear fit methodology is accurate within the $k = 2$ uncertainty of the measurement (0.50% in the blue-green and 0.56% in the red using the new test apparatus).

Beyond the 380–910 nm range, spectrograph data were outside the accuracy objectives because of low lamp output in the UV and attenuation from water in the NIR resulting in a low signal-to-noise ratio (SNR) at both ends of the spectral domain. Consequently, data from the microradiometers was used to calculate a linear fit describing the EPE immersion factors for both the microradiometer and spectrograph components. The average RPD differences when comparing the legacy microradiometer factors to the newly measured microradiometer factors were 0.63% in the UV, 0.57% in the blue, 0.45% in the green, 0.37% in the red, and 0.38% in the NIR.

When the upgrades to the immersion factor test facilities are fully implemented as part of routine procedures, rather than one-of-a-kind experiments as presented here, the characterization will be repeated to determine the most accurate EPE immersion factors for future deployments. The use of the linear fit extrapolation for the spectrograph in the UV and NIR will be further investigated by repeating the characterization experiment with an increased lamp output and improved lamp monitoring capabilities. In addition, the integration times of the spectrograph will be optimized to improve the SNR at the shortest and longest wavelengths.

8.11.3 Radiometric Stability

The solicitation requires spectral radiometric stability of the order of 1% per deployment (with NIST traceability).

The spectral radiometric stability is estimated to be approximately 0.3% per deployment and is computed by comparing pre- and post-campaign calibrations, optical bench measurements with transfer radiometer monitoring, and CQM observations. To ensure the stability does not exceed 1% per deployment, CQM data are used to track stability.

If the time series of CQM data forecast that the stability for an instrument deployment might approach 1%, the instrument radiance quartz window or irradiance cosine collector (as appropriate) is replaced. The C-PHIRE class of radiometers are designed to ensure this anticipated maintenance procedure is not difficult, because it is the most likely source of short-term degradation for an autonomous deployment system.

Prior to replacement, the radiometer(s) are calibrated, so a time series of calibration drift due to stability degradation can be created, and then retroactively applied to the applicable instrument observations as part of a PROSIT reprocessing. After replacement, the radiometer(s) are calibrated. If the aperture replacement does not return all detectors to a new stability baseline, outlier individual detectors (e.g., microradiometers) are investigated and individual components replaced as necessary (e.g., individual filter stacks).

8.11.4 Autonomous Field Operation

The solicitation requires a capability of autonomous field operation.

The autonomous platform in the HARPOONS project is an SV3 Wave Glider, which is used to tow an in-water optical (TOW-FISH) profiling package while making simultaneous above-water solar reference, GPS, and PAR measurements. All the instruments sample automatically under automated DACPRO control hosted on a MacMini (Mac OS X) computer stored inside the forward SV3 dry box. Supporting atmospheric observations from the above-water C-OSPREy instrument suite are also obtained using an autonomous DACPRO control that is architecturally similar to the in-water SV3 software.

The deployment location of the SV3 is expected to be in near proximity of a shore station to ensure a field maintenance and emergency response capability, which means validation measurements in the vicinity of the SV3 are anticipated. During the validation measurements WiFi communications allow the status and health of the above- and in-water instruments to be confirmed. The deployment location for C-OSPREy is expected to be at or near the shore station, thus making it easier for personnel to visit on a daily basis.

8.11.5 Maintaining Internal Calibration

The solicitation requires a capability of maintaining internal calibration throughout the 3–5 yr mission.

The internal calibration is designed for a 15 y time period that was initiated in 2010 (Hooker et al. 2012a) and is maintained through the use of a Lamp Library that includes NIST standard lamps plus NIST-traceable calibrations of operational components, e.g., a high precision shunt and multimeter (Sects. 8.4.5 and 8.6.1). These components are further supplanted through the use of legacy

transfer radiometers and the next-generation CXL (Sects. 11.2 and 11.3, respectively), which all have NIST-traceable calibrations. Additional calibration monitoring is provided by the CQM (Chap. 12).

8.11.6 Sustainability and Field Maintenance

The solicitation requires that in consideration of the entire life cycle of the instrument, the system shall be built with consideration to sustainability and field maintenance of the deployed system(s).

The sustainability of the HARPOONS instrumentation over the entire life cycle of the instruments is established by relying on COTS radiometers built primarily out of COTS components. In terms of the principal detector systems, the hyperspectral component is built by Carl Zeiss Spectroscopy GmbH (Jena, Germany) and the microradiometer array is built by BSI (San Diego, California). In both cases, important support electronics are also COTS components. Field maintenance of the HARPOONS instrumentation was demonstrated during the Monterey Bay and Puerto Rico deployments (Sects. 8.8.5 and 8.8.7.8, respectively).

8.11.7 Laboratory and Field Characterized

The solicitation requires fully laboratory and field characterized to all of the above requirements versus NIST standards prior to deployment.

The instrumentation developed for the HARPOONS project are fully laboratory characterized (Sects. 8.4–8.6), as evidenced also by the detailed uncertainty budget (Sect. 8.11.2). The complete field characterization involves dark current measurements and stability monitoring using the CQM (Sect. 12.4) and celestial viewing opportunities, e.g., the Moon, a solar eclipse (Sect. 8.8.9), etc.

8.11.8 Autonomous Data Delivery

The solicitation requires fully autonomous delivery of data, in the proper format, fidelity, and latency, to enable the NASA mission science.

All data are recorded as ASCII text using a format compliant with the SeaBASS architecture (Sect. 8.7.1) as first established by Hooker et al. (1994). The optical data are recorded as raw digital counts with field characterization of the dark currents, so all data can be reprocessed from the lowest to highest level at any time after data acquisition, thereby ensuring fidelity of the data during and after the satellite mission. Delivery of the data files is fully autonomous with a latency spanning shortly after cast completion to immediately after the SV3 is recovered, thereby enabling NASA mission science.

8.11.9 Quantification of Uncertainties

The solicitation expects complementary routine field efforts would also support any future satellite mission to

verify data quality through the quantification of uncertainties affecting data products.

The HARPOONS field campaigns include the contemporaneous use of complementary validation exercises, e.g., *in situ* instrumentation and seawater samples for laboratory analyses. These exercises are used to verify data quality through the quantification of uncertainties affecting data products, as required by the solicitation. It is important to recall that the C-PHIRE instruments by themselves support this requirement, because they have two independent detector systems that can be continuously intracompared.

8.11.10 TRL Assessment

The solicitation requires the TRL of the instrument be advanced. The required deliverable from the solicitation is a fully tested, field deployable instrument at TRL 6 with the instrument ready to support a future mission with verified data quality and uncertainties sufficient for space product validation.

There are five principal systems associated with HARPOONS CVR field activities that are designed to provide or support the derivation of C-PHIRE data products:

1. The in-water TOW-FISH profiler (E_d and L_u), which is towed behind the SV3 from the Float;

2. The above-water instruments mounted on the SV3 mast plate to provide solar reference measurements (E_s and shadow band E_i) plus PAR and GPS, as well as antennas to facilitate communications with the SV3;

3. The C-OSPREy sun photometer (E, L_i, and L_T) mounted on a tracker with a quad detector, which is supported with a solar reference similar to what is mounted on the SV3 (the wavelength domain is more expansive);

4. The CXR laboratory transfer radiometer in a radiance embodiment (CXL); and

5. The CQM portable source for stability monitoring.

A sixth component, validation, does not use additional C-PHIRE instrumentation, but nonetheless provides required data to verify C-PHIRE data quality through the quantification of uncertainties influencing the derivation of data products, e.g., C-OPS with C-PrOPS, IOP sensors, laboratory analyses of water samples, Cimel and Micro-Tops II sun photometers, etc.

The entry TRL value for the five systems designed to provide or support the derivation of C-PHIRE data products is 3 in each case due to subsystems in development, but most subsystems quickly achieved a TRL 6 value and above, because the history of the technologies involved were frequently rather advanced prior to initiating the HARPOONS project. A summary of the TRL values as a function of project quarters for the five C-PHIRE instrument systems are presented left to right in Table 17 as follows: the TOW-FISH profiler (*Pro.*), the two solar references (*Ref.*), the C-OSPREy sun photometer (*Sun*), the CXR radiance instrument (*CXL*); and the portable source (*CQM*).

Table 17. A summary of the TRL values as a function of project quarters for the four C-PHIRE radiometer systems plus the CQM portable source. The $\rightarrow$ symbol indicates entering the TRL value, and the $\Rightarrow$ symbol indicates exiting the TRL value. TRL values exceeding solicitation requirements are shown in bold typeface.

TRL	HARPOONS				
Value	Pro.	Ref.	Sun	CXL	CQM
$\rightarrow 3$	Q 1	Q 1	Q 1	Q 1	Q 1
$3 \Rightarrow$	Q 2	Q 2	Q 2	Q 3	Q 5
$\rightarrow 4$	Q 4	Q 4	Q 7	Q 6	Q 6
$4 \Rightarrow$	Q 6	Q 5	Q 7	Q 6	Q 6
$\rightarrow 5$	Q 7	Q 5	Q 8	Q 7	Q 7
$5 \Rightarrow$	Q 7	Q 5	Q 9	Q 7	Q 7
$\rightarrow 6$	Q 7	Q 6	Q 9	Q 7	Q 7
$6 \Rightarrow$	Q 8	Q 8	Q 9	Q 8	Q 8
$\rightarrow \mathbf{7}$	**Q 8**	**Q 8**	**Q 10**	**Q 10**	**Q 10**
$\mathbf{7} \Rightarrow$	**Q 9**	**Q 9**	**Q 10**	**Q 10**	**Q 10**
$\rightarrow \mathbf{8}$	**Q 9**	**Q 9**	**Q 11**	**Q 11**	**Q 11**
$\mathbf{8} \Rightarrow$	**Q 10**	**Q 10**	**Q 11**	**Q 11**	**Q 11**
$\rightarrow \mathbf{9}$	**Q 11**	**Q 11**	**Q 12**	**Q 12**	**Q 12**
$\mathbf{9} \Rightarrow$	**Q 11**	**Q 11**	**Q 13**	**Q 12**	**Q 13**

S.B. Hooker, R.N. Lind, J.H. Morrow, J.W. Brown, R.M. Kudela, H.F. Houskeeper, and K. Suzuki

Glossary

AA   AIS Antenna
AC   Alternating Current
ADCP   Acoustic Doppler Current Profiler
AIR   Adobe Integrated Runtime
AIS   Automatic Identification System
AMPS   Adaptable Modular Power System
AOD   Aerosol Optical Depth
AOPs   Apparent Optical Properties
APU   Auxiliary Power Unit
AS   ActionScript
ASP   Active Server Page
ASCII   American Standard Code for Information Interchange

BioGPS   Biospherical Global Positioning System
BioSHADE   Biospherical Shadow band Accessory for Diffuse Irradiance
BSI   Biospherical Instruments Incorporated

C-HyR   Compact-Hybridspectral Radiometer
C-OPS   Compact-Optical Profiling System
C-OSPREy   Compact-Optical Sensors for Planetary Radiant Energy
C-PHIRE   Compact-Profiling Hybrid Instrumentation for Radiometry and Ecology
C-PrOPS   Compact-Propulsion Option for Profiling Systems
CA   Cellular Antenna
CCU   Command and Control Unit
CDOM   Colored Dissolved Organic Matter
CFML   Coldfusion Markup Language
CGI   Common Gateway Interface
CGS   Compact Grating Spectrometer
CIRPAS   Center for Interdisciplinary Remotely-Piloted Aircraft Studies
COMPACT   Compact Portable Advanced Characterization Tank
COTS   Commercial-Off-The-Shelf
CQM   Compact Quality Monitor
CSS   Cascading Style Sheets
CVR   Calibration, Validation, and Research
CXL   C-PHIRE Transfer Radiance (radiometer)
CXR   C-PHIRE Transfer Radiometer

D1   Debug (port)
DACPRO   Data Acquisition and Control for Photometric and Radiometric Observations
DC   Direct Current
DGR   Dangerous Goods Regulations
DLL   Dynamic Link Library
DRT   Directional Response Tester
DUN   Dunnage

EAE   EPIC Above-water Irradiance (radiometer)
EAL   EPIC Above-water Radiance (radiometer)
EAL(E)   EPIC Above-water Radiance (calibrated for) Irradiance
EAL(L)   EPIC Above-water Radiance (calibrated for) Radiance
ECMA   European Computer Manufacturers Association
EPE   EPIC Profiling (in-water) Irradiance (radiometer)
EPIC   Enhanced Performance Instrument Class
EPL   EPIC Profiling (in-water) Radiance (radiometer)
ERA   EPIC Remote Atmospheric (interface)
ERI   EPIC Remote Interface
ERP   EPIC Remote Profiling (interface)

FAD   Fish Aggregation Device
FASCAL   Facility for Automated Spectroradiometric Calibrations
FEL   Not an acronym, but a lamp designation.
FET   Field-Effect Transistor
FLH   Fluorescence Line Height
FOV   Field of View
FTDI   Future Technology Devices International
FWHM   Full Width at Half Maximum

G   Graphical (programming language)
G1–G3   General (purpose expansion ports)
GmbH   *Gesellschaft mit beschränkter Haftung*, which designates a private company with limited liability in Germany.
GPS   Global Positioning System
GSFC   Goddard Space Flight Center
GSM   Global System for Mobile (communication)
GUI   Graphical User Interface
GUV   Ground-Based UV (transfer radiometer)

HARPOONS   Hybridspectral Alternative for Remote Profiling of Optical Observations for NASA Satellites
HazMat   Hazardous Material
HeNe   Helium Neon (laser)
HEPA   High Efficiency Particulate Air
HgAr   Mercury Argon (lamp)
HOBI   Hydro-Optics, Biology, and Instrumentation
HPLC   High Performance Liquid Chromatography
HSG   Hyperspectral Spectrograph
HT   Heat Treatment
HTML   Hypertext Markup Language
HV   High Voltage
HVA   Half View Angle
HyControl   Hybrid Control (box)
HyPower   Hybridspectral Power (box)
HyPower2   Hybridspectral Power 2-port (box)
HyPower2+   Hybridspectral Power 2-port (advanced box)
HySEAS3D   Hybrid System for Environmental AOP Sampling of the Sea Surface Demonstration

I/O   Input/Output
ICA   Irradiance Collector Assembly
InGaAs   Indium Gallium Arsenide
IOPs   Inherent Optical Properties
IPPC   International Plant Protection Convention
IR&D   Internal Research and Development

ISO International Organization for Standardization (not an acronym)
ISPM International Standards for Phytosanitary Measures

LAN Local Area Network
LED Light-Emitting Diode
LRI Liquid Robotics, Incorporated

MB Methyl Bromide (fumigation)
MLML Moss Landing Marine Laboratories
MLO Mauna Loa Observatory
MO Mobile-Originated
MOBy Marine Optical Buoy
MODIS Moderate Resolution Imaging Spectroradiometer
MMS Monolithic Miniature-Spectrometer
MPP Multi-Pinned Phase
MPU Modular Payload Unit
MT Mobile-Terminated
MXML Maximum Experience Markup Language

NASA National Aeronautics and Space Administration
ND Neutral Density
NI National Instruments
NIR Near-Infrared
NIST National Institute of Standards and Technology
NRA NASA Research Announcement
NRE Non-Recurring Engineering (costs)

O1–O2 System (ports)
OC Ocean Color
OC3M Ocean Color Three-Band MODIS (algorithm)
OC4 Ocean Color Four-Band (SeaWiFS algorithm)
OD Outer Diameter
OS Operating System
OSPREy Optical Sensors for Planetary Radiant Energy
OXE OSPREy Transfer (radiometer) Irradiance
OXL OSPREy Transfer (radiometer) Radiance
OXR OSPREy Transfer Radiometer

PACE Plankton, Aerosol, Cloud, ocean Ecosystem
PAR Photosynthetically Available Radiation
PCA Printed Circuit Assembly
PDC Power Domain Controller
PE Polyethylene
PHP Hypertext Preprocessor
PK Power Key
PP Polypropylene or (CCU) Pressurization Port (depending on usage)
PROSIT Processing of Radiometric Observations of Seawater using Information Technologies
PTFE Polytetrafluoroethylene

RCA Radiance Collector Assembly
RIA Rich Internet Application
RS-232 Recommended Standard 232
RS-422 Recommended Standard 232
RS-485 Recommended Standard 485

S/N Serial Number
S1–S4 Sensor (ports)
SBD Short Burst Data
SBE SeaBird Electronics
SBIR Small Business Innovative Research

SeaBASS SeaWiFS Bio-Optical Archive and Storage System
SIF Science Innovation Fund
SDT Science Definition Team
SeaHARRE SeaWiFS HPLC Analysis Round-Robin Experiment
SeaWiFS Sea-viewing Wide Field-of-view Sensor
SiP Silicon Photodetector
SMA Subminiature (version) A
SMC Sensor Management Computer
SNR Signal-to-Noise Ratio
SRT Spectral Response Tester
SSF Slit Scattering Function
STARR Spectral Trifunction Automated Reference Reflectometer
SV2 Wave Glider Surface Vessel Second-generation
SV3 Wave Glider Surface Vessel Third-generation
SWIR Short-Wave Infrared

T-MAST Telescoping Mount for Advanced Solar Technologies
TOW-FISH Towable Optical Wave-Following *In Situ* Hybrid
TCP/IP Transmission Control Protocol/Internet Protocol
TRL Technology Readiness Level
TTL Transistor-Transistor Logic
Type A An uncertainty evaluated by statistical methods.
Type B An uncertainty evaluated by non-statistical methods.

U1 Umbilical (port)
UAV Unmanned Airborne Vehicle
UCSC University of California Santa Cruz
UPR University of Puerto Rico
UPS Uninterruptible Power Supply
USB Universal Serial Bus
USV Unmanned Surface Vessel
UTC Coordinated Universal Time
UV Ultraviolet

VAC Voltage Alternating Current
VIS Visible
VMC Vehicle Management Computer

WETLabs Western Environmental Technology Laboratories
WGMS Wave Glider Management System
WiFi Wireless Fidelity
WPM Wood Packaging Material

XGUV Transfer Ground-Based UV (radiometer)
XML Extensible Markup Language
XTRA Expandable Technologies for Radiometric Applications

Symbols

0^- The null depth immediately below the water surface.
0^+ The height immediately above the water surface.

a A fit parameter.

b A fit parameter.

c A fit parameter.

$\mathbb{C}$ The stray light correction matrix.

C_0 A fit coefficient.

C_1 A fit coefficient.

C_2 A fit coefficient.

C_3 A fit coefficient.

d The distance from the lamp source from the collector surface.

$d_{i,j}$ The matrix element of $\mathbb{D}$ (with i and j indicating row and column, respectively).

$\mathbb{D}$ The stray light distribution matrix.

$E(\lambda)$ The above-water spectral direct solar irradiance.

$E_a(\lambda)$ The measured irradiance in air.

$E_d(\lambda))$ The in-water spectral downward irradiance.

$E_d(0^+, \lambda)$ The above-water spectral global solar irradiance.

$E_i(\lambda)$ The above-water spectral indirect (sky) irradiance.

$E_s(\lambda)$ The above-water spectral global solar irradiance.

$E_w(z, \lambda)$ The measured irradiance in (usually pure) water at depth z.

F_0 The hypothetical irradiance outside the Earth atmosphere.

F_E The immersion factor for irradiance.

F_L The immersion factor for radiance.

$G(\lambda_s)$ A gaussian function applied to a spectral segment.

i An index variable.

$\mathbb{I}$ The identity matrix.

j An index variable.

k The coverage factor for the uncertainty estimate.

$K_d(\lambda)$ The in-water E_d spectral diffuse attenuation coefficient.

$K_{L_u}(\lambda)$ The in-water L_u spectral diffuse attenuation coefficient.

$K_w(\lambda)$ The spectral diffuse attenuation coefficient for pure water.

l_c The lamp-to-plaque calibration distance.

L_E A radiance instrument calibrated to measure irradiance.

$L_i(\lambda)$ The above-water spectral indirect (sky) radiance.

L_L A radiance instrument calibrated to measure radiance.

l_r The reference distance.

$L_T(\lambda)$ The total above-water spectral total radiance from the sea surface.

$L_u(\lambda)$ The in-water spectral upwelling radiance.

$L_W(\lambda)$ The spectral water-leaving radiance.

$[L_W(\lambda)]_N$ The spectral normalized water-leaving radiance.

$[L_W(\lambda)]_N^{ex}$ The spectral exact (normalized) water-leaving radiance.

$M_D(\lambda_s)$ The net monitor signal (i.e., dark signal removed) observed using the discharge lamp.

$\widetilde{M}_D(\lambda_s)$ The monitor detector signal for the light observed using the discharge lamp, i.e., HgAr wavelength standard, (subscript D).

$M_X(\lambda_s)$ The net monitor signal (i.e., dark signal removed) observed using the xenon lamp.

$\widetilde{M}_X(\lambda_s)$ The monitor detector signal for the light observed using the xenon lamp (subscript X).

$M_X'(\lambda_s)$ The net monitor signal observed using the xenon lamp with a wavelength correction function $\Delta\lambda(\lambda)$ applied for the wavelength range of interest.

$n_g(\lambda)$ The refractive index of the radiance aperture, i.e., quartz window.

$n_w(\lambda)$ The refractive index of seawater.

$N_s(z)$ The number of samples obtained by depth z.

p An arbitrary functional variable.

$R_{rs}(\lambda)$ The spectral remote sensing reflectance.

$\vec{S}$ The column vector of the measured net (dark corrected) signal.

$\vec{S}_{IB}$ The contribution of the net spectrograph signal due to the *in band* (subscript IB) response.

$\vec{S}_{SL}$ The contribution from stray light (subscript SL).

t_1 A fit parameter.

t_2 A fit parameter.

t_3 A fit parameter.

T The test instrument signal (voltage) with the dark current removed.

$T_i(\lambda_s)$ The net test instrument signal (i.e., dark signal removed).

$\widetilde{T}_i(\lambda_s)$ The test instrument signal for the light observed at each channel i as a function of SRT wavelength λ_s using the xenon lamp as the light source.

$T_i'(\lambda_s)$ The net test instrument signal observed using the xenon lamp with a wavelength correction function $\Delta\lambda(\lambda)$ applied for the wavelength range of interest. (subscript s).

T_p The transmittance through the water path.

T_s The transmittance through the water surface.

u The uncertainty.

$V_r(z)$ The vertical resolution achieved at depth z.

$W(z, \lambda)$ The change with water depth z of the refracted solid angle subtended by the collector as viewed from the lamp filament.

z The water depth or path length.

γ The relative spectral response function.

$\gamma_i(\lambda)$ The relative spectral response function for channel i.

$\widehat{\gamma}_i(\lambda)$ The normalized relative spectral response function, wherein the γ_i values are normalized by the maximum spectral value.

$\gamma_i^c(\lambda)$ The convolution of $\widehat{\gamma}_i(\lambda)$ with the slit function of the monochromator.

$\gamma_i^d(\lambda)$ The deconvolved relative spectral response function.

$\Gamma(\lambda)$ The NIST-traceable responsivity of the monitor detector provided by the manufacturer.

$\Delta\lambda$ A wavelength shift or difference.

ϵ The cosine error.

$\bar{\varepsilon}$ The average cosine error.

θ The incidence or rotation angle (depending on usage).

λ The wavelength.

λ_{18} The 18 spectral fixed-wavelength channels of a radiometer.

λ_{19} The 19 spectral fixed-wavelength channels of a radiometer.

$\lambda_{2,048}$ The spectral 2,048 pixels of the CGS.

λ_c The centroid wavelength.

λ_f A spectral segment.

λ_s A spectral segment.

λ_Σ The combination of the SiP and CGS spectral domains.

τ The shift of λ for the convolution.

ϕ The azimuth or rotation angle of the instrument (depending on usage).

$\psi(\lambda)$ The slit function of the monochromator.

References

Austin, R.W., and G. Halikas, 1976: The index of refraction of seawater. *SIO Ref. 76–1*, Vis. Lab., Scripps Institution of Oceanography, La Jolla, California, 64 pp.

Gordon, H.R., and K. Ding, 1992: Self shading of in-water optical instruments. *Limnol. Oceanogr.,* **37,** 491–500.

Gueymard, C., 2003: Direct solar transmittance and irradiance predictions with broadband models. Part I: detailed theoretical performance assessment. *Solar Energy,* **74,** 355–379.

Hooker, S.B., 2010: "The Telescoping Mount for Advanced Solar Technologies (T-MAST)." In: Morrow, J.H., S.B. Hooker, C.R. Booth, G. Bernhard, R.N. Lind, and J. W. Brown, Advances in Measuring the Apparent Optical Properties (AOPs) of Optically Complex Waters. *NASA Tech. Memo. 2010–215856,* NASA Goddard Space Flight Center, Greenbelt, Maryland, 66–71.

——, 2014: Mobilization Protocols for Hybrid Sensors for Environmental AOP Sampling (HySEAS) Observations. *NASA Tech. Pub. 2014–217518*, NASA Goddard Space Flight Center, Greenbelt, Maryland, 105 pp.

——, and J.W. Brown, 1985: CENTER: A software package for center estimation. *Comp. Phys. Comm.,* **38,** 421–433.

——, C.R. McClain, J.K. Firestone, T.L. Westphal, E-n. Yeh, and Y. Ge, 1994: The SeaWiFS Bio-Optical Archive and Storage System (SeaBASS), Part 1. *NASA Tech. Memo. 104566, Vol. 20,* S.B. Hooker and E.R. Firestone, Eds., NASA Goddard Space Flight Center, Greenbelt, Maryland, 40 pp.

——, and G. Zibordi, 2005: Platform perturbations in above-water radiometry. *Appl. Opt.,* **44,** 553–567.

——, G. Bernhard, J.H. Morrow, C.R. Booth, T. Co-mer, R.N. Lind, and V. Quang, 2012a: Optical Sensors for Planetary Radiant Energy (OSPREy): Calibration and Validation of Current and Next-Generation NASA Missions. *NASA Tech. Memo. 2012–215872*, NASA Goddard Space Flight Center, Greenbelt, Maryland, 117 pp.

——, L. Clementson, C.S. Thomas, L. Schlüter, M. Allerup, J. Ras, H. Claustre, C. Normandeau, J. Cullen, M. Kienast, W. Kozlowski, M. Vernet, S. Chakraborty, S. Lohrenz, M. Tuel, D. Redalje, P. Cartaxana, C.R. Mendes, V. Brotas, S.G.P. Matondkar, S.G. Parab, A. Neeley, and E.S. Egeland, 2012b: The Fifth SeaWiFS HPLC Analysis Round-Robin Experiment (SeaHARRE-5). *NASA Tech. Memo. 2012–217503,* NASA Goddard Space Flight Center, Greenbelt, Maryland, 98 pp.

——, J.H. Morrow, and A. Matsuoka, 2013: Apparent optical properties of the Canadian Beaufort Sea, part II: The 1% and 1 cm perspective in deriving and validating AOP data products. *Biogeosci.,* **10,** 4,511–4,527.

——, and J.W. Brown, 2018: Processing of Radiometric Observations of Seawater using Information Technologies (PRO-SIT): In-Water User Manual. *NASA Tech. Memo.,* (in prep.)

Kostkowski, H.J., 1997: *Reliable Spectroradiometry*, Spectroradiometry Consult., La Plata, Maryland, 609 pp.

Kreuter, A., and M. Blumthaler, 2009: Stray light correction for solar measurements using array spectrometers. *Rev. Sci. Instr.,* **80,** 096108, doi.org/10.1063/1.3233897.

Lide D.R., 1993: *CRC Handbook of Chemistry and Physics, 74th Ed.*, CRC Press, Boca Raton, Florida, 2,031 pp.

Petzold, T.J., and R.W. Austin, 1988: Characterization of MER-1032. *Tech. Memo. EV–001–88t*, Vis. Lab., Scripps Institution of Oceanography, La Jolla, California, 56 pp.

Pidwirny, M., 2006: "Earth-Sun Relationships and Insolation." In: *Fundamentals of Physical Geography, 2nd Ed.* `http://www.physicalgeography.net/fundamentals/6i.html`.

Schmid, B., and C. Wehrli, 1995: Comparison of Sun photometer calibration by use of the Langley technique and the standard lamp. *Appl. Opt.,* **34,** 4,500–4,512.

——, J. Michalsky, R. Halthore, M. Beauharnois, L. Harrison, J. Livingston, P. Russell, B. Holben, T. Eck, and A. Smirnov, 1999: Comparison of aerosol optical depth from four solar radiometers during the fall 1997 ARM intensive observation period. *Geophys. Res. Lett.,* **26,** 2,725–2,728.

McLean, S., B. Schofield, G. Zibordi, M. Lewis, S. Hooker, and A. Weidemann, 1997: Field evaluation of anti-biofouling compounds on optical instrumentation. *SPIE Proc. Ocean Optics XIII,* **2963,** 708–713.

Mobley, C.D., 1999: Estimation of the remote-sensing reflectance from above-surface measurements. *Appl. Opt.,* **38,** 7,442–7,455.

Morel, A., and B. Gentili, 1991: Diffuse reflectance of oceanic waters: its dependence on sun angle as influenced by the molecular scattering contribution. *Appl. Opt.* **30,** 4,427–4,438.

——, and ——, 1993: Diffuse reflectance of oceanic waters. II. Bidirectional aspects. *Appl. Opt.,* **32,** 6,864–6,879.

——, and ——, 1996: Diffuse reflectance of oceanic waters, III. Implication of bidirectionality for the remote sensing problem. *Appl. Opt.,* **35,** 4,850–4,862.

Mueller, J., 2000: "Overview of Measurement and Data Analysis Protocols." In: Fargion, G.S., and J.L. Mueller, Ocean Optics Protocols for Satellite Ocean Color Sensor Validation, Revision 2. *NASA Tech. Memo. 2000–209966,* NASA Goddard Space Flight Center, Greenbelt, Maryland, 87–97.

S.B. Hooker, R.N. Lind, J.H. Morrow, J.W. Brown, R.M. Kudela, H.F. Houskeeper, and K. Suzuki

——, 2002: "Overview of Measurement and Data Analysis Protocols." In: Mueller, J.L., and G.S. Fargion, Ocean Optics Protocols for Satellite Ocean Color Sensor Validation, Revision 3, Volume I. *NASA Tech. Memo. 2002–210004/Rev3–Vol.I,* NASA Goddard Space Flight Center, Greenbelt, Maryland, 123–137.

——, 2003: "Overview of Measurement and Data Analysis Methods." In: Mueller, J.L., and 17 Coauthors, Ocean Optics Protocols for Satellite Ocean Color Sensor Validation, Revision 4, Volume III: Radiometric Measurements and Data Analysis Protocols. *NASA Tech. Memo. 2003–211621/Rev4–Vol.III*, NASA Goddard Space Flight Center, Greenbelt, Maryland, 1–20.

——, and R.W. Austin, 1992: Ocean Optics Protocols for Sea-WiFS Validation. *NASA Tech. Memo. 104566, Vol. 5,* S.B. Hooker and E.R. Firestone, Eds., NASA Goddard Space Flight Center, Greenbelt, Maryland, 43 pp.

——, and R.W. Austin, 1995: Ocean Optics Protocols for Sea-WiFS Validation, Revision 1. *NASA Tech. Memo. 104566, Vol. 25,* S.B. Hooker, E.R. Firestone, and J.G. Acker, Eds.,

NASA Goddard Space Flight Center, Greenbelt, Maryland, 66 pp.

Slusser, J., J. Gibson, D. Bigelow, D. Kolinski, P. Disterhoft, K. Lantz, and A. Beaubien, 2000: Langley method of calibrating UV filter radiometers. *J. Geophys. Res.,* **105,** 4,841–4,849.

Sperling, A., S. Winter, K-H. Raatz, and J. Metzdorf, 1996: *Entwicklung von Normallampen für das UV-B Meßprogramm, PTB-Ber. PTB-Opt-52*, Physikalisch-Technische Bundesanstalt, Braunschweig, Germany. 60 pp.

Taylor, B.N., and C.E. Kuyatt, 1994: Guidelines for Evaluating and Expressing the Uncertainty of NIST Measurement Results. *NIST Tech. Note 1297,* U.S. Department of Commerce, National Institute of Standards and Technology, Washington, DC, 20 pp.

Yoon, H.W., C.E. Gibson, and P.Y. Barnes, 2002: Realization of the National Institute of Standards and Technology detector-based spectral irradiance scale. *Appl. Opt.*, **41,** 5,879–5,890.